Development of an *f*–element separation chemistry using solid electrolytes

A Dissertation Presented for the
Doctor of Philosophy
Degree
The University of Tennessee, Knoxville

Kristian Guy Myhre
December 2016

Dedication

To my beautiful and precious wife, whom I adore endlessly:
I have never loved you so much and I will never love you so little again, Bethany.

Acknowledgements

It is a nearly impossible task to decide where to start in thanking those who have helped me get to this point. Certainly, it is truly impossible to decide where to end, as there have been too many people that have helped me along the way to count.

First and foremost, I want to thank my wife and family. Bethany, you are the most amazing wife and more than I deserve. I have been and continue to be extremely blessed by your supportive and endless love. I am beyond excited to continue sharing every day of my life with you. Mom, thank you for enabling and encouraging me to pursue an education that I enjoyed. Dad, thank you for showing me that family comes first and that hard work coupled with integrity is its own reward. Kameron and Kjasa, thank you for keeping me humble in the way only siblings can. I want to also thank my in–laws, who have been an immensely important part of my life in Tennessee.

I want to sincerely thank those at the University of Tennessee and Oak Ridge National Laboratory for giving me so many wonderful opportunities during my time in graduate school. I am especially thankful to Dr. Lee Riedinger for accepting me into the Bredesen Center for my graduate studies as well as personally ensuring my time as a graduate student was successful. The Radiochemical Engineering Development Center has been an extremely exciting place to carry out my dissertation research. The opportunities and support I have been provided as a member of the Nuclear Materials Processing group have been unbelievable. I am also extremely thankful to all of my graduate committee members, each of which has been instrumental in my graduate education. I look forward to continuing to work with all of them.

I want to also thank those that encouraged me throughout the pursuit of my undergraduate degree and helped grow my passion for chemistry, particularly in the areas of separation chemistry, radiochemistry, and electrochemistry.

Abstract

The *f*–elements (lanthanides and actinides) have numerous applications and are critically important to many industries, including the energy, security, and medical industries. One of the barriers to increased use and availability of the *f*–elements is the difficulty in separating them from each other due to their similar chemistries. This is especially true of the trivalent *f*–elements (lanthanides and minor actinides). The development of separation techniques that maximize the differences in the physicochemical properties of the *f*–elements is therefore an important area of research. For these reasons, an effort was undertaken to explore the use of solid electrolyte materials to accomplish separations of the *f*–elements. The results of this work have led to the development of a novel separation method at Oak Ridge National Laboratory for accomplishing *f*–element separations using inorganic solid electrolyte materials, specifically beta´´–alumina. The use of beta´´–alumina was both investigated both as an ion exchanger and selective membrane. Given the large dependence of superionic conductivity upon the valence of mobile ions, oxidation state control of the ions to be separated was explored. The high–temperature regimes (greater than 300°C) required for superionic conduction of multivalent metal ions in beta´´–alumina necessitated the use of molten salts as a medium to contain ions to interact with the solid electrolyte. These studies also included the development of Laser Induced Breakdown Spectroscopy for determining the concentrations of *f*–elements in the alumina based materials.

Preface

"Captain, you almost make me believe in luck." – Spock

Table of Contents

List of Tables

List of Figures

Abbreviations

REDC	Radiochemical Engineering Development Center
HFIR	High Flux Isotope Reactor
ORNL	Oak Ridge National Laboratory
BDPA	beta"-alumina
LIBS	Laser Induced Breakdown Spectroscopy
XPS	X-ray Photoelectron Spectroscopy
PLS	Partial Least Square
PC	Principal Component
LOD	Limit of Detection
SLR	Simple Linear Regression
RMSE	Root Mean Square Error

Chapter 1: Introduction and motivation

1.1 Use of f–elements in society

The *f*–elements, comprised of the lanthanides ($_{57}$La – $_{71}$Lu) and actinides ($_{89}$Ac – $_{103}$Lr), have numerous applications and are critically important to many industries, including the energy, security, and medical industries. Neodymium, for example, is used in NdFeB magnets and optical materials, such as in Nd:YAG lasers [1]. Europium is used commonly used for its phosphorescent characteristics in electronic displays and as anti–counterfeiting phosphors in the euro currency [1, 2]. Actinium, specifically the alpha–emitting radionuclide ^{225}Ac, is being investigated for use in various modalities of alpha radioimmunotherapy for the treatment of numerous types of cancer [3, 4]. Uranium, perhaps the most prolifically known *f*–element, is used as the fuel for nuclear energy production, which currently generates roughly 20% of the United States' and 14% of world's electricity [5]. Indeed, despite being unfamiliar by name to many, the *f*–elements are an integral part of daily activities around the globe, particularly in an era where advanced technologies are increasingly used and commonplace. An important aspect of using the *f*–elements in electronic, optical, magnetic, medical and other advanced technology applications is the purity of the raw materials, since even minute impurities can decrease performance of *f*–element materials.

1.2 Project motivation

The similar physicochemical properties of the *f*–elements result in many of the lanthanides and actinides (especially the transplutonium actinides, also known as the minor actinides) sharing extraordinarily similar chemistries [1, 6–10]. The lanthanides

and minor actinides have an overwhelming preference for the trivalent oxidation state as well as cationic radii that are close in size. The difference in trivalent cationic radii of the lanthanides and minor actinides, when ranked in order of radii, average a difference of only 0.9%. Separations of *f*–elements adjacent on the periodic table are therefore particularly difficult to accomplish, such as the lanthanide pair Eu and Sm or actinide pair curium and americium. This results in long chemical processing schemes involving numerous intricate separation steps in order to reach the purities required when processing materials containing a large number of different *f*–elements. These separations are further complicated by the often radioactive nature of the *f*–element species to be separated, thereby altering the separation chemistries being used via radiolytic effects [11]. Many of the routinely used separation methods rely upon organic and aqueous solvents and materials, which are far more radiation sensitive compared to inorganic solvents and materials.

A prime example of the need for improved *f*–element separation technologies is the possibility of a nuclear fuel cycle involving the complete or at least partial reprocessing of used nuclear fuel. Although used nuclear fuel is not reprocessed in the United States currently, there are many ongoing major research and development efforts ranging in scope from fundamental to applied to everything in–between [12]. A major difficulty in the reprocessing of used nuclear fuel is the separation of the lanthanides and minor actinides from each other. The used nuclear fuel that has been produced in the United States consists predominately of uranium oxide based. After being used to produce electricity in a nuclear reactor, a large build–up of activation and fission products

are present in the irradiated fuel. One metric ton of used nuclear fuel from a standard Pressurized Water Reactor after a 10 year cooling period contains, in addition to the remaining uranium and other fission products, roughly: 8.5 kg of plutonium, 0.13 kg of the minor actinides (neptunium, americium, and curium), and 10.1 kg of the lanthanides [6, 13]. A large amount of the products in the fuel consist of the lanthanides and minor actinides, accounting for roughly two percent of the used nuclear fuel's mass. At the same time, a large amount of uranium oxide fuel is technically unused. While the presence of certain activation and fission products called "poisons" cause the used nuclear fuel to be unusable after a certain amount of irradiation, the remaining uranium could be reused if purified through reprocessing since the ^{235}U content has not been fully depleted. In most used nuclear fuel reprocessing schemes, the lanthanides and minor actinides follow each other closely given their similar physicochemical properties. It is, however, desirable to separate the americium from the curium and lanthanides in order to reduce the radiotoxicity of the waste from nuclear energy [12].

The separation of the lanthanides and minor actinides is also of critical importance to the production of heavy elements at Oak Ridge National Laboratory's (ORNL) High Flux Isotope Reactor (HFIR) and Radiochemical Engineering Development Center (REDC) facilities. These facilities routinely produce transuranic radioisotopes, such as ^{252}Cf and ^{249}Bk, for use as neutron, fission fragment, heat, and other radiation sources as well as targets for super–heavy element discovery [14–16]. Neutron irradiation of the americium/curium targets used for ^{252}Cf production produces large amounts of the lanthanides are through fission reactions. Since re–use of the

americium/curium target material is highly desired, the lanthanides have to be separated from the americium/curium material. Additionally, although the feedstock that is used as target material is comprised of both americium and curium, it would be ideal for the target material to be purely heavy curium, specifically ^{246}Cm and ^{248}Cm [16].

Improved *f*–element separations are also needed for improving the production of lanthanide radioisotopes. For instance, ^{155}Eu is uniquely useful in nuclear battery applications as a beta–emitting radioisotope due to its long half–life ($t_{1/2}$ = 4.753 years), low gamma emissions, and decay to stable ^{155}Gd [17]. The major route for producing no–carried–added ^{155}Eu is to irradiate a ^{154}Sm target with neutrons in a nuclear reactor, such as the HFIR. The ^{154}Sm captures a neutron and then quickly decays from ^{155}Sm to ^{155}Eu. The difficulty in producing high–purity ^{155}Eu comes from the similar chemistries of Eu and Sm. The two elements are adjacent on the Periodic Table with trivalent cationic radii differing only by 1% [18]. The amount of ^{155}Eu produced is much smaller than the amount of ^{154}Sm target material, with roughly 1 – 3 milligrams of ^{155}Eu produced per gram of ^{154}Sm [19]. Similarly, to separating Am and Cm from each other, the separation of Eu and Sm is one of the most difficult in the production of purified lanthanides. This is demonstrated well by the closely related partition coefficients of trivalent Eu and Sm in common extractants used for solvent extraction separations of the lanthanides [1]. For this reason, selective reduction of Eu in the presence of Sm using a zinc amalgam is often used industrially after numerous solvent extraction steps [1, 2, 19]. The Eu^{2+} is then precipitated out of the liquid phase, which is where Sm^{3+} remains dissolved.

For the reasons mentioned here, it is highly desirable that highly effective *f*–element separation approaches be explored and developed, particularly those relevant to the separation of the lanthanides and minor actinides.

1.3 Scope of work

A novel method for accomplishing separations involving the *f*–elements has been investigated. This new separation approach relies upon differences in the behavior of multivalent cationic species of solid electrolytes, specifically the beta″–alumina (BDPA) solid electrolyte material. It offers an approach to separating the *f*–elements that does not utilize organic materials, which can be significantly more susceptible to radiation damage than inorganic materials. Instead, inorganic chloride salts and simple metal oxide materials are used to accomplish separations. Ultimately, the work presented herein lays the groundwork for future research and development efforts that will investigate the use of solid electrolytes to accomplish separations involving the *f*–elements. It is hoped that future work will include investigating this and related separation methods using solid electrolytes for application in the production of purified stable rare earth materials, lanthanide and actinide radioisotopes, heavy element production, as well as nuclear fuel reprocessing.

Separations were achieved by ion exchange reactions both into and out of BDPA as well as selective electrolysis into BDPA. The lanthanide pair Eu and Sm were predominately used throughout these studies to investigate this new separation approach. The separation of Eu and Sm was chosen for its relevance to the rare earth production

industry and radioisotope production at ORNL. The solid electrolyte material BDPA was chosen for these initial studies for several reasons. A surprisingly large number of cations, ranging from monovalent to trivalent and including the lanthanides (except Pm), have been reported as participating in ion exchange reactions with BDPA [20–25]. Additionally, BDPA is a robust, non–hazardous, and relatively inexpensive material that is commercially available. Because ion exchange reactions with BDPA typically require temperatures greater than 300 °C and often 600 °C, molten chloride salts were investigated as solvents for exchanging with BDPA instead of aqueous or organic solvents. This work also involved the development of Laser Induced Breakdown Spectroscopy (LIBS) as a method for quantifying the amount of Eu and Sm in samples of BDPA. This was necessary since BDPA is an alumina based ceramic material and very difficult to chemically or physically prepare for other analysis methods, such as Inductively Coupled Plasma Mass Spectrometry or Inductively Coupled Plasma Optical Emission Spectroscopy. X–ray Photoelectron Spectroscopy (XPS) studies were carried out in order to understand the oxidation state behavior of Eu and Sm in BDPA, which was found to play a large role in the ion exchange reactions.

1.4 References

(1) Lucas, J.; Lucas, P.; Le Mercier, T.; Rollat, A.; Davenport, W. Rare Earths Purification, Separation, Precipitation and Calcination. In *Rare Earths*; Elsevier, 2015; pp 69–91.

(2) Goonan, T. G. Rare Earth Elements — End Use and Recyclability. *U.S. Geol. Surv. Sci. Investig. Rep. 2011-5094* **2011**, 1–15

(3) Boll, R. A.; Malkemus, D.; Mirzadeh, S. Production of Actinium-225 for Alpha Particle Mediated Radioimmunotherapy. *Appl. Radiat. Isot.* **2005**, *62* (5), 667–679 DOI: 10.1016/j.apradiso.2004.12.003.

(4) Scheinberg, D. A.; McDevitt, M. R. Actinium-225 in Targeted Alpha-Particle Therapeutic Applications. *Curr. Radiopharm.* **2011**, *4* (4), 306–320 DOI: 10.2174/1874471011104040306.

(5) Tester, J. W.; Drake, E. M.; Driscoll, M. J.; Golay, M. W.; Peters, W. A. *Sustainable Energy: Choosing Among Options*, 2nd ed.; The MIT Press, 2012.

(6) Veliscek-Carolan, J. Separation of Actinides from Spent Nuclear Fuel: A Review. *Journal of Hazardous Materials*. 2016, pp 266–281.

(7) Nash, K. L.; Choppin, G. R. Separations Chemistry for Actinide Elements: Recent Developments and Historical Perspective. *Sep. Sci. Technol.* **1997**, *32* (1–4), 255–274 DOI: 10.1080/01496399708003198.

(8) Cotton, S. *Lanthanide and Actinide Chemistry*, 2nd ed.; John Wiley & Sons, Ltd: West Sussex, **2006**.

(9) Moyer, B. A.; Lumetta, G. J.; Mincher, B. J. 11 – Minor Actinide Separation in the Reprocessing of Spent Nuclear Fuels: Recent Advances in the United States. In *Reprocessing and Recycling of Spent Nuclear Fuel*; Elsevier Ltd, 2015; pp 289–312.

(10) Modolo, G.; Geist, A.; Miguirditchian, M. 10 – Minor Actinide Separations in the Reprocessing of Spent Nuclear Fuels: Recent Advances in Europe. In *Reprocessing and Recycling of Spent Nuclear Fuel*; Elsevier Ltd, 2015; pp 245–287.

(11) Mincher, B. J. 8 – Radiation Chemistry in the Reprocessing and Recycling of Spent Nuclear Fuels. In *Reprocessing and Recycling of Spent Nuclear Fuel*; Elsevier Ltd, 2015; pp 191–211.

(12) Nash, K. L.; Nilsson, M. 1 – Introduction to the Reprocessing and Recycling of Spent Nuclear Fuels. In *Reprocessing and Recycling of Spent Nuclear Fuel*; Elsevier Ltd, 2015; pp 3–25.

(13) Glatz, J.-P.; Souček, P.; Malmbeck, R. 3 – Key Challenges in Advanced Reprocessing of Spent Nuclear Fuels. In *Reprocessing and Recycling of Spent Nuclear Fuel*; Elsevier Ltd, 2015; pp 49–62.

(14) I. W. Osborne-Lee and C. W. Alexander.; Californium-252: a remarkable versatile radioisotope. *ORNL/TM-12706*. Oak Ridge National Laboratory, **1995**.

(15) Oganessian, Y. T.; Abdullin, F. S.; Bailey, P. D.; Benker, D. E.; Bennett, M. E.; Dmitriev, S. N.; Ezold, J. G.; Hamilton, J. H.; Henderson, R. A.; Itkis, M. G.; Lobanov, Y. V.; Mezentsev, A. N.; Moody, K. J.; Nelson, S. L.; Polyakov, A. N.; Porter, C. E.; Ramayya, A. V.; Riley, F. D.; Roberto, J. B.; Ryabinin, M. A.; Rykaczewski, K. P.; Sagaidak, R. N.; Shaughnessy, D. A.; Shirokovsky, I. V.; Stoyer, M. A.; Subbotin, V. G.; Sudowe, R.; Sukhov, A. M.; Taylor, R.; Tsyganov, Y. S.; Utyonkov, V. K.; Voinov, A. A.; Vostokin, G. K.; Wilk, P. A. Eleven New Heaviest Isotopes of Elements Z=105 to Z=117 Identified among the Products of Bk^{249} + Ca^{48} Reactions. *Phys. Rev. C - Nucl. Phys.* **2011**, *83* (5), 1–14 DOI: 10.1103/PhysRevC.83.054315.

(16) Roberto, J. B.; Alexander, C. W.; Boll, R. A.; Burns, J. D.; Ezold, J. G.; Felker, L. K.; Hogle, S. L.; Rykaczewski, K. P. Actinide Targets for the Synthesis of Super-Heavy Elements. *Nucl. Phys. A* **2015**, *944*, 99–116 DOI: 10.1016/j.nuclphysa.2015.06.009.

(17) Litz, M.; Isotope Beta-Battery Approaches for Long-Lived Sensors: Technology Review. *ARL-TR-7048*. Army Research Laboratory Report, **2014**.

(18) Shannon, R. D. Revised Effective Ionic Radii and Systematic Studies of Interatomic Distances in Halides and Chalcogenides. *Acta Crystallogr. Sect. A* **1976**, *32* (5), 751–767 DOI: 10.1107/S0567739476001551.

(19) Myhre, K. G., Du, M.; *Production of No-Carrier-Added ^{155}Eu from ^{154}Sm Target Material*. Presented at the 2014 Symposium on Separation Science and Technology for Energy Applications, Oak Ridge, TN, October, **2014**.

(20) Farrington, G. C.; Dunn, B.; Thomas, J. O. The Lanthanide Beta´´-aluminas: A New Family of Fluorescent Solid Electrolytes. *Appl. Phys. A Solids Surfaces* **1983**, *32*, 159–161.

(21) Breiter, M. W.; Maly-Schreiber, M.; Allitsch, G.; Linhardt, P. Properties of Polycrystalline Beta´´-alumina Isomorphs. *Solid State Ionics* **1988**, *28–30*, 369–372.

(22) Wen, Z.-Y.; Lin, Z.-X.; Tian, S.-B. Preparation and Ionic Conduction Property of Polycrystalline Eu^{2+} Beta´´-alumina. *Solid State Ionics* **1990**, *40/41*, 91–94.

(23) Tietz, F.; Urland, W. Investigations on Lanthanide-Ion-Exchange Beta and Beta´´-alumina. *J. Alloys Compd.* **1993**, *192*, 78–80.

(24) Sattar, S.; Ghosal, B.; Underwood, M. L.; Mertwoy, H.; Saltzberg, M. A.; Frydrych, W. S.; Rohrer, G. S.; Farrington, G. C. Synthesis of Di- and Trivalent Beta´´-aluminas by Ion Exchange. *J. Solid State Chem.* **1986**, *65*, 231–240.

(25) Farrington, G. C.; Dunn, B. Divalent Beta´´-aluminas: High Conductivity Solid Electrolytes for Divalent Cations. *Solid State Ionics* **1982**, *7*, 267–281 DOI: 10.1016/0167-2738(82)90023-6.

Chapter 2: Background

2.1 Separation of the lanthanides and minor actinides

Lanthanide and actinide intra– and inter–group separations are very difficult to accomplish, with separations involving the lanthanides and minor actinides particularly troublesome. This is due mainly to their preference for the trivalent cationic state and similar size, which lead to very similar chemistries [1-5]. Additionally, it is often the case that the lanthanides and actinides to be separated are highly radioactive and separations are thereby complicated by radiolysis [6]. This is particularly troublesome for hydrometallurgical separations utilizing aqueous solutions and organic molecules, which are the most widely employed separation methods today.

Solvent extraction, precipitation/coprecipitation, and ion exchange methods have historically been the most commonly employed methods for accomplishing separations involving the lanthanides and actinides. Precipitation of fluoride salts was used at the laboratory scale to accomplish early separations of uranium and plutonium [1]. The bismuth phosphate process was utilized during the Manhattan project to produce the plutonium for the Fat Man nuclear bomb used in World War II [1]. The resource intensive precipitation separation methods were then replaced with solvent extraction processes for large–scale actinide separations. The Plutonium Uranium Reduction Extraction (PUREX) process was eventually developed in the 1950's [1]. The PUREX process and its variants are still used today to process large quantities of used nuclear fuel in countries such as France as well as irradiated actinide targets. A byproduct of the PUREX process is a mixed aqueous raffinate solution containing a large mixture of heavy metals in nitric acid, which include the lanthanide fission products and minor

actinide activation products. In order to reduce the amount of radioactive high level waste required for disposition in a geological repository, whether through consolidation or minor actinide burn–up in a fast reactor, a separation of the lanthanides and minor actinides is required.

The TRUEX (TransUranic EXtraction), TRPO (TRialkyl Phosphine Oxides), and DIAMEX (DIAMide Extraction) processes have and continue to be developed for removing the trivalent lanthanides and minor actinides from PUREX raffinate solutions to reduce the amount of high level waste produced from used nuclear fuel reprocessing [1, 6–9]. These methods all make use of solvating extractants. TRUEX and TRPO use phosphine oxides whereas DIAMEX uses malonamides. These methods do not, however, accomplish a separation of the trivalent lanthanides and minor actinides from each other. Thus, further processing is required if the minor actinides are to be burnt up in a fast spectrum reactor or disposed of separately. In the case of heavy element production, such as for ^{252}Cf, additional processing steps would also be required to recover the americium and curium from the lanthanides for future use as a feedstock material [11].

It is well known that the separation of the trivalent lanthanides and minor actinides from each other can be accomplished through selective complexation with molecules containing soft–donor groups with nitrogen, sulfur, and phosphorous [1-5]. The minor actinides bond more strongly with soft-donor ligands compared to the lanthanides due to the higher covalent character of the bonding. This comes from the higher involvement of the 5*f* electrons of the actinides compared to the 4*f* electrons of the lanthanides in bonding [4]. The difference in involvement is due to the 4*f* electrons being

shielded by the $5s^2$ and $5p^6$ orbitals. The $5f$ electrons are less effectively shielded and therefore participate in bonding to a greater degree. Among the methods that rely upon these differences is the TALSPEAK (Trivalent Actinide Lanthanide Separation with Phosphorous–reagent Extraction from Aqueous Komplexes) process, which uses the partitioning of the actinides into an aqueous phase containing a complexant, such as aminopolyacetic acid, and the lanthanides into an organic phase containing a extractant, such as di(2–ethlhexyl) phosphoric acid (HDEHP or HA) [11]. Closely related to the TALSPEAK process, the reverse TALSPEAK process involves the loading of both the lanthanides and actinides into an organic phase and subsequent selective stripping of the actinides into an aqueous phase [12]. Another approach is the TRAMEX process, in which the actinides are extracted into a tertiary amine containing organic phase from a highly concentrated lithium chloride solution containing the lanthanides and actinides [13]. The ALSEP (Actinide Lanthanide SEParation) process, which is recently under development, uses an acidic extractant in combination with a neutral extractant to separate the lanthanides and minor actinides [7]. Ion exchange column separations have also been investigated [14, 15]. However, a major drawback is the production of gases and low–stability of the ion exchange resins under radiolytic conditions. It should be noted that all of these methods separate the lanthanides and minor actinides while they remain in the stable trivalent oxidation state.

Approaches that utilize oxidation states other than the trivalent have been and continue to be investigated for separating the lanthanides and minor actinides [16-20]. Americium, unlike the lanthanides and curium, can be oxidized and stabilized in aqueous

solutions to the pentavalent and hexavalent oxidation states. Thus, a separation of americium from the lanthanides and curium can be accomplished. Processes that take this approach include the SESAME process [17]. Oxidizing agents such as sodium bismuthate have also been used to accomplish separations of the lanthanides and/or minor actinides [20].

Most of the hydrometallurgical techniques that have been investigated to date to achieve a separation between actinides and lanthanides have been described above. Major drawbacks of the current techniques include: (1) use of materials highly susceptible to radiolysis; (2) use of expensive ligands; (3) separation processes that are difficult to scale; and (4) production of large quantities of complicated chemical and radiological waste.

It should be noted that pyroprocessing techniques are also being seriously explored for reprocessing used nuclear fuel by the United States, South Korea, and other countries [21-24]. In contrast to PUREX and other organic/aqueous based methods, pyroprocessing involves the use of molten salts (e.g. LiCl–KCl or NaCl–KCl) and molten metals (e.g. cadmium or bismuth). Although variants certainly exist, the favored approach is to electrochemically reduce spent oxide fuel, which comprises the vast majority of used nuclear fuel in the United States. The electrochemical reduction is carried out once the oxide fuel has been dissolved into a molten salt, such as Li_2O–LiCl. Reduced oxide fuel or metallic fuel is then dissolved in a molten salt, such as LiCl–KCl, and electrorefining is carried in order to purify uranium for reuse. In several pyroprocessing schemes, plutonium and minor actinides follow with uranium in the

processing scheme and are incorporated in mixed fuels. However, the used molten salts contain significant amounts of the lanthanides as well as residual minor actinides. It is highly desirable for these contaminated pyroprocessing salts to be recycled in order to reduce the volume of highly radioactive waste going to a final geological repository [25]. Current methods under serious consideration are crystallization, distillation, precipitation, and zeolite occlusion [25, 26]. Crystallization works to some extent but is not highly effective and requires lengthy processing times. Distillation requires large differences in vapor pressures between the species to be separated from each other and again lengthy process times. The precipitation of lanthanide fission product and minor actinide elements (as oxides/oxychlorides or phosphates) from molten salt eutectics has also been investigated. After the precipitation step, the molten salt is cooled and the two phases (purified salt and precipitated lanthanides) are mechanically separated. This can lead to significant contamination due to the spreading of salt material during the mechanical processing. Issues with precipitation also include the requirements of either high temperatures and corrosive environment (oxygen sparging for oxide/oxychlorides approach) or very accurately knowing the salt composition (phosphate approach). The favored method, zeolite occlusion, involves the ion exchange of contaminants in molten salts with inorganic zeolite materials [26]. Drawbacks of this approach include large volumes of waste produced and temperature stability of the zeolite material itself. All of the methods mentioned do not aim to accomplish a separate of the lanthanides from the minor actinides.

2.2 Separations using solid electrolytes

A relatively unexplored method of accomplishing separations involving the *f*–elements is to use solid electrolytes, which are materials exhibiting macroscopic ionic conduction with conductivities on the same order as room temperature liquid electrolyte solutions (10^{-3} to 10 Ω^{-1} cm^{-1}) [27-29]. Overwhelmingly, solid electrolytes have been researched and developed for use in battery, sensor, and fuel cell technologies [27-33]. Solid electrolytes offer enhanced lifetimes, higher energy densities, and increased safety when used in battery technologies [32, 33]. The largest application of solid electrolytes in the battery arena is for lithium ion batteries. Applications of solid electrolytes have included sensor technologies, such as for the measurement of oxygen and hydrogen content in gaseous and liquid media [31]. The possibility of measuring hydrogen isotope ratios has even been investigated [34]. Fuel cell technologies rely upon the use of oxide and other ion conducting solid electrolyte materials, such as in solid oxide fuel cells [30, 31].

A solid electrolyte can be broken down into two pieces: the immobile scaffold structure and the mobile ionic species [27, 28]. Whether a specific solid electrolyte conducts a given species depends upon the characteristics of the solid electrolyte and experimental parameters (e.g. temperature or pressure). The scaffold structure or framework of the solid electrolyte, which is immobile, must provide a pathway for the mobile ionic species to be conducted through. Some solid electrolytes are conductive towards only one mobile species, such as is often the case with lithium ion conductors, while others can conduct multiple elements at the same time. In order for

a given solid electrolyte material to be used for a separation, it must exhibit different conductivities towards the different elements to be separated from each other. When a solid electrolyte conducts multiple elements/species, the difference in conductivity between the mobile ionic species is dependent upon characteristics such as polarizability, ionic radius, valency, and mass. For instance, the conductivities of several trivalent cations, including several of the lanthanides, have been shown to have markedly different conductivity values in the tungstates and molybdates with the $Sc_2(WO_4)_3$–type structure [35, 36]. The difference in conductivities arises largely from polarizability and ionic radii size. One of the largest effects on relative conductivities of two mobile ions is the valence state. Both divalent and trivalent Eu cations are both mobile in the BDPA solid electrolyte but their conductivities are several orders of magnitude different from each other [37]. A key takeaway is that solid electrolytes are selective towards which ion or ions are conducted. It would therefore seem natural to explore the use of solid electrolytes to separate elements from each other. However, relatively few examples of using solid electrolytes in elemental separation techniques exist in comparison to the other applications mentioned.

Perhaps the most studied application of solid electrolytes for separations is that of producing high–purity oxygen from air, for which ceramic oxygen ion conducting solid electrolytes have used to “pump” oxygen away from the other components of ambient air [38, 39]. Typically, the separation apparatus is comprised of a ceramic solid electrolyte membrane separating two compartments. Oxygen ions migrate

through the solid electrolyte membrane from one compartment to the other. It is possible to drive the oxygen separation using either an applied potential or pressure difference. For example, Dongsheng *et al.* investigated the use of $Ce_{0.9}Gd_{0.1}O_{1.95}$ as the oxygen ion conducting ceramic solid electrolyte membrane for onboard oxygen generation in airplanes [38]. They found the use of an electrical driving force to be the best option for that application and were able to produce 99.9% pure oxygen with a recovery rate of 85%. There are also a few instances of a ceramic solid electrolyte membrane being used to separate lithium from other alkali metals. Kunugi *et al.* used a perovskite-type oxide, $La_{0.55}Li_{0.35}TiO_3$, to separate lithium from an aqueous solution containing equimolar amounts of LiCl, NaCl, and KCl [40]. Although successful, the lithium ion conducting ceramic solid electrolyte material did not have a great stability in water. A recent study by Hoshino similarly extracted lithium selectivity from seawater using a lithium ion conducting solid electrolyte. However, the solid electrolyte used is a glassy-ceramic material that is significantly more stable in aqueous solutions with a nominal composition of Li_2O-Al_2O_3-SiO_2-P_2O_5-TiO_2-GeO_2 [41]. It is interesting to note that Hoshino was able to recover lithium from seawater while producing electricity rather than consuming it. Researchers at Sandia National Laboratory have investigated the selective conduction of lithium and potassium from a molten LiCl–KCl salt containing impurities such as cesium, with the goal being to recycle used salts from pyroprocessing operations [42]. It was found that NaSICON–type and garnet–structured lithium lanthanum tantalite (LLTO) solid electrolytes could be used to selectively conduct lithium and potassium in the presence of cesium.

Subsidiaries of CoorsTek have published documents stating the separation of hydrogen, lithium, sodium, and oxygen from complicated aqueous and organic waste streams [43, 44]. In each of the discussed studies, the solid electrolyte is used as a membrane type separator in which at least two compartments are separated by the solid electrolyte material thereby allowing only certain ions to pass between compartments. There are several other possible approaches to using solid electrolytes to separate elements from each other, including ion exchange reactions.

Although they have not been investigated specifically for separations, a great deal of work that has been done to study ion exchange reactions involving solid electrolytes [tango]. The main purpose in those studies has been to synthesize metastable compounds not accessible through direct synthetic routes. A prime example of this is the exchange of mono–, di–, and even trivalent cations with beta–alumina and BDPA [45-51]. Toropov and Stukalova first performed ion exchange reactions with beta–alumina initially containing sodium to prepare calcium, strontium, barium, and rubidium containing derivatives [50]. Yao and Kummer later investigated ion exchange reactions of the monovalent cations from molten salts with sodium containing beta–alumina [51]. An important observation from their work was that a fractionation of the two elements involved in the ion exchange reaction occurred due to the stabilities of each species between the molten salt and solid electrolyte phases. For a reaction between potassium and sodium chloride salts with beta–alumina, it was found that potassium favored the molten salt and sodium the solid electrolyte phases [51]. This behavior was reversed when the chloride melt was

replaced with an iodide melt. Farrington and co-workers further studied ion exchange reactions of divalent and trivalent cations with BDPA [45-47]. Several of the lanthanides were exchanged into the BDPA, including Eu and Sm.

This work is intended to answer the question of whether or not solid electrolytes can be used to accomplish separations involving the *f*–elements.

2.3 References

(1) Nash, K. L.; Choppin, G. R. Separations Chemistry for Actinide Elements: Recent Developments and Historical Perspective. *Sep. Sci. Technol.* **1997**, *32* (1–4), 255–274 DOI: 10.1080/01496399708003198.

(2) Moyer, B. A.; Lumetta, G. J.; Mincher, B. J. 11 – Minor Actinide Separation in the Reprocessing of Spent Nuclear Fuels: Recent Advances in the United States. In *Reprocessing and Recycling of Spent Nuclear Fuel*; 2015; pp 289–312.

(3) Modolo, G.; Geist, A.; Miguirditchian, M. 10 – Minor Actinide Separations in the Reprocessing of Spent Nuclear Fuels: Recent Advances in Europe. In *Reprocessing and Recycling of Spent Nuclear Fuel*; 2015; pp 245–287.

(4) Cotton, S. *Lanthanide and Actinide Chemistry*; John Wiley & Sons, Ltd: Chichester, UK, 2006.

(5) Jensen, M. P.; Chiarizia, R.; Ulicki, J. S.; Spindler, B. D.; Murphy, D. J.; Hossain, M. M.; Roca-Sabio, A.; de Blas, A.; Rodríguez-Blas, T. Solvent Extraction Separation of Trivalent Americium from Curium and the Lanthanides. *Solvent Extr. Ion Exch.* **2015**, *33* (4), 329–345 DOI: 10.1080/07366299.2015.1046292.

(6) Mincher, B. J. 8 – Radiation Chemistry in the Reprocessing and Recycling of Spent Nuclear Fuels. In *Reprocessing and Recycling of Spent Nuclear Fuel*; 2015; pp 191–211.

(7) Lumetta, G. J.; Gelis, A. V.; Carter, J. C.; Niver, C. M.; Smoot, M. R. The Actinide-Lanthanide Separation Concept. *Solvent Extr. Ion Exch.* **2014**, *32* (4), 333–347 DOI: 10.1080/07366299.2014.895638.

(8) Horwitz, E. P.; Kalina, D. G.; Diamond, H.; Vandegrift, G. F.; Schulz, W. W. The TRUEX process: A process for the extraction of the transuranic elements from nitric acid wastes utilizing modified PUREX solvent. Solvent Extr. Ion Exch. 1985, 3, 75–109.

(9) Courson, O.; Lebrun, M.; Malmbeck, R.; Pagliosa, G.; Römer, K.; Sätmark, B.; Glatz, J.-P. Partitioning of minor actinides from HLLW using the DIAMEX process. Part 1: Demonstration of extraction performances and hydraulic behavior of the solvent in a continuous process. Radiochim. Acta 2000, 88(12), 857–863.

(10) Malmbeck, R.; Courson, O.; Pagliosa, G.; Römer, K.; Sätmark, B.; Glatz, J.-P.; Baron, P. Partitioning of minor actinides from HLLW using the DIAMEX process. Part 2: “Hot” continuous counter-current experiment. Radiochim. Acta 2000, 88(12), 865–871.

(11) Patton, B. D.; Benker, D.; Collins, E. D.; *Recovering americium and curium from mark-42 target materials – new processing approaches to enhance separations and integrate waste stream disposition – 12228*. WM2012 Conference, February 26 – March 1, **2012**, Phoenix, Arizona, USA.

(12) Nilsson, M., Nash, K.L Review Article: A review of the development and operational characteristics of the TALSPEAK process. Solvent Extr. Ion Exch. **2007**, 25, 665–701.

(13) Baybarz, R. D.; Kinser, H. B.; Separation of Transplutoniums and Lanthanides by Tertiary Amine Extraction. *ORNL-3244*. Oak Ridge National Laboratory Technical Report, **1962**.

(14) Myasoedov, B. F.; Maryutina, T. A.; Litvina, M. N.; Malikov, D. A.; Kulyako, Y. M.; Spivakov, B. Y.; Hill, C.; Adnet, J.-M.; Lecomte, M.; Madic, C. Americium(III)/curium(III) separation by countercurrent chromatography using malonamide extractants. Radiochim. Acta 2005, 93, 9–15.

(15) Kraak, W.; Van Der Heijden, W. A. Anion exchange separation between americium and curium and between several lanthanide elements. J. Inorg. Nucl. Chem. 1966, 28, 221–224.

(16) Mason, G. W.; Bollmeier, A. F.; Peppard, D. F. Partition of oxidized americium from actinides(III) and lanthanides(III). J. Inorg. Nucl. Chem. 1970, 32, 1011–1022.

(17) Donnet, L.; Adnet, J. M.; Faure, N.; Bros, P.; Brossard, P.; Josso, F. Development of the SESAME Process. *Proc. 5th Int. Inf. Exch. Meet. Actin. Fission Prod. Partitioning Transmutat. Nov. 25–27, 1998* **1999**, 161.

(18) Runde, W. H.; Mincher, B. J. Higher oxidation states of americium: Preparation, characterization and use for separations. Chem. Rev. 2011, 111, 5723–5741.

(19) Burns, J. D.; Shehee, T. C.; Clearfield, A.; Hobbs, D. T. Separation of americium from curium by oxidation and ion exchange. Anal. Chem. 2012, 84, 6930–6932.

(20) Mincher, B. J.; Martin, L. R.; Schmitt, N. C. Tributylphosphate extraction behavior of bismuthate-oxidized americium. Inorg. Chem. 2008, 47, 6984–6989.

(21) Souček, P.; Malmbeck, R. 17 – Pyrochemical Processes for Recovery of Actinides from Spent Nuclear Fuels. In *Reprocessing and Recycling of Spent Nuclear Fuel*; 2015; pp 437–456.

(22) Lewin, R. G.; Harrison, M. T. 15 – International Developments in Electrorefining Technologies for Pyrochemical Processing of Spent Nuclear Fuels. In *Reprocessing and Recycling of Spent Nuclear Fuel*; 2015; pp 373–413.

(23) Lee, H. 16 – Oxide Electroreduction and Other Processes for Pyrochemical Processing of Spent Nuclear Fuels: Developments in Korea. In *Reprocessing and Recycling of Spent Nuclear Fuel*; 2015; pp 415–436.

(24) Koyama, T.; Iizuka, M. 18 – Pyrochemical Fuel Cycle Technologies for Processing of Spent Nuclear Fuels: Developments in Japan. In *Reprocessing and Recycling of Spent Nuclear Fuel*; 2015; pp 457–519.

(25) Frank, S.; Ebert, W.; Riley, B.; Park, H. S.; Cho, Y. Z.; Lee, C. H.; Jeon, M. K.; Yang, J. H.; Eun, H. C.; Waste Stream Treatment and Waste Form Fabrication for Pyroprocessing of Used Nuclear Fuel. *INL/EXT/14-34014*. Idaho National Laboratory Technical Report, **2015**.

(26) Park, H.-S.; Kim, I.-T.; Cho, Y.-J.; Son, M.-S.; Eun, H.-C. Removal Behavior of Cs from Molten Salt by Using Zeolitic Materials. *J. Radioanal. Nucl. Chem.* **2010**, *283*, 267–272 DOI: 10.1007/s10967-009-0351-9.

(27) Stimming, U.; Tu, H. Solid-State Electrochemistry. In *Fundamentals of Electrochemistry*; Wiley, 2005.

(28) Anwane, S. W. Solid Electrolytes: Principles and Applications. In *Advanced Energy Materials*; Scrivener Publishing LLC, 2014; pp 259–294.

(29) Knauth, P.; Tuller, H. L. Solid-State Ionics: Roots, Status, and Future Prospects. *J. Am. Ceram. Soc.* **2004**, *85* (7), 1654–1680 DOI: 10.1111/j.1151-2916.2002.tb00334.x.

(30) Mahato, N.; Banerjee, A.; Gupta, A.; Omar, S.; Balani, K. Progress in Material Selection for Solid Oxide Fuel Cell Technology: A Review. *Prog. Mater. Sci.* **2015**, *72*, 141–337 DOI: 10.1016/j.pmatsci.2015.01.001.

(31) Pasciak, G.; Prociow, K.; Mielcarek, W.; Gornicka, B.; Mazurek, B. Solid Electrolytes for Gas Sensors and Fuel Cells Applications. *J. Eur. Ceram. Soc.* **2001**, *21*, 1867–1870.

(32) Liu, D.; Zhu, W.; Feng, Z.; Guerfi, A.; Vijh, A.; Zaghib, K. Recent Progress in Sulfide-Based Solid Electrolytes for Li-Ion Batteries. *Mater. Sci. Eng. B Solid-State Mater. Adv. Technol.* **2016**, *213* DOI: 10.1016/j.mseb.2016.03.005.

(33) Kim, J. G.; Son, B.; Mukherjee, S.; Schuppert, N.; Bates, A.; Kwon, O.; Choi, M. J.; Chung, H. Y.; Park, S. A Review of Lithium and Non-Lithium Based Solid State Batteries. *J. Power Sources* **2015**, *282* DOI: 10.1016/j.jpowsour.2015.02.054.

(34) Matsumoto, H.; Hayashi, H.; Iwahara, H. Electrochemical Hydrogen Isotope Sensor Based on Solid Electrolytes. *J. Nucl. Sci. Technol.* **2002**, *39* (4), 367–370 DOI: 10.1080/18811248.2002.9715205.

(35) Adachi, G. Y.; Imanaka, N.; Tamura, S. Ionic Conducting Lanthanide Oxides. *Chem. Rev.* **2002**, *102* (6), 2405–2429 DOI: 10.1021/cr0103064.

(36) Imanaka, N.; Tamura, S. Development of Multivalent Ion Conducting Solid Electrolytes. *Bull. Chem. Soc. Jpn.* **2011**, *84* (4), 353–362 DOI: 10.1246/bcsj.20100178.

(37) Ghosal, G.; Mangle, E.; Topp, M.; Dunn, B.; Farrington, G. C. Preparation, Ion Transport, and Spectroscopy of Eu(II) and Eu(III) Beta´´ Alumina. *Solid State Ionics* **1983**, *9–10*, 273–276 DOI: 10.1016/0167-2738(83)90246-1.

(38) Dyer, P. N.; Richards, R. E.; Russek, S. L.; Taylor, D. M. Ion Transport Membrane Technology for Oxygen Separation and Syngas Production. *Solid State Ionics* **2000**, *134* (1–2), 21–33 DOI: 10.1016/S0167-2738(00)00710-4.

(39) Jiang, D.; Bu, X.; Sun, B.; Lin, G.; Zhao, H.; Cai, Y.; Fang, L. Experimental Study on Ceramic Membrane Technology for Onboard Oxygen Generation. *Chinese J. Aeronaut.* **2016**, *29* (4), 863–873 DOI: 10.1016/j.cja.2016.06.003.

(40) Kunugi, S.; Inaguma, Y.; Itoh, M. Electrochemical Recovery and Isotope Separation of Lithium Ion Employing Lithium Ion Conductive Perovskite-Type Oxides. *Solid State Ionics* **1999**, *122* (1–4), 35–39 DOI: 10.1016/S0167-2738(99)00073-9.

(41) Hoshino, T. Innovative Lithium Recovery Technique from Seawater by Using World-First Dialysis with a Lithium Ionic Superconductor. *Desalination* **2015**, *359*, 59–63 DOI: 10.1016/j.desal.2014.12.018.

(42) Spoerke, E.; Wheeler, J.; Ihlefeld, J.; Blea, M.; Brown-Shaklee, H.; Rodriguez, M. *Ion Selective Ceramics for Waste Separations: Performance and Design of Ion Selective Ceramic Membrane for Molten Salt Recycle*; 2014.

(43) Joshi, A. V; Steppan, J. J.; Taylor, D. M.; Elangovan, S. Solid Electrolyte Materials, Devices, and Applications. *J. Electroceramics* **2004**, *13* (1–3), 619–625 DOI: 10.1007/s10832-004-5168-x.

(44) SelectIon Technologies. “Technologies”. SelectIon Technologies official company website. www.select-ion.com/technologies.php (accessed October 1st, 2016).

(45) Sattar, S.; Ghosal, B.; Underwood, M. L.; Mertwoy, H.; Saltzberg, M. A.; Frydrych, W. S.; Rohrer, G. S.; Farrington, G. C. Synthesis of Di- and Trivalent Beta´´-aluminas by Ion Exchange. *J. Solid State Chem.* **1986**, *65*, 231–240.

(46) Farrington, G. C.; Dunn, B. Divalent Beta´´-aluminas: High Conductivity Solid Electrolytes for Divalent Cations. *Solid State Ionics* **1982**, *7*, 267–281 DOI: 10.1016/0167-2738(82)90023-6.

(47) Seevers, R.; Denuzzio, J.; Farrington, G. C. Ion Transport in Ca^{2+}, Sr^{2+}, Ba^{2+}, and Pb^{2+} Beta´´-aluminas. *J. Solid State Chem.* **1983**, *50*, 146–152 DOI: 10.1016/B978-0-12-403985-8.50018-1.

(48) Tietz, F.; Urland, W. Investigations on Lanthanide-Ion-Exchange Beta and Beta´´-alumina. *J. Alloys Compd.* **1993**, *192*, 78–80.

(49) Clearfield, A. Role of Ion Exchange in Solid-State Chemistry. *Chem. Rev.* **1988**, *88*, 125–148 DOI: 10.1021/cr00083a007.

(50) Toropov, N. A.; Stukalova, M. M.; *C. R. Acad. Sci. SSR.* **1939**, *24*, 249.

(51) Yao, Y.-F. Y.; Kummer, J. T. Ion Exchange Properties of and Rates of Ionic Diffusion in Beta-Alumina. *J. Inorg. Nucl. Chem.* **1967**, *29* (9), 2453–2475 DOI: 10.1016/0022-1902(67)80301-4.

Chapter 3: Quantification of rare earth elements in alumina matrix via laser induced breakdown spectroscopy

3.1 Disclosure

This chapter is based on the manuscript submitted to Spectrochimica Acta Part B: Atomic Spectroscopy (In Review). The full list of authors includes Kristian G. Myhre, Mihir J. Mehta, Madhavi Z. Martin, and Miting Du. The role of Kristian G. Myhre was to design and perform experiments, process and analyze data, and prepare the manuscript for submission.

3.2 Abstract

The development of laser induced breakdown spectroscopy as a technique for quantification of Eu and Sm concentrations in ceramic aluminum oxide samples was accomplished for application to studying lanthanide separation processes. Metal oxide powders of Eu and/or Sm were mixed with aluminum oxide at varying concentrations and pressed into pellets. Both univariate and multivariate linear regression methodologies were used to build calibration curves from data subsets of the laser induced breakdown spectroscopy measurements of the pellets. A comparison between the univariate and multivariate methodologies is presented. A linear behavior was seen over the total lanthanide concentration range from 0.086 to 12.358 weight percent (wt %). The calculated limits of detection for the univariate calibration curves were determined to range from 0.001 to 0.108 wt % and 0.001 and 0.183 wt % for Eu and Sm, respectively. The calculated limits of detection for the multivariate calibration curves were determined to range from 0.013 to 0.019 wt % and 0.005 to 0.015 wt % for Eu and Sm, respectively. The univariate analyses yielded slightly better figures of merit compared to the

multivariate analyses. However, multivariate analysis was much more readily implemented.

3.3 Introduction

The rare earth elements are used in many advanced science and technology applications. However, separating the rare earths from each other is extremely difficult. This is especially true for lanthanide pairs adjacent to each other on the periodic table, such as Eu and Sm [1]. As such, a great deal of research and development effort is put forth toward improving current separation methods and developing new ones. Recently, work carried out at ORNL has investigated the novel use of BDPA as a separation material for separating lanthanides from each other [2]. Several approaches to using BDPA to accomplish separations have been investigated with a common parameter of interest being the concentration of the rare earths in the BDPA material at various points in the experimental procedure.

Previously, Neutron Activation Analysis (NAA) has been used to quantitatively determine the elemental concentrations of the rare earths, such as Eu and Sm, in the BDPA matrix [2]. NAA is advantageous because it has a very high sensitivity, is not matrix dependent, and requires little to no preparation of the samples [3]. The ability to analyze samples without sample preparation is particularly useful given the chemical and physical robustness of alumina ceramics such as BDPA [4]. Many other and more common analytical techniques, such as Inductively Coupled Plasma Mass Spectrometry (ICP–MS), require difficult sample digestion steps and dilutions by several orders of

magnitude to be performed prior to analysis. However, a major drawback to NAA is that the samples become radioactive and remain so for a long period of time, given the long half–lives of many lanthanide activation products. This prevents the exact same samples from being analyzed multiple times throughout the separation process and therefore inhibits a more accurate picture of the separation process from being constructed. It also requires the use of a neutron source with a high flux, such as ORNL's High Flux Isotope Reactor, for high–sensitivity measurements, which is not a commonly available resource. It is therefore desirable to use a different technique capable of quantitatively determining the concentrations of the rare earths in BDPA that would be essentially nondestructive and applicable to the robust alumina matrix. For these reasons, Laser Induced Breakdown Spectroscopy (LIBS) was investigated for use in quantifying Eu and Sm concentrations in an alumina matrix.

LIBS is a technique capable of analyzing a wide variety of sample matrices, including physically and chemically robust ceramic matrices such as BDPA, without the need of lengthy and cumbersome sample preparation [5]. LIBS involves the formation of a plasma on the surface of the material being analyzed which then emits light representative of the elemental composition of the plasma. The plasma is formed from a small amount (few hundred nanograms) of laser–ablated material and therefore is effectively nondestructive. This technique is especially advantageous when analyzing samples that are difficult to digest, as is the case with ceramics such as high–density alumina. However, it can be difficult to obtain quantitative information from LIBS measurements for reasons including: signal interference from self–adsorption by the

sample or interaction with the surrounding atmosphere; matrix effects due to inhomogeneity in samples; and differences in plasma formation from shot to shot due to variability in the laser pulse parameters, as well as the physicochemical nature of the samples of interest [6].

A variety of methodologies have nonetheless been successfully utilized to obtain quantitative information from LIBS measurements [5–7]. The most commonly used involve the building of some form of a linear regression model using a set of standards. It is often the case that the standards used must have essentially the same matrix as the unknown samples to overcome the common issue of matrix effects. For example, a regression model for quantification of Eu and Sm concentrations in samples with a carbon matrix, as was built by Martin *et al.*, would likely not be useful for analyzing samples with an aluminum oxide matrix, despite all other parameters and instrumentation being the same [8]. Regression models measure the response values in the LIBS spectral data for standards and correlate them with known concentrations of the analytes of interest [6]. Regression models fall into two categories, namely univariate and multivariate. The former correlates one value of response in the LIBS spectral data to one value of analyte concentration. The latter correlates multiple response values in the LIBS spectral data to determine the concentration of one or more analytes. Other methodologies are under development which are calibration–free have shown promise but require a significant amount of additional work prior to widespread implementation [7].

This paper focuses on a comparison of the application of univariate and multivariate linear regression analysis methodologies to the quantification of Eu and Sm in an alumina oxide matrix.

3.4 Materials and Characterization

3.4.1 Instrumentation

LIBS measurements were performed at ORNL's Radiochemical Engineering Development Center. The measurements were taken using a LIBSCAN–150 Laser Induced Breakdown Spectrometer system from Applied Photonics Ltd., based in the United Kingdom. The laser used in the system was a passively Q–switched Nd:YAG laser (manufactured by Applied Photonics Ltd.). The mean pulse energy of the laser is 161 mJ with a standard deviation of 2.25 mJ and the output wavelength is 1064 nm. Measurements from six spectrometers were stitched together to give a wavelength measurement range of 182.27 nm to 909.37 nm. The characteristics of the LIBS system are listed in Table 3.1. The LIBSoft software package (version 16.1) from Applied Photonics Ltd was used to perform the LIBS measurements.

3.4.2 Sample preparation

The samples used as calibration standards were prepared by mixing high–purity metal oxide powders of Sm and/or Eu (purity >99.95%, Alfa Aesar) with high purity Al_2O_3 (purity >99.99%, Alfa Aesar). The lanthanide concentrations in ten single element standards containing either Eu or Sm ranged from 0.086 to 12.358 wt %. The four multi–

element standards that contained both Sm and Eu had individual lanthanide concentrations ranging from 0.860 to 5.300 wt %. After each metal oxide powder mixture was prepared, the mixtures were pressed into pellets using a manual hydraulic press with a pressure of approximately 15 ton cm^{-2}. A blank pellet of pure Al_2O_3 was prepared in addition to those containing Eu and/or Sm. The pellets formed had a diameter of 1 cm and average thickness of 2 mm. The pellets were put under pressure for approximately two minutes, and no binder was used to form the pellets. The pellets were stored in small plastic bags after being pressed prior to and after performing the LIBS measurements.

3.4.3 Acquisition of the spectral data

Spectral data were acquired at three locations on each side of the pellets for a total of six locations on each pellet. The data for each spot were acquired using ten shots of the laser. No conditioning shots were used. Inert argon gas was flowed at a constant rate prior to and throughout the LIBS measurements. The integration time used was 1.10 ms and the integration delay was 1.27 μs.

3.4.4 Selection of the emission lines for univariate analysis

Several useful emission lines were identified from a survey of the literature on LIBS measurements of Eu and Sm in conjunction with processing the spectral data produced in this study [8–11]. Many of the spectral lines noted in the literature were present in the measured spectra and found to be correctly assigned to each element. However, many of the emission lines noted in the literature had a significant amount of

noise or interference, making them undesirable for use in building univariate regression models. Three emission lines each for Eu and Sm as well as two for Al were selected for use in building the univariate regression models. This was accomplished by comparing the spectral lines found in the spectra of pure Al_2O_3, Eu_2O_3–Al_2O_3, and Sm_2O_3–Al_2O_3 pellets. The selected emission lines used to build the univariate regression models are given in Table 3.2.

3.4.5 Construction of the calibration curves

Several different approaches to constructing the calibration curves were implemented. The first two approaches both used a univariate simple linear regression (SLR) model and the background–subtracted integrated area of the respective Eu and Sm emission lines, which are listed in Table 3.2. The first approach correlated the known concentration of an analyte in a standard to the normalized value of an integrated emission line to give a response signal (S_E). The integrated area of a nearby background region was used to normalize the data [11]. It is important to note that the region used for the background in this approach should be as close to the emission line as possible and always measured by the same spectrometer. The signal (S_α) of each emission line for analyte A at wavelength α was therefore calculated by the equation

$$S_\alpha = \frac{A_\alpha - B_\beta}{B_\beta}$$

with A_α being the integral of the emission line at wavelength α and B_β the integral of the background at wavelength β [11]. The second methodology instead normalized the

integral of the emission line to a background subtracted internal standard (I), as given by the equation

$$S_\alpha = \frac{A_\alpha - B_\beta}{I_\gamma - C_\delta}$$

with C_δ being the integral of the background for the internal standard at wavelength δ [12]. Three emission lines of Eu and Sm, given in Table 3.2, were investigated using each of the two univariate approaches. The internal standard used for the second approach was either the emission line of Al at 308.205 or 309.281 nm. Thus, a set of nine calibration curves was produced for both Eu and Sm by the univariate SLR methodologies. Outlier values for the calculated S_α signal values were defined as being more than 1.5 interquartile ranges above or below the first and third quartiles, respectively. The outliers were removed from the data subsequent to identification and were not used to build the calibration curves. The integrals of the emission lines and background areas were calculated using the PLASUS SpecLine software package (version 2.1). The data were then exported into Microsoft Excel for graphing and linear fitting.

The third approach was to build multivariate regression models using partial least square (PLS) regression analysis, which is the most commonly used chemometric technique to determine concentrations from LIBS measurements [6]. PLS regression analysis correlates one or more dependent variables (i.e., concentrations) to two or more independent variables (i.e., spectral data). The PLS–1 algorithm is used for single element concentrations, whereas the PLS–2 algorithm is used for calculating the concentrations of multiple elements from the same set of data. The Unscrambler® X

(version 10.4) software package made by CAMO Software was used to perform the PLS regression analysis. Both untreated and pretreated LIBS data were used to construct the multivariate regression models. No pretreatment of the data was carried out prior to PLS regression analysis. Single element calibration curves were constructed using the PLS–1 algorithm on the single element standards. Multi–element calibration curves were constructed using the PLS–2 algorithm on both the single and multi–element standards. Outliers were identified and removed from the analysis routine. In total, four models and six calibration curves were constructed using multivariate PLS regression analysis. The first model was constructed using the LIBS spectral data from the Eu_2O_3–Al_2O_3 single element standards. The second model used the Sm_2O_3–Al_2O_3 single element standards. The third model used the Al_2O_3 and Eu_2O_3–Al_2O_3 multi–element standards, and the fourth model used all of the standards.

3.5 Results and Discussion

3.5.1 Selection of emission lines for univariate analysis

Full range spectra representative of those collected throughout this study are presented in Figure 3.1. The four spectra shown in Figure 3.1 are for pure Al_2O_3 as well as Al_2O_3 mixed with Eu_2O_3 and/or Sm_2O_3. It can be seen that LIBS measurements of samples containing both Eu and Sm produce more complex spectra compared to the pure Al_2O_3 and single analyte (Eu or Sm) mixtures. As has been noted elsewhere by Martin *et al.*, LIBS measurements of rare earth mixtures can yield dense and often overlapping emission lines [8]. This can cause difficulties in selecting emission lines for use in

univariate analysis routines, which quickly becomes a tedious task. Regardless, the spectra shown in Figure 3.1 were plotted together and used to identify emission lines without overlap for use in building the univariate SLR analysis models. Three emission lines were found for Eu and Sm, as well as two for Al. The selected emission lines are given in Table 3.2. Previous work by others in quantifying Eu and Sm did not use several of the emission lines identified in this study [8–11]. Differences in instrumentation and the sample matrix could have led to different lines being identified and useful for quantification. Certain emission lines can be either absent or present due to differences in self–adsorption effects when comparing samples with different matrices.

3.5.2 Calibration curves from univariate analysis

Nine different calibration curves were built using univariate SLR analysis for Eu and Sm in the single element and multi–element Al_2O_3 samples. Thus, thirty–six calibration curves were built in total using univariate methodologies. Figure 3.2 shows graphs of the univariate calibration curves with the highest values of the coefficient of determination (R^2) from each set of nine. Tables 3.3 and 3.4 list the figures of merit for each of the univariate SLR calibration curves that were built. The figures of merit used were the R^2 value as well as the root mean square error (RMSE) and limit of detection (LOD), both in units of analyte wt % of the total sample mass. The LOD was calculated using the equation

$$\text{LOD} = \frac{3\sigma_\alpha}{\text{b}}$$

with σ_α being the standard deviation at wavelength α and b being the slope of the calibration curve equation [6]. The first two calibration curves in Figure 3.2 were built from the LIBS measurements of single element standards containing only one of the lanthanides, either Eu or Sm, in an Al_2O_3 matrix. The second two calibration curves were built from the LIBS measurements of standards containing both Eu and Sm in an Al_2O_3 matrix. Ten different concentrations of the lanthanides ranging from 0.086 to 12.360 wt % were used for the single element standards. Four different concentrations of the lanthanides ranging from 0.860 to 5.300 wt % were used for the multi–element standards.

The calibration curves built from the multi–element standards have unsurprisingly better statistics with the average figures of merit being higher in all three categories. The multi–element standards, which were fewer in number, were in the concentration region of best (most linear) response resulting in lower percent errors and closer linear fits to the measured data. Indeed, calibration curves built from the single element standards using the same four concentrations as the multi–element standards yielded slightly improved figures of merit. One source of error that causes this difference is the interferences inherent with having an increasing number of elements present in the samples. The overlap of peaks is a particular issue when analyzing samples with a large variety of elements. The lanthanide series has a particularly large number of peaks that overlap. However, careful selection of the emission lines as described earlier was able to largely overcome these issues and maintain high figures of merit for the calibration curves built

from multi–element standards. A second source of interference aside from overlapping peaks is an increase in the background, as shown in Figure 3.1.

It can be seen from Tables 3.3 and 3.4 that normalizing the measured LIBS data to a nearby background region generally results in a poorer calibration compared to normalizing to either of the Al emission lines. Additionally, normalization to the Al 308.205 nm emission line on average resulted in slightly higher quality calibrations than normalization to the Al 309.281 nm emission line. The best emission lines to use for building a univariate calibration curve for Eu and Sm appear to be 390.693 nm and 474.556 nm, respectively. This designation is based upon a consideration of all three figures of merit.

3.5.3 Calibration curves from multivariate analysis

Six calibration curves were built in total using multivariate PLS regression analysis to quantify Eu and Sm concentrations in an Al_2O_3 matrix. The six calibration curves, shown in Figure 3.3, consisted of: Eu from the Eu_2O_3–Al_2O_3 single element standards; Sm from the Sm_2O_3–Al_2O_3 single element standards; Sm from the Al_2O_3 and Eu_2O_3–Sm_2O_3–Al_2O_3 multi–element standards; Eu from the Al_2O_3 and Eu_2O_3–Sm_2O_3–Al_2O_3 multi–element standards; Sm from all of the standards; and Eu from all of the standards. Figure 3.4 shows graphs of the percentage of explained variance as a function of the number of principal components (PCs) in the multivariate model. Convention is that fewer PCs are better, and more than ten is likely integrating undesirable noise into the model. The optimized number of PCs determined by the analysis software ranged

from 3 to 5 for the multivariate models produced in this work. High R^2 values were obtained for the calibration curves from multivariate analysis, with the lowest being 0.9083 for Eu from all of the standards. Table 3.5 lists the figures of merit for each of the multivariate PLS calibration curves that were built.

3.6 Conclusion

Univariate and multivariate methodologies for building linear calibration curves from LIBS measurements were applied for quantifying the concentrations of Eu and Sm in an Al_2O_3 matrix. Univariate calibration curves were built in two ways. The first was to normalize the background–subtracted integrated emission line to a nearby background region. The second was to normalize the background–subtracted integrated emission line to one of two background–subtracted integrated aluminum emission lines. It was found that normalizing to one of the aluminum emission lines yielded high–quality calibration curves, as evidenced by higher R^2 values, as well as lower RMSE and LOD values. Additionally, the univariate calibration curves were built using two different types of datasets, specifically single element standards and multi–element standards. The single element standards were either Eu or Sm in Al_2O_3. The multi–element standards were both Eu and Sm in Al_2O_3. The multi–element standards yielded higher–quality calibration curves compared to those built from the single element standards. This is largely due to the concentration ranges used to build the calibration curves. The single element standards spanned a larger concentration range than the multi–element standards. Calibration curves were also built using multivariate PLS regression analysis. Three

different types of datasets were used; single element standards, multi–element standards, and all of the standards. The presence of both Eu and Sm complicated the analysis, as evidenced by the generally worse figures of merit for the multivariate calibration curves built from LIBS measurements of all of the standards. The best figures of merit for both univariate and multivariate analysis were very close together, with the univariate analysis yielding slightly better figures of merit. However, multivariate analysis was significantly easier to implement compared to univariate analysis. Given the similar figures of merit and ease of implementation, multivariate SLR analysis was used throughout the remainder of the studies described herein to determine the concentrations of Eu and Sm in alumina samples by LIBS.

3.7 Acknowledgements

Research sponsored by the Laboratory Directed Research and Development Program at Oak Ridge National Laboratory, managed by UT–Battelle, LLC, for the U.S. Department of Energy. This manuscript has been authored by UT–Battelle, LLC under Contract No. DE–AC05–00OR22725 with the U.S. Department of Energy. The United States Government retains and the publisher, by accepting the article for publication, acknowledges that the United States Government retains a non–exclusive, paid–up, irrevocable, world–wide license to publish or reproduce the published form of this manuscript, or allow others to do so, for United States Government purposes. The Department of Energy will provide public access to these results of federally sponsored

research in accordance with the DOE Public Access Plan (http://energy.gov/downloads/doe–public–access–plan).

3.8 References

(1) Xie, F., Zhang, T. A., Dreisinger, D., Doyle, F. (2014). A critical review on solvent extraction of rare earths from aqueous solutions. Minerals Engineering, 56, 10–28. http://doi.org/10.1016/j.mineng.2013.10.021.

(2) Myhre, K. G., Du, M. (2015). Development of a Novel Lanthanide and Actinide Separation Method Utilizing Solid Electrolytes. 2015 International Chemical Congress of Pacific Basin Societies. Honolulu, Hawaii, United States.

(3) Blaauw, M. (1993). The Holistic Analysis of Gamma–ray Spectra in Instrumental Neutron Activation Analysis. Interfacultair Reactor Instituut van de Technische Universiteit, Delft.

(4) Ćurković, L., Jelača, M. F., Kurajica, S. (2008). Corrosion behavior of alumina ceramics in aqueous HCl and H2SO4 solutions. Corrosion Science, 50(3), 872–878. http://doi.org/10.1016/j.corsci.2007.10.008.

(5) R. Noll. Laser–induced Breakdown Spectroscopy, Springer, 2012.

(6) El Haddad, J., Canioni, L., Bousquet, B. (2014). Good practices in LIBS analysis: Review and advices. Spectrochimica Acta – Part B Atomic Spectroscopy, 101, 171–182. http://doi.org/10.1016/j.sab.2014.08.039.

(7) Tognoni, E., Cristoforetti, G., Legnaioli, S., Palleschi, V. (2010). Calibration–Free Laser–Induced Breakdown Spectroscopy: State of the art. Spectrochimica Acta – Part B Atomic Spectroscopy, 65, 1–14. http://doi.org/10.1016/j.sab.2009.11.006.

(8) Martin, M., Martin, R. C., Allman, S., Brice, D., Wymore, A., Andre, N. (2015). Quantification of rare earth elements using laser–induced breakdown spectroscopy. Spectrochimica Acta – Part B Atomic Spectroscopy, 114, 65–73. http://doi.org/10.1016/j.sab.2015.10.005.

(9) Weisberg, A., Lakis, R. E., Simpson, M. F., Horowitz, L., Craparo, J. (2014). Measuring Lanthanide Concentrations in Molten Salt Using Laser–Induced Breakdown Spectroscopy (LIBS). Applied Spectroscopy, 68(9), 937–948. http://doi.org/10.1366/13–07390.

(10) Devangad, P., Unnikrishnan, V. K., Nayak, R., Tamboli, M. M., Muhammed Shameem, K. M., Santhosh, C., Kumar, G. A., Sardar, D. K. (2016). Performance evaluation of Laser Induced Breakdown Spectroscopy (LIBS) for quantitative analysis of rare earth elements in phosphate glasses. Optical Materials, 52, 32–37. http://doi.org/10.1016/j.optmat.2015.12.001.

(11) Alamelu, D., Sarkar, A., Aggarwal, S. K. (2008). Laser–induced breakdown spectroscopy for simultaneous determination of Sm, Eu and Gd in aqueous solution. Talanta, 77, 256–261. http://doi.org/10.1016/j.talanta.2008.06.021.

(12) Sanghapi, H. K., Jain, J., Bol'shakov, A., Lopano, C., McIntyre, D., Russo, R. (2016). Determination of elemental composition of shale rocks by laser induced breakdown spectroscopy. Spectrochimica Acta Part B: Atomic Spectroscopy, 122, 9–14. http://doi.org/10.1016/j.sab.2016.05.011.

Chapter 4: Oxidation state behavior of Eu and Sm in beta´´–alumina by X–ray photoelectron spectroscopy

4.1 Disclosure

This chapter is based on two manuscripts with slight revisions added for coherence. The first manuscript has been submitted to Surface Science Spectra (Accepted). The full list of authors includes Kristian G. Myhre, Harry M. Meyer III, and Miting Du. The role of Kristian G. Myhre was to design and perform all experiments, process and analyze all data, and prepare the manuscript for submission. The second manuscript is in preparation for submission to a journal. The full list of authors includes Kristian G. Myhre and Miting Du. The role of Kristian G. Myhre was to design and perform all experiments, process and analyze all data, and prepare the manuscript for submission.

4.2 Abstract

The oxidation state behavior of Eu and Sm in BDPA after high temperature ion exchange reactions was studied using XPS. Derivatives of BDPA containing were synthesized to contain various mixtures of Eu and Sm using high temperature ion exchange reactions under various atmospheric conditions (air, argon, and vacuum) between $LnCl_3$ salts and Na–BDPA. The ratio of Eu to Sm was varied with ratios of Eu to Sm ranging from 1:0, 3:1, 1:1, 1:3, and 0:1. It was found that Eu^{3+} was selectively reduced to Eu^{2+} during the ion exchange reaction of $LnCl_3$ salts with Na–BDPA. The reduction of Eu to its divalent state was found to be dependent upon the ratio of Eu to Sm. It was also found to depend upon the atmosphere conditions of the ion exchange

reaction. The Sm in both pure Sm and mixed Ln BDPA samples was measured to remain Sm^{3+}.

4.3 Introduction

BDPA has been widely studied as a solid electrolyte to conduct Na^{+} ions in sodium sulfur batteries of interest for use in large–scale energy storage settings [1]. Numerous other applications of BDPA derivatives containing various ions have been investigated. These include as ion selective electrode materials for pyroprocessing safeguards and optical materials for lasers technologies [2-4]. Recently, BDPA has been investigated at ORNL as an ion exchange material for use in separating Eu and Sm from each other [5].

An important aspect of the separation process is the oxidation state behavior of Eu and Sm in the BDPA material throughout the separation (see Chapter 5 and Chapter 6). Depending upon the oxidation states of Eu and Sm in the BDPA, either Eu or Sm will be preferentially extracted from the BDPA using a molten salt, such as NaCl. The difference in conductivities between Ln^{2+} and Ln^{3+} species in BDPA can be utilized to selectively extract the more conductive Ln^{2+} species. For instance, Eu^{2+} has a conductivity value in BDPA four orders of magnitude greater than Eu^{3+} [6]. In the case of separating Eu from Sm using this approach, Eu is reduced and stabilized to Eu^{2+} in BDPA while Sm remains Sm^{3+}. An ion exchange reaction between a molten salt, such as NaCl, and the Eu^{2+}/Sm^{3+}–BDPA material could therefore involve the selective extraction of Eu^{2+} out of the BDPA

material given that the higher mobility should lead to faster ion exchange kinetics with the Na^{+}.

The synthesis of Eu–BDPA containing both $Eu^{2+}$and Eu^{3+} have been reported in the literature previously [6-10]. Those studies predominately relied upon the luminescent properties of the Eu/Sm–BDPA to show the presence of $Eu^{2+}$and/or Eu^{3+} in BDPA. Mössbauer spectroscopy utilizing the 21.6 keV transition of ^{151}Eu (47.81% natural isotopic abundance) has also been used [10]. A noted difficulty was the determination of the Eu^{2+} to Eu^{3+} ratio. Comparison between studies is further complicated given the noted dependence of the Eu^{2+} to Eu^{3+} ratio on the processing history. It has been observed the thermal history and exposure to moisture can both effect the structural properties of BDPA derivatives [11]. XPS measurements have been utilized to answer some of the questions regarding the oxidation state behavior of Eu in the BDPA structure. A discussion on the dependence of the reduction of Eu on total Ln concentration and atmospheric conditions during ion exchange of Eu and Sm into BDPA containing Na is presented.

4.4 Materials and Characterization

4.4.1 Sample Preparation

$EuCl_3$ (anhydrous, 99.99%) and $SmCl_3$ (anhydrous, 99.9%) were purchased from Alfa Aesar. $EuCl_3$ hydrate (REacton, 99.9% REO) and $SmCl_3$ hydrate (REacton, 99.9% REO) were purchased from Alfa Aesar. NH_4Cl (analytical reagent) was purchased from Mallinckrodt. Mixtures of the $LnCl_3$ were produced by mixing the appropriate amounts

of the anhydrous or hydrated chlorides with an agate mortar and pestle. The hydrated chlorides were then mixed with a large molar excess of NH_4Cl with an agate mortar and pestle. Na–BDPA was purchased as large pieces from Ionotec Ltd. The larges pieces were subsequently cut into smaller pieces with dimensions of about 2 mm x 2 mm x 1 mm using diamond tooling. The Na–BDPA pieces were buried in an excess of the mixed lanthanide chloride powders inside of high–purity quartz ampoules. Some of the samples were sealed under high vacuum to achieve an oxygen depleted atmosphere with reduced pressure. The other samples were in open quartz ampoules and reacted with either static air or flowing argon gas at pressure nominally ambient. All of the samples were heated for 24 hours at 650 °C in a large crucible furnace to achieve the synthesis by ion exchange of the lanthanide BDPA derivatives, as described previously in the literature. The only exception is that the hydrated $EuCl_3$–$SmCl_3$ mixture with an excess amount of NH_4Cl was heated to 700 °C under an argon atmosphere. After the samples were heated for 24 hours, the residual $EuCl_3$–$SmCl_3$ was removed using a small amount of water. Each sample was then patted dry with a Kimwipe and mounted on a glass slide using an adhesive strip for XPS analysis.

4.4.2 X–ray photoelectron spectroscopy

The XPS measurements of the Eu– and/or Sm–BDPA samples were taken using a Thermo Scientific K–Alpha system operated in constant energy analyzer mode. The XPS instrument has a double–focusing hemispherical analyzer and position sensitive detector with 128 detector elements. The excitation source was a water–cooled aluminum–coated

anode. The source energy was 1486.68 eV and strength was 72 W. The beam size was 400 × 400 μm and the analyzer width was 60 × 60 mm. Survey scans were taken to identify the elements present in the samples. Subsequently, narrow region scans were taken to obtain higher resolution data on the peaks of interest. The samples were not charging, and no energy scale correction was needed. The binding energies measured by the spectrometers were calibrated using the Au $4f_{7/2}$ peak at 83.9 eV, Ag $3d_{5/2}$ peak at 368.2 eV and Cu $2p_{3/2}$ peak at 932.6 eV. Thermo Avantage software version 4.61 was used to carry out the background subtraction as well as the determinations of peak positions and FWHM values. The atomic concentrations were calculated using the Al Scofield sensitivity factors in the Thermo Avantage software version 4.61. The major peaks of interest used in this study to determine the oxidation states of Eu and Sm were in the 3d regions of Eu and Sm (highlighted in Figure 4.1). Specifically, the Eu $3d_{5/2}$ emission lines at 1126.3 eV and 1136.3 eV were used to quantify the amount of Eu^{2+} and Eu^{3+}, respectively [12, 13]. The Sm^{3+} $3d_{3/2}$ and $3d_{5/2}$ emission lines at 1111.9 eV and 1084.5 eV, respectively, were present in all spectra [14, 15]. No evidence of Sm^{2+} of was observed.

4.5 Results and Discussion

Carrillo–Cabrera *et al.* proposed a mechanism for the reduction of $Eu^{3+}$to Eu^{2+} in the BDPA structure, which is comprised of alternating layers of Al_2O_3 spinel layers and conduction planes containing oxygen and mobile cations, such as Eu and Sm [6]. The first step is for oxygen to be removed from the conduction plane in the BDPA structure

containing Eu^{3+}. The removal of the oxygen is proposed to leave behind two electrons trapped in the oxygen vacancy. The second step is for two Eu^{3+}atoms to be reduced to Eu^{2+} by electron trapping. Finally, the leftover oxygen vacancy moves into the spinel block of the BDPA structure. If this is the mechanism, it is reasonable to assume that the presence and partial pressure of oxygen should effect the reduction of Eu. It is therefore logical that a lower oxygen pressure in the atmosphere surrounding the BDPA would favor the reduction of Eu^{3+} to Eu^{2+} within the BDPA structure. The preparation of Eu/Sm–BDPA samples under various atmospheric conditions was carried out to elucidate the effect of oxygen and pressure on the reduction of Eu^{3+} to Eu^{2+}. The spectra collected from XPS measurements of Eu/Sm–BDPA samples prepared under various atmospheric conditions from anhydrous $EuCl_3$–$SmCl_3$ mixtures with a Eu to Sm ratio of about 1:1 are given in Figure 4.2 (Eu 3d region spectra). The XPS spectra in the Eu 3d region of a Eu/Sm–BDPA sample prepared from the reaction of Na–BDPA and a $EuCl_3$–$SmCl_3$ [50:50] hydrate mixture with an excess of NH_4Cl at 700 °C for 24 hours under an argon atmosphere is also given in Figure 4.2. The corresponding Sm 3d region spectra are given in Figure 4.3.

All four spectra of Figure 4.2 show evidence of both Eu^{2+} and Eu^{3+}. The percentages of Eu present as Eu^{2+} in the samples prepared under air and argon were both about 12%. The only difference between the two samples is that one was prepared with oxygen present and the other without (both at or near to ambient pressure). A much higher Eu^{2+} content of 32% was measured in the Eu/Sm–BDPA sample prepared under vacuum. It is therefore evident that the reduction of Eu^{3+} to Eu^{2+} during the ion exchange

reaction depends upon the presence of oxygen and the overall pressure of the surrounding atmosphere. This correlates well with previous work on the preparation of Eu^{2+}–BDPA and Eu^{3+}–BDPA materials with 100% of the Eu in one oxidation state. To synthesize pure Eu^{3+}–BDPA, a chlorine gas atmosphere was required to prevent the reduction of Eu^{3+} in the chloride and/or BDPA [7]. Previous work has studied the decomposition of $EuCl_3$ to $EuCl_2$ in alkali chloride molten salts with chloride ions acting as the oxidant [16, 17]. At the same time, the reduction of Eu^{3+} to Eu^{2+} in Eu–BDPA samples using thermal treatment under vacuum has also been described [6-8]. Given the results from this work, the reduction of Eu^{3+} to Eu^{2+} in both the chloride phase and BDPA phase is likely for the samples prepared under vacuum.

It was also of interest to study the dependence of the reduction of Eu^{3+} to Eu^{2+} on the percent of Eu in the total Ln content. This is important for application to separations since the percentage of Eu in the total amount of Ln will vary both in the raw materials and during processing if multiple separation stages are used. In order to understand this dependence, ion exchange reactions between Na–BDPA and $EuCl_3$–$SmCl_3$ mixtures were carried out with varying amounts of Eu and Sm (1:0, 3:1, 1:1, 1:3, and 0:1). Figure 4.4 is a graph of the percent Eu^{2+} out of the total Eu^{3+} content as a function of the percent Eu out of the total Ln content (sum of Eu and Sm). Figure 4.5 is a graph of the percent Eu^{2+} out of the total Ln content as a function of the percent Eu out of total Ln content. The results from XPS measurements of Eu/Sm–BDPA samples prepared through ion exchange reactions in both air and argon atmospheres are presented in Figure 4.4 and Figure 4.5.

Figure 4.4 shows that the amount of Eu^{2+} relative to Eu^{3+} increases as the Eu concentration decreases relative to the total Ln concentration, which is a sum of Eu and Sm. At the same time, it can be seen in Figure 4.5 that the percentage of Eu^{2+} does not appear to increase at all relative to the total Ln concentration. In other words, while the amount of total Eu in the sample decreases, the amount of Eu^{2+} in the sample does not decrease.

4.6 Conclusion

Derivatives of BDPA containing Eu and/or Sm at ratios ranging from 1:0, 33:1, 1:1, 1:3, and 0:1 were prepared through high–temperature ion exchange reactions with $LnCl_3$ salts. XPS measurements of the samples were carried out to understand the oxidation state behavior of Eu and Sm in BDPA as a function of several ion exchange reaction conditions. It was found that Eu was reduced from Eu^{3+} to Eu^{2+} in all instances, albeit to varying degrees. Ion exchange reactions in air and argon atmospheres at ambient pressures resulted in the same percentage of Eu as Eu^{2+}, which was 12%. The percentage of Eu present as Eu^{2+} was increased to 32% with all reaction conditions the same except for the sample being sealed under high vacuum in a quartz ampoule. It was therefore determined that both the presence of oxygen and partial pressure of oxygen play a key role in the reduction of Eu during ion exchange reactions of $LnCl_3$ salts and Na–BDPA. The percentage of Eu present as Eu^{2+} was found to increase as the ratio of Eu to Sm decreased in the starting chloride salts. However, the percentage of Eu^{2+} out of the total Ln content was found to be stable. The total Ln content loaded into the BDPA samples

varied only slightly 6 wt %. These trends were found to be true for ion exchange reactions carried out in both ambient air and high vacuum atmospheric conditions, with the latter yielding higher percentages of Eu^{2+} in the final Eu/Sm–BDPA material. It is still unclear as to whether the reduction of Eu^{3+} to Eu^{2+} occurs in the chloride phase, BDPA phase, or a combination of thereof. It is likely that the Eu is reduced in the chloride phase for the samples prepared in argon and air atmospheres. A combination of the Eu being reduced in the chloride phase and BDPA phase is expected for the samples prepared under vacuum.

4.7 Acknowledgments

The authors thank Jason Craig for sealing samples in quartz tubes and Randy Parten for cutting and grinding various samples. Research sponsored by the Laboratory Directed Research and Development Program at Oak Ridge National Laboratory, managed by UT–Battelle, LLC, for the U.S. Department of Energy. This manuscript has been authored by UT–Battelle, LLC under Contract No. DE–AC05–00OR22725 with the U.S. Department of Energy. The United States Government retains and the publisher, by accepting the article for publication, acknowledges that the United States Government retains a non–exclusive, paid–up, irrevocable, world–wide license to publish or reproduce the published form of this manuscript, or allow others to do so, for United States Government purposes. The Department of Energy will provide public access to these results of federally sponsored research in accordance with the DOE Public Access Plan (http://energy.gov/downloads/doe–public–access–plan).

4.8 References

(1) Wen, Z.; Cao, J.; Gu, Z.; Xu, X.; Zhang, F.; Lin, Z. Research on Sodium Sulfur Battery for Energy Storage. *Solid State Ionics* **2008**, *179* (27–32), 1697–1701 DOI: 10.1016/j.ssi.2008.01.070.

(2) Gese, N. J.; Jue, J.-F.; Serrano, B. E.; Fredrickson, G. L.; Potentiometric Sensor for Real-Time Remote Surveillance of Actinides in Molten Salts. *INL/CON-12-24475*. Idaho National Laboratory Technical Report, **2012**.

(3) Zink, P. A.; Jue, J.; Serrano, B. E.; Fredrickson, G. L.; Cowan, B. F.; Herrmann, S. D.; Li, S. X.; Potentiometric Sensor for Real-Time Monitoring of Multivalent Ion Concentrations in Molten Salt. *INL/CON-10-17752*. Idaho National Laboratory Technical Report, **2010**.

(4) Dunn, B.; Thomas, J. O.; Farrington, G. C. Beta′′ Alumina: A Solid Electrolyte as a Solid-State Laser Host. In *Spectroscopy of Solid-State Laser-Type Materials*; Di Bartolo, B., Ed.; Springer US: Boston, MA, 1987; pp 467–474.

(5) Myhre, K. G., Du, M. (2015). Development of a Novel Lanthanide and Actinide Separation Method Utilizing Solid Electrolytes. 2015 International Chemical Congress of Pacific Basin Societies. Honolulu, Hawaii, United States.

(6) Carrillo-Cabrera, W.; Thomas, J. O.; Farrington, G. C. The Eu^{3+} Eu^{2+} Reduction Process in Eu^{3+} Beta′′-alumina. *Solid State Ionics* **1986**, *19*, 645–652.

(7) Sattar, S.; Ghosal, B.; Underwood, M. L.; Mertwoy, H.; Saltzberg, M. A.; Frydrych, W. S.; Rohrer, G. S.; Farrington, G. C. Synthesis of Di- and Trivalent Beta′′-aluminas by Ion Exchange. *J. Solid State Chem.* **1986**, *65*, 231–240.

(8) Wen, Z.-Y.; Lin, Z.-X.; Tian, S.-B. Preparation and Ionic Conduction Property of Polycrystalline Eu^{2+} Beta′′-alumina. *Solid State Ionics* **1990**, *40/41*, 91–94.

(9) Saltzberg, M. A.; Farrington, G. C. Eu-O Bonding and Spectroscopy in Beta′′-alumina. *J. Solid State Chem.* **1989**, *83*, 272–281.

(10) Saltzberg, M. A.; Thomas, J. O.; Wappling, R. Mossbauer Spectroscopy Studies of the Reduction of Eu(III) in Beta′′-alumina. *Solid State Ionics* **1988**, *28–30*, 1563–1566.

(11) Rohrer, G. S.; Farrington, G. C. The Reactivity of Selected Divalent Beta′′-aluminas with Water. *Mat. Res. Bull.* **1988**, *23*, 1747–1755.

(12) Taheri, M.; Konuma, M.; Razavi, F. S. X-Ray Photoemission Spectroscopy Investigation of Ce_{1-X} Eu_XCrO_3 Nano-Powders. *Surf. Interface Anal.* **2016** DOI: 10.1002/sia.6069.

(13) Vercaemst, R.; Poelman, D.; Fiermans, L.; Van Meirhaeghe, R. L.; Laflere, W. H.; Cardon, F. A Detailed XPS Study of the Rare Earth Compounds EuS and EuF_3. *J. Electron Spectros. Relat. Phenomena* **1995**, *74* (1), 45–56 DOI: 10.1016/0368-2048(95)02349-6.

(14) Yan, Y.; Li, K.; Dai, Y.; Chen, X.; Zhao, J.; Yang, Y.; Lee, J. M. Synthesis of 3D Mesoporous Samarium Oxide Hydrangea Microspheres for Enzyme-Free Sensor of Hydrogen Peroxide. *Electrochim. Acta* **2016**, *208*, 231–237 DOI: 10.1016/j.electacta.2016.05.037.

(15) Kumbhar, V. S.; Lokhande, A. C.; Gaikwad, N. S.; Lokhande, C. D. One-Step Chemical Synthesis of Samarium Telluride Thin Films and Their Supercapacitive Properties. *Chem. Phys. Lett.* **2016**, *645*, 112–117 DOI: 10.1016/j.cplett.2015.12.042.

(16) Kim, T. J.; Jeong, Y. K.; Kang, J. G.; Jung, Y.; Ahn, D. H.; Lee, H. S. In Situ Analysis for Spontaneous Reduction of Eu^{3+} in LiCl Pyroprocessing Media at 923 K. *J. Radioanal. Nucl. Chem.* **2010**, *286* (1), 283–286 DOI: 10.1007/s10967-010-0651-0.

(17) Park, Y.J.; Kim, T. J.; Cho, Y. H.; Jung, Y. J.; Im, H. J.; Song, K. S.; Jee, K. Y.; EPR investigation on a quantitative analysis of Eu(II) and Eu(III) in LiCl/KCl eutectic molten salt. *Bull Korean Chem Soc*. **2008,** *29*, 127–129

Chapter 5: Separation of Eu and Sm by ion exchange reactions between molten salts and beta´´–alumina

5.1 Disclosure

This chapter is based on two manuscripts with slight revisions added for coherence. The first manuscript is in approval process for submission to a journal (in the ORNL Publication Tracking System). The full list of authors includes Kristian G. Myhre, Justin R. Knowles, and Miting Du. The role of Kristian G. Myhre was to design and perform all experiments, process and analyze all data, and prepare the manuscript for submission. The second manuscript is in preparation for submission to a journal. The full list of authors includes Kristian G. Myhre, Mihir J. Mehta, and Miting Du. The role of Kristian G. Myhre was to design and perform all experiments, process and analyze all data, and prepare the manuscript for submission.

5.2 Abstract

Separations of Eu and Sm were accomplished using ion exchange reactions between molten chloride salts and the solid electrolyte BDPA. Ion exchange reactions involving the extraction of Eu and Sm both into and out of BDPA were investigated. Different exchange salts, atmospheres, and reaction times were investigated. Although separations of Eu and Sm were accomplished through ion exchange reactions of Eu and Sm into BDPA, the more effective separations were achieved through ion exchange reactions that either selectively extracted Eu or Sm out of BDPA. In particular, 38% of the original Eu content in a sample of BDPA loaded with Eu and Sm with a high percentage of Eu as Eu^{2+} was extracted without any detectable Sm.

5.3 Introduction

The rare earth elements are critical for many applications due to their unique physicochemical properties; the energy, medical, security, and electronics industries rely upon them [1-6]. A few examples of their widespread use include Eu in phosphors for electronics and anti–counterfeiting of banknotes, Nd and Sm in magnets for electronics, and Y in solid–state laser crystals [2]. An important aspect of using the rare earths is the elemental purity. Miniscule impurities can drastically alter the properties of materials, as is exemplified by rare earth impurities in Nd magnets. The capability to produce purified rare earths is founded upon the effectiveness of the separation technologies used.

The separation of the lanthanides from each other is an extremely difficult task due to their similar physicochemical properties, such as preferred valence state and size [3-5]. This is especially true for the rare earth elements that are adjacent to each other on the Periodic Table, such as Eu and Sm. The current methods used industrially to separate the rare earths from each other fall into the category of solvent extraction [3-5]. Simply, solvent extraction achieves separations based upon differences in the partition coefficients of the rare earths between multiple liquid phases. In almost all cases, the solvent extraction process involves several stages. Additionally, it is very often necessary for certain rare earth pairs to be further purified using auxiliary methods. This is the case with Eu and Sm, which are further separated from each other involving a selective reduction step using a zinc amalgam [3-5]. The typical solvent extraction process results in the side production of large volumes of chemically complex organic and aqueous liquid waste that is difficult and expensive to dispose of. Needless to say, it is highly

desirable from multiple viewpoints, such as cost of production and environmental management, that more effective and efficient separation technologies be developed.

A novel approach to accomplishing separations of the lanthanides using solid electrolytes has been explored. This approach involves ion exchange reactions between BDPA and molten chloride salts. Results from a variety of ion exchange reactions are presented. Additionally, a theoretical explanation of the separation results from the ion exchange reactions is presented.

5.4 Materials and Characterization

5.4.1 Materials and Equipment

$EuCl_3$ (anhydrous, 99.99%) and $SmCl_3$ (anhydrous, 99.9%) were purchased from Alfa Aesar. $EuCl_3$ hydrate (REacton, 99.9% REO) and $SmCl_3$ hydrate (REacton, 99.9% REO) were purchased from Alfa Aesar. Calcium chloride ($CaCl_2$, anhydrous, >97%) and sodium chloride (NaCl, anhydrous, >99%) were purchased from Sigma–Aldrich. NH_4Cl (analytical reagent) was purchased from Mallinckrodt. Mixtures of the salts were produced by grinding the salts together using a mortar and pestle. Na–BDPA (70 mm x 70 mm x 2 mm) was purchased as large pieces from Ionotec Ltd. The Na–BDPA used was magnesium stabilized and produced as a dense polycrystalline ceramic using electrophoretic deposition techniques. The Na–BDPA was cut into smaller pieces with average dimensions of about 2 mm x 2 mm x 1 mm using diamond tooling.

The furnace used to heat the samples was a CV11 series crucible furnace purchased from the Mellen Company. The furnace is capable of reaching 1100 ˚C. Each

reaction was carried out in a high–purity quartz tube. The reactions under vacuum were carried out using closed quartz tubes sealed under high vacuum. The reactions under an inert argon gas atmosphere were carried out using a steady flow of argon gas into the furnace chamber.

5.4.2 Ion Exchange Reactions

Ion exchange reactions between molten salts and BDPA were carried out in quartz tubes heated inside of a high–temperature furnace. The starting material was either purchased Na–BDPA or previously exchanged BDPA loaded with Eu and Sm. For each ion exchange reaction, the BDPA ceramic piece was buried completely within the exchange salt.

5.4.3 Oxidation State Determination

XPS was utilized to determine the oxidation states of Eu and Sm in the BDPA samples. The XPS measurements were taken using the same set up and methodology described earlier in Chapter 4. Large survey scans were taken to identify the elements present in the samples. Subsequently, narrow region scans were taken to obtain higher resolution data on the peaks of interest.

5.4.4 Quantification of Eu and Sm in BDPA

LIBS measurements were taken before and after ion exchange reactions to quantify the amount of Eu and Sm in each of the BDPA samples. The data was then

analyzed using the multivariate approach previously described in Chapter 3 based on the multivariate PLS linear regression analysis model built from all of the standards in the calibration set. The RMSE values for Eu and Sm in this model were 0.010 wt % and 0.009 wt %, respectively. The LOD values for Eu and Sm in this model were 0.013 wt % and 0.005 wt %. The ratio of Eu to Sm at the surface of the samples before and after ion exchange reactions as determined LIBS analysis was compared to results from XPS. The measurements from the two techniques were found to be in fairly good agreement. It should be noted that the analysis depths for XPS and LIBS differ greatly, with XPS having an analysis depth of about 10 nm and LIBS one of about 1.8 μm (as shown earlier). The LIBS measurements resulted in obtaining four concentration profiles (one for each large side of the sample taken before and after ion exchange) per sample. An example concentration profile is shown in Figure 5.1. The average concentration values for each sample were then calculated by fitting the concentration profiles with a linear trend line. The y–intercept of each trend line equation was taken to be the average concentration in that sample. This yielded calculated values for the total Eu and Sm concentrations that were in line with previous NAA measurements of a variety of Eu/Sm–BDPA samples.

5.4.5 Separation Efficacy Evaluation

Three different types of values were calculated to evaluate the efficacy of each ion exchange reaction as a separation of Eu and Sm. Specifically, these values were the

separation factor, percentage extracted of a given species, and quotient of the distribution coefficients. The separation factor was calculated using the equation:

$$SF_A = \frac{A_f}{B_f} * \frac{B_i}{A_i}$$

where A_f and B_f are the final concentrations A_i and B_i are the initial concentrations of the two elements to be separated from each other [6]. The percentage extracted of a given species was calculated by the subtracting the quotient of the final concentration to the initial concentration from 1. Finally, the quotient of the distribution coefficients was calculated using the equation:

$$D_{ex} = \frac{\%E_A}{\%E_B} * \frac{1-\%E_B}{1-\%E_A}$$

where $\%E_A$ and $\%E_B$ are the percentage extracted of species A and B [6]. It should be noted that in the separation results presented herein, the quotient of the distribution coefficients is always put in terms of the species being extracted out of the starting material.

5.5 Results and Discussion

5.5.1 Driving forces behind ion exchange reactions

Ion exchange reactions between a solid and liquid phase were used to accomplish a separation of Eu and Sm from each other. The solid phase was BDPA and the liquid phase was a molten salt, such as $EuCl_3$–$SmCl_3$ or NaCl. The ion exchange reaction between ions in BDPA and a molten salt can be represented by

$$\overline{RM^{n+}} + A^{n+}X_n \rightleftharpoons \overline{RA^{n+}} + M^{n+}X_n$$

with R represents the BDPA framework, M^{n+} is a cation with a positive charge of n, A^{n+} is a cation with a charge of n, and X is an anion with a charge of one [7]. A large molar excess of the molten salt can be used to drive the reaction to the products side with an excess of the molten salt remaining (not shown in the above equation). In this work, ion exchange reactions involving more than two species were investigated. Specifically, the extraction of Eu and Sm into and out of BDPA under a variety of ion exchange conditions was investigated. For these ion exchange reactions, there are thermodynamic and kinetic driving forces involved to varying degrees.

The thermodynamic driving force accomplishes a separation by the fractionation of one element over another between a molten salt liquid phase and a solid BDPA phase. In this case, the reaction is thermodynamically driven since the system is given enough time to equilibrate. The fractionation occurs due to differences in the stabilities of each species between the BDPA and molten salt phases. As mentioned in Chapter 2, Yao and Kummer investigated several ion exchange reactions of monovalent cations from molten salts with Na in the beta–alumina solid electrolyte [7]. The fractionation of the two elements involved in the ion exchange reaction occurred due to the stabilities of each species between the molten salt and solid electrolyte phases. A prime example is that of K and Na ions exchanging between molten salts and beta–alumina [7]. For chloride molten salts, it was found that K favored the molten salt phase and Na the solid electrolyte phase [7]. Interestingly, the behavior was reversed when an iodide based melt was used. This behavior was reversed when the chloride melt was replaced with an iodide based molten salt.

The second type of ion exchange separation is one accomplished by utilizing differences in the diffusion coefficients of the Eu and Sm ionic species in BDPA. The driving force is therefore kinetic in nature. Previous work by Farrington *et al.* has shown the conductivity of Eu^{2+} to be four orders of magnitude higher than Eu^{3+} in single crystals of BDPA [8]. The Eu-BDPA single crystals were prepared by performing high temperature ion exchange reactions between Eu chloride salts and Na-BDPA single crystals with sizes roughly 3 mm by 2 mm by 0.3 mm in size. A molar excess of Eu was used in order to fully replace the Na content. The reactions were found to reach equilibrium, as measured using gravimetric and radiometric methods, with more than 99% of the Na content replaced with Eu after around 24 hours of heating. For the radiometric measurements, the Na-BDPA starting material was doped with the radioisotope ^{22}Na prior to the subsequent reaction with the Eu chloride salts. Although the conductivity of Sm^{3+} in BDPA does not appear to have been previously measured, it could be expected that Sm^{3+} would have a similar conductivity to Eu^{3+} given their similar physicochemical properties [2]. Therefore, Eu^{2+} should be significantly more mobile than Sm^{3+} in the BDPA structure. The difference in diffusion coefficients, which are directly related to the ionic conductivities, can then possibly be utilized to accomplish a separation through ion exchange between a cation, such as Na^{+}, in a molten salt and the Eu and Sm ionic species in Eu/Sm–BDPA. Similarly, Chapter 6 involves the separation of Eu and Sm through the selective conduction of Eu^{2+} from Sm^{3+}.

5.5.2 Separation of Eu and Sm through extraction into BDPA

Ion exchange reactions between Na–BDPA and $EuCl_3$–$SmCl_3$ [50:50] mixtures were carried out in order to prepare Eu/Sm–BDPA starting materials for subsequent ion exchange reactions to selectively extract Eu or Sm out of the BDPA structure. Two sets of conditions were used to prepare the Eu/Sm–BDPA starting materials, each resulting in different amounts of Eu^{2+} present during the loading of Eu and Sm into the BDPA samples. For both sets, however, the total lanthanide content loaded into the BDPA was measured to be about 6 wt % using LIBS. This equates to roughly 1 mg of total Ln loaded into each BDPA chip. The first batch of samples was prepared by heating several pieces of Na–BDPA with a $EuCl_3$–$SmCl_3$ [50:50] hydrate mixture and an excess amount of NH_4Cl to 700 ˚C for 24 hours under an argon atmosphere. The NH_4Cl served to dehydrate and chlorinate the $EuCl_3$–$SmCl_3$ [50:50] hydrate mixture. The second batch of samples involved a slightly more complicated preparation procedure. First, several pieces of Na–BDPA were heated to 650 ˚C for 24 hours under an argon atmosphere with a $EuCl_3$–$SmCl_3$ [50:50] hydrate mixture and an excess amount of NH_4Cl. The samples were then cleaned of residual powder on them through washing with deionized water. The Eu/Sm–BDPA samples were then heated to 900 ˚C for 16 hours under an argon atmosphere. Originally, the intent was to increase the amount of Eu^{2+} present in the Eu/Sm–BDPA samples. However, the opposite result was observed. Figure 5.2 shows the Eu 3d regions scanned using XPS of the two different starting material types. The starting material type prepared using two heating periods had a Eu^{2+} percentage out of total Eu of 12% as measured on the surface by XPS. The other starting material had a Eu^{2+}

percentage out of total Eu of 32% as measure on the surface by XPS. In both cases, the amount of Eu^{2+} increased with depth as measured by XPS after sputtering the surface with argon.

5.5.3 Separation of Eu and Sm through extraction out of BDPA

Ion exchange reactions between various molten chloride salts and Eu/Sm–BDPA were carried out to investigate the separation of Eu and Sm through selective extraction out of BDPA. The molten chloride salts investigated were pure NaCl (melting point of 801 ˚C), CsCl–NaCl [0.807:193] (melting point of 491 ˚C), and $CaCl_2$–NaCl [0.521:0.479] (melting point of 504 ˚C) [9]. The ion exchange reactions with NaCl were carried out at 815 ˚C and those for the other two salts were carried out at 550 ˚C. The time and atmospheric conditions were varied amongst the numerous separation experiments. Additionally, the two different starting Eu/Sm–BDPA materials described in the previous section were used. A major difference between the two starting Eu/Sm–BDPA materials was a higher percentage of Eu^{2+}. The results from the ion exchange reactions between the described starting materials and chloride salts are given in Tables 5.1 through 5.5. The largest D_{ex} value of 1.3×10^7 with 38% of the Eu being extracted from the Eu/Sm-BDPA starting material (high Eu^{2+} content starting) was achieved. No Sm was detected as being extracted and therefore the D_{ex} value was calculated using the Sm LOD value of 0.005 wt %. Interestingly, Sm was selectively extracted in all of the ion exchange reactions with the low Eu^{2+} content starting material. Overall, the most

effective separations were accomplished using CsCl-NaCl molten salt as the extraction salt for both the high and low Eu^{2+} content starting material.

5.5.4 Separation model

For ion exchange reactions between Na–BDPA and $EuCl_3$–$SmCl_3$ [50:50] mixtures both in air and vacuum, Eu is preferentially extracted into the BDPA structure. If we assume the Ln and Na species to be equivalent to their metal oxide forms when introduced into the BDPA structure, this outcome is to be expected from thermodynamic considerations. With the assumption that mobile ions in the BDPA structure are equivalent to their oxide forms, the enthalpies for the reactions between $EuCl_3$ and $SmCl_3$ with Na–BDPA could be estimated to be

$$2\ SmCl_3 + 3\ Na_2O \rightarrow Sm_2O_3 + 6\ NaCl \qquad -980\ kj/mol$$

$$2\ EuCl_3 + 3\ Na_2O \rightarrow Eu_2O_3 + 6\ NaCl \qquad -998\ kj/mol$$

using available thermodynamic data [10]. Therefore, Eu would be favored in the BDPA structure over Sm.

It is important to realize that the difference in stabilities of the Eu and Sm chlorides in the molten salt phase plays an important role in the ion exchange reactions. This is evidenced the differences between the ion exchange reactions presented in section 5.5.3 of CsCl-NaCl and $CaCl_2$-NaCl with Eu/Sm-BDPA. In all cases of separations with the low Eu^{2+} content Eu/Sm-BDPA, higher separation factors were achieved using CsCl-NaCl as the extractions salt. If it is assumed that the dominant species to being extracted out of the low Eu^{2+} content Eu/Sm-BDPA to be Eu^{3+} and Sm^{3+}, then this behavior would

be due to the difference in stabilities of Eu^{3+} and Sm^{3+} in the chloride phase. This can be explained when the relative availability of the chloride anion is considered for each of the two molten chloride salts, which is significantly higher in the CsCl-NaCl melt than in the $CaCl_2$-NaCl melt. It has been shown previously that the trivalent lanthanides are fairly uncoordinated by chloride anions in $CaCl_2$-NaCl melts due to the preferred formation of the $CaCl_4^{2-}$ complex compared to the $LnCl_6^{3-}$ complex [11]. However, the formation of $LnCl_6^{3-}$ is preferred in CsCl-NaCl melts since the Cs^+ cation is too large to strongly bond with the chloride anions comparatively to the Ln^{3+} species [12]. It would therefore be expected that the Ln^{3+} is favored in the CsCl-NaCl melt compared to the $CaCl_2$-NaCl melt.

There are several additional factors that need to be considered when building an understanding of the mechanics of these separation processes. It is important to realize that the BDPA has two main lattice sites for mobile cations [13]. One is the Beevers–Ross (BR) site and the other is the mid–Oxygen (mO) site. The BR site is octahedral (eight-coordinate), which is the most common coordination of trivalent lanthanides in their respective oxides, whereas the mO site is tetrahedral (four-coordinate) [14-25]. Generally, Ln^{3+} ions prefer the BR site and typical site occupancies have been measured to be greater than 90% [15, 19, 20]. This preference comes from the coordination of the Ln^{3+} ions and more covalent nature of the bonds in the BR site compared to the mO site, which has been describe extremely ionic [15, 16, 19, 20]. It has also been noted that the Ln^{3+} preference for the BR site increases with decreasing ionic size [17]. Thus, Eu^{3+} is favored over Sm^{3+} in the BR site given the ionic radii for Eu^{3+} and Sm^{3+} are 94.7 pm and

95.8 pm, respectively [26]. Finally, it has interestingly been found in studying mixed Ln^{3+}/Na^{+}–BDPA systems that the Na^{+} will replace the Ln^{3+} ions in the mO sites before those in the BR sites [18]. With these considerations in mind, that Eu^{3+} would be preferentially extracted into and Sm^{3+} preferentially extracted out of BDPA makes sense.

Given the drastic differences in the results from ion exchange reactions aiming to selectively extract either Eu or Sm out of the two different Eu/Sm–BDPA starting materials, it appears as if there is a large dependence upon the concentration of Eu^{2+}. This can be explained by considering the site occupations again. In mixed Eu^{2+}/Eu^{3+}-BDPA systems, the site occupancies for Eu have been measured to be roughly 70% mO and 30% BR [25]. If it is assumed that the preference of Eu^{2+} is also for the BR site compared to Eu^{3+} and Sm^{3+} and Na will exchange with ions in the mO sites first, then there must be enough Eu^{2+} present to reside within the BR sites for the Na to exchange with the Eu^{2+} ions. Thus, it is expected that all or at least the majority of Eu^{2+} in the low Eu^{2+} content starting materials resides in BR sites. It should be pointed out that another explanation is possible since the Eu/Sm–BDPA starting material with the lower amount of Eu^{2+} was heated to 900 ˚C. This could have resulted in the BDPA structure partially collapsing within itself, leaving the Eu species trapped within the collapsed BDPA structure. It has been noted by TANGO *et al.* that heating can cause significant rearrangement of the mobile species in BDPA [18]. Future studies using structural characterization and modeling are needed to better understand the role of the mobile ion site occupancies and overall structure of BDPA derivatives in the ion exchange reactions.

5.6 Conclusions

The results from this initial study have shown the development of a novel method for separating Eu and Sm from each other using ion exchange reactions between molten chloride salts and the solid electrolyte BDPA. Depending on the conditions of the ion exchange, separation factors greater than or close to 1.5 can be achieved using selective extraction of Eu into BDPA. Even greater separations can be achieved through the selective extraction of Eu or Sm out of Eu/Sm–BDPA material. The best separation achieved was the ion exchange between Eu/Sm-BDPA with a high Eu^{2+} starting content and CsCl-NaCl at 550 °C in air for 2 hours. However, it is apparent that the extraction of Eu and Sm from Eu/Sm–BDPA is greatly influenced by the ratio of Eu^{2+}/Eu^{3+} in the starting Eu/Sm-BDPA material. If the Eu^{2+} content is low enough, then the Sm is preferentially extracted rather than Eu. It was proposed that this is due to the two lattice sites within the conduction plane of BDPA. The largest quotient of the distribution coefficient value was calculated to 1.3×10^7 for the extraction of Eu out of a Eu/Sm–BDPA sample with a relatively high percentage of Eu^{2+} in the starting Eu/Sm-BDPA material. Further studies are needed to confirm the findings described herein. It is suggested that future work include a robust investigation through structural characterization and modeling techniques. It is especially of interest to better understand the role of site occupancies in the separations.

5.7 Acknowledgements

The authors would like to thank Jason Craig for his help in preparing and sealing quartz ampoules. The authors would like to thank the NAA team (David Glasgow, Justin Knowles, and Riley Hunley) for their help in performing and analyzing the results from NAA. The authors would also like to thank Madhavi Martin for her assistance in understanding how to use LIBS. Research sponsored by the Laboratory Directed Research and Development Program at Oak Ridge National Laboratory, managed by UT–Battelle, LLC, for the U.S. Department of Energy. This manuscript has been authored by UT–Battelle, LLC under Contract No. DE–AC05–00OR22725 with the U.S. Department of Energy. The United States Government retains and the publisher, by accepting the article for publication, acknowledges that the United States Government retains a non–exclusive, paid–up, irrevocable, world–wide license to publish or reproduce the published form of this manuscript, or allow others to do so, for United States Government purposes. The Department of Energy will provide public access to these results of federally sponsored research in accordance with the DOE Public Access Plan (http://energy.gov/downloads/doe–public–access–plan).

5.8 References

(1) Goonan, T. G. Rare Earth Elements — End Use and Recyclability. *U.S. Geol. Surv. Sci. Investig. Rep. 2011-5094* **2011**, 1–15 DOI: U.S. Geological Survey Scientific Investigations Report 2011-5094.

(2) Cotton, S. *Lanthanide and Actinide Chemistry*, 2nd ed.; John Wiley & Sons, Ltd: West Sussex, 2006.

(3) Lucas, J.; Lucas, P.; Le Mercier, T.; Rollat, A.; Davenport, W. Rare Earths Purification, Separation, Precipitation and Calcination. In *Rare Earths*; Elsevier, 2015; pp 69–91.

(4) Zhang, J.; Zhao, B.; Schreiner, B. *Separation Hydrometallurgy of Rare Earth Elements*; Springer International Publishing: Switzerland, 2016.

(5) Xie, F.; Zhang, T. A.; Dreisinger, D.; Doyle, F. A Critical Review on Solvent Extraction of Rare Earths from Aqueous Solutions. *Miner. Eng.* **2014**, *56*, 10–28 DOI: 10.1016/j.mineng.2013.10.021.

(6) Sandell, E. B. Meaning of the Term "Separation Factor." *Anal. Chem.* **1968**, *40* (4), 834–835 DOI: 10.1021/ac60260a010.

(7) Yao, Y.-F. Y.; Kummer, J. T. Ion Exchange Properties of and Rates of Ionic Diffusion in Beta-Alumina. *J. Inorg. Nucl. Chem.* **1967**, *29* (9), 2453–2475 DOI: 10.1016/0022-1902(67)80301-4.

(8) Ghosal, G.; Mangle, E.; Topp, M.; Dunn, B.; Farrington, G. C. Preparation, Ion Transport, and Spectroscopy of Eu(II) and Eu(III) Beta´´ Alumina. *Solid State Ionics* **1983**, *9–10*, 273–276 DOI: 10.1016/0167-2738(83)90246-1.

(9) Data from FTsalt – FACT salt databases. http://www.crct.polymtl.ca/fact/documentation/FTsalt/FTsalt_Figs.htm (accessed November 1st, 2016).

(10) Jain, A.; Hautier, G.; Ong, S. P.; Moore, C. J.; Fischer, C. C.; Persson, K. A.; Ceder, G. Formation Enthalpies by Mixing GGA and GGA + U Calculations. *Phys. Rev. B - Condens. Matter Mater. Phys.* **2011**, *84* (4), 1–10 DOI: 10.1103/PhysRevB.84.045115.

(11) Castrillejo, Y.; Bermejo, M. R.; Díaz Arocas, P.; Martínez, A. M.; Barrado, E. Electrochemical Behavior of Praseodymium (III) in Molten Chlorides. *J. Electroanal. Chem.* **2005**, *575* (1), 61–74 DOI: 10.1016/j.jelechem.2004.08.020.

(12) Kuznetsov, S.; Gaune-Escard, M. Electrochemistry and Thermodynamics of $EuCl_3$ and $EuCl_2$ in Alkali Chloride Melts. *J. Nucl. Sci. Technol.* **2002**, *39*, 628–631 DOI: 10.1080/00223131.2002.10875546.

(13) Wen, Z.; Cao, J.; Gu, Z.; Xu, X.; Zhang, F.; Lin, Z. Research on Sodium Sulfur Battery for Energy Storage. *Solid State Ionics* **2008**, *179* (27–32), 1697–1701 DOI: 10.1016/j.ssi.2008.01.070.

(14) Wang, Y.; Cormack, A. N. Study of Ion Distribution in Nd(III) Doped Beta´´-alumina through Atomistic Simulation. *J. Electroceramics* **1997**, *1:2*, 179–192.

(15) Kohler, J.; Urland, W. Dependence of Pr^{3+} Distributions on the Composition of Pr^{3+}-Beta´´-alumina. *J. Solid State Chem.* **1996**, *124*, 169–175.

(16) Saltzberg, M. A.; Farrington, G. C. Eu-O Bonding and Spectroscopy in Beta´´-alumina. *J. Solid State Chem.* **1989**, *83*, 272–281.

(17) Kohler, J.; Urland, W. Ionic Conductivity in Na^+/Pr^{3+}-beta´´-Al2O3 Crystals. *J. Solid State Chem.* **1996**, *127*, 161–168.

(18) Davies, P. K.; Petford, A.; O'Keeffe, M. Investigations of Cation Order in Nd-, Gd- and Eu-Beta´´ Alumina Using High Resolution T.E.M. *J. Chem. Inf. Model.* **1986**, *18/19* (9), 624–630 DOI: 10.1017/CBO9781107415324.004.

(19) Carrillo-Cabrera, W.; Thomas, J. O.; Farrington, G. C. The Ionic Distribution in Trivalent Gd^{3+} Beta´´-alumina. *Solid State Ionics* **1983**, *9* & *10*, 245–248.

(20) Carrillo-Cabrera, W.; Thomas, J. O.; Farrington, G. C. The Structure of the Lanthanide Gd^{3+}, Eu^{3+} and Nd^{3+} Beta´´-aluminas. *Solid State Ionics* **1988**, *28–30* (PART 1), 317–323 DOI: 10.1016/S0167-2738(88)80057-2.

(21) Tietz, F.; Urland, W. Investigations on Lanthanide-Ion-Exchange Beta and Beta´´-alumina. *J. Alloys Compd.* **1993**, *192*, 78–80.

(22) Laberge, M.; Simkin, D. J.; Dunn, B. Site-Selective Resonance Fluorescence of Eu^{3+}-Exchanged Sodium Beta´´-alumina. *J. Chem. Phys.* **1992**, *96* DOI: 10.1063/1.462892.

(23) Dunn, B.; Yang, D. L.; Vivien, D. Spectroscopic Studies of Nd^{3+}-Exchanged Beta´´-alumina. *J. Solid State Chem.* **1988**, *73*, 235–242.

(24) Farrington, G. C.; Dunn, B.; Thomas, J. O. The Lanthanide Beta´´-aluminas: A New Family of Fluorescent Solid Electrolytes. *Appl. Phys. A Solids Surfaces* **1983**, *32*, 159–161.

(25) Carrillo-Cabrera, W.; Thomas, J. O.; Farrington, G. C. The Eu^{3+} Eu^{2+} Reduction Process in Eu^{3+} Beta´´-alumina. *Solid State Ionics* **1986**, *19*, 645–652.

(26) Shannon, R. D. Revised Effective Ionic Radii and Systematic Studies of Interatomic Distances in Halides and Chalcogenides. *Acta Crystallogr. Sect. A* **1976**, *32* (5), 751–767 DOI: 10.1107/S0567739476001551.

Chapter 6: Reduction of Eu in molten $CsCl–MgCl_2$ and subsequent separation from Sm using a beta´´–alumina membrane

6.1 Disclosure

This chapter is based on a manuscript in preparation for submission to a journal. The full list of authors includes Kristian G. Myhre and Miting Du. The role of Kristian G. Myhre was to design and perform all experiments, process and analyze all data, and prepare the manuscript for submission.

6.2 Abstract

Electrolysis through a solid electrolyte BDPA membrane was utilized to achieve fast and high–quality separation of Eu from Sm. A mixture of Eu_2O_3 and Sm_2O_3 was dissolved in a molten CsCl–$MgCl_2$ eutectic at 550 ˚C under an argon atmosphere. In this molten salt mixture, the reduction of Eu^{3+} to Eu^{2+} appears to have occurred spontaneously. A voltage was applied across the electrochemical cell for a short period of time to selectively conduct the Eu^{2+} into the BDPA membrane. Analysis of the starting solution, ending solution, and BDPA membrane using LIBS indicates that a nearly complete separation of Eu from Sm was achieved. LIBS was used to quantify the amount of Eu and Sm in the BDPA membrane after electrolysis. The separation factor of Eu was calculated to be 940 with a percent error of 9.8 % and total Eu recovery of 5.3%.

6.3 Introduction

There are several instances of solid electrolytes being used as membranes for separations [1-8]. Oxide ion conducting solid electrolytes have been used in oxygen pumps, which produce purified oxygen from air [1, 2]. The separation of Li^+ from

aqueous solutions, such as mixed alkali halide solutions and seawater, has also been investigated [3, 4]. Researchers at Sandia National Laboratory have even investigated the use of Li and K ion conducting solid electrolytes to separate Li and K from used pyroprocessing salt waste streams [5]. It does not appear, however, that solid electrolytes have been previously investigated to selectively separate multivalent cations from each other using selective superionic conduction through or into a solid electrolyte membrane.

A difficult aspect of working with molten chloride salts as a high–temperature solvent and the lanthanide chlorides is their oxygen/moisture sensitivity. Without the use of carefully prepared reagents and an inert atmosphere glove box, it can be essentially impossible to dissolve lanthanide oxides into molten chloride salts in a normal fume hood or other place with ambient conditions. This is because the lanthanide chlorides quickly react to become insoluble oxychlorides in the presence of oxygen and/or moisture [9-11]. It is often the case that extreme chemical methods need to be used to insure the dissolution of the lanthanide oxides into molten chloride salts. These include sparging with Cl_2 or dry HCl as well as the addition of solid chlorinating agents, such as $ZrCl_4$ [12, 13]. A couple instances of adding small amounts $MgCl_2$ to molten alkali halide salt mixtures has been used to dissolve lanthanide oxides [14, 15]. The use of $MgCl_2$ is preferable to the other mentioned methods of chlorinating the lanthanide oxides for use in scaled up hot cell operations given the more mundane nature of $MgCl_2$. The chlorination of Sm_2O_3 and Eu_2O_3 by $MgCl_2$ should be thermodynamically favored given the calculated heats of reaction

$$3\ MgCl_2 + Sm_2O_3 \rightarrow 2\ SmCl_3 + 3\ MgO \qquad -115\ kj/mol$$

$$3\ MgCl_2 + Eu_2O_3 \rightarrow 2\ EuCl_3 + 3\ MgO \qquad -97\ kj/mol$$

which can be calculated using available thermodynamic data [16].

The dissolution of Eu_2O_3 and Sm_2O_3 into a molten CsCl–$MgCl_2$ [0.807:0.193] eutectic was investigated for use as a starting solution for the separation of Eu and Sm using the solid electrolyte membrane approach. The CsCl-$MgCl_2$ eutectic with a melting point of 491 °C was chosen instead of pure $MgCl_2$ because of the lower melting temperature. Pure $MgCl_2$ has a melting temperature of 714 °C [17]. The Cs is not expected to interfere with the chlorination since the Cs^+ ion is very large and does not strongly bond with chloride anions [18]. Additionally, the Cs^+ ion is too large to be incorporated into the BDPA structure and should not interfere with the conduction of the Ln species [19].

6.4 Materials and Characterization

6.4.1 Materials

$MgCl_2$ was purchased from Sigma–Aldrich. CsCl was purchased from Alfa Aesar. Eu_2O_3 and Sm_2O_3 were purchased from Sigma–Aldrich. The CsCl and $MgCl_2$ were weighed out and mixed together using a mortar and pestle to make a CsCl–$MgCl_2$ [0.807:0.193] mixture, which was then stored in an oven at over 100 ˚C for several days before use. Eu_2O_3, Sm_2O_3, and the CsCl–$MgCl_2$ mixture were mixed together using a mortar and pestle to make a mixture containing about 0.8 wt % of both Eu_2O_3 and Sm_2O_3. Glassy carbon electrodes were used as electrodes and were purchased from HTW (Germany). A Na–BDPA disc (10 mm diameter, 1 mm thick) was purchased from

Ionotec, Ltd. PELCO high–temperature carbon paste was purchased from Ted Pella, Inc. The Na–BDPA disc was attached to a quartz basket using the carbon paste as directed to attach ceramics to quartz. Figure 6.1 is a picture of the quartz basket with the Na–BDPA disc attached resting in the quartz container.

6.4.2 Dissolution of Eu_2O_3 and Sm_2O_3

Cyclic voltammetry was used to measure the dissolution of Eu_2O_3 and Sm_2O_3 into a molten CsCl–$MgCl_2$ mixture at 550 ˚C. A scan speed of 1 V s^{-1} was used. Measurements were taken every 15 minutes after the furnace had equilibrated for 1 hour at 550 ˚C. The potentiostat used is a Versastat3-200 Advanced DC Voltammetry System which was purchased from Princeton Applied Research. Throughout the entire experiment, a steady flow of argon gas into the furnace chamber was maintained.

6.4.3 Electrolysis

After the CsCl–$MgCl_2$–Eu_2O_3–Sm_2O_3 mixture had been given 1 hour to equilibrate, 5 V was applied across the electrochemical cell for 20 minutes. Afterwards, the voltage and furnace were turned off. The sample was let to cool with the flow of argon gas continuing.

6.4.4 Quantification of separation

LIBS was used to quantify the amount of Eu and Sm that had been electrochemically implanted into the BDPA membrane. The photoemission line at

412.941 nm was used for Eu and the one at 425.624 nm was used for Sm. Both peaks were background subtracted and normalized to the Al photoemission peak at 308.205 nm. Multiple spots on the BDPA membrane were measured in order to better estimate the bulk content of Eu. The method for calculating the concentration of Eu and Sm in an alumina matrix is using the mentioned photoemission lines is outlined in Chapter 3. Part of the BDPA membrane measured to have Eu in it was able to be recovered without any visible amounts of carbon paste. The recovered Eu-BDPA pieces were then weighed to calculate a percent recovery of Eu.

6.5 Results and Discussion

Figure 6.3 shows a cyclic voltammogram taken of a $CsCl–MgCl_2–Eu_2O_3–Sm_2O_3$ mixture at 550 ˚C under an argon atmosphere. Two redox couples can be seen, which correspond to the Eu^{3+}/Eu^{2+} and Sm^{3+}/Sm^{2+} redox pairs. The presence of these redox pairs indicates that at least some of the Eu_2O_3 and Sm_2O_3 had dissolved into the $CsCl–MgCl_2$ molten salt. The first cyclic voltammogram was taken after the sample had been let to heat at 550 ˚C for 1 hour. After several subsequent measurements, it appeared that the dissolution of the lanthanide oxides was either complete or at equilibrium from the very first measurement since no change was noticed.

After electrolysis of the solid electrolyte membrane cell at 5 V for 20 minutes, the furnace and power supply were turned off and let to cool. Once cooled, the electrochemical cell was disassembled using a small amount of water to separate the solidified salts and quartz cell pieces. LIBS measurements were then performed on the

BDPA membrane with the measurements being taken on the side exposed to the receiving solution, as shown in Figure 6.2. The separation factor was then calculated using univariate analysis methodology described in Chapter 3. Part of the BDPA membrane measured to have Eu in it was then physically separated from the quartz basket that it was pasted to. The recovered Eu-BDPA pieces were measured to contain roughly 6 wt % Eu and a total of 6% of the original Eu content was measured to be recovered in the Eu/Sm-BDPA membrane. This corresponds to 5.3 mg of Eu recovered from the [50:50] mixture of Eu and Sm oxide.

6.6 Conclusions

A fast and high–quality separation of Eu and Sm was accomplished using the solid electrolyte BDPA as a selective membrane to conduct Eu^{2+} from a mixture of CsCl–$MgCl_2$ with Eu_2O_3 and Sm_2O_3 dissolved into it. The Eu^{3+} appears to have been reduced to Eu^{2+} spontaneously within the CsCl–$MgCl_2$ molten salt. This could occur through the precipitation of MgO, thereby leaving excess chloride to reduce the Eu^{3+} through the formation of Cl_2. A separation factor of 940 with a percent error of 9.8% was achieved. 5.3 mg of Eu was recovered from about 0.2 g of a [50:50] mixture of Eu and Sm oxide dissolved in CsCl-$MgCl_2$. There was no detectable amount of Sm with the separated Eu.

6.7 Acknowledgments

Research sponsored by the Laboratory Directed Research and Development Program at Oak Ridge National Laboratory, managed by UT–Battelle, LLC, for the U.S.

Department of Energy. This manuscript has been authored by UT–Battelle, LLC under Contract No. DE–AC05–00OR22725 with the U.S. Department of Energy. The United States Government retains and the publisher, by accepting the article for publication, acknowledges that the United States Government retains a non–exclusive, paid–up, irrevocable, world–wide license to publish or reproduce the published form of this manuscript, or allow others to do so, for United States Government purposes. The Department of Energy will provide public access to these results of federally sponsored research in accordance with the DOE Public Access Plan (http://energy.gov/downloads/doe–public–access–plan).

6.8 References

(1) Dyer, P. N.; Richards, R. E.; Russek, S. L.; Taylor, D. M. Ion Transport Membrane Technology for Oxygen Separation and Syngas Production. *Solid State Ionics* **2000**, *134* (1–2), 21–33 DOI: 10.1016/S0167-2738(00)00710-4.

(2) Jiang, D.; Bu, X.; Sun, B.; Lin, G.; Zhao, H.; Cai, Y.; Fang, L. Experimental Study on Ceramic Membrane Technology for Onboard Oxygen Generation. *Chinese J. Aeronaut.* **2016**, *29* (4), 863–873 DOI: 10.1016/j.cja.2016.06.003.

(3) Kunugi, S.; Inaguma, Y.; Itoh, M. Electrochemical Recovery and Isotope Separation of Lithium Ion Employing Lithium Ion Conductive Perovskite-Type Oxides. *Solid State Ionics* **1999**, *122* (1–4), 35–39 DOI: 10.1016/S0167-2738(99)00073-9.

(4) Hoshino, T. Innovative Lithium Recovery Technique from Seawater by Using World-First Dialysis with a Lithium Ionic Superconductor. *Desalination* **2015**, *359*, 59–63 DOI: 10.1016/j.desal.2014.12.018.

(5) Spoerke, E.; Wheeler, J.; Ihlefeld, J.; Blea, M.; Brown-Shaklee, H.; Rodriguez, M. *Ion Selective Ceramics for Waste Separations: Performance and Design of Ion Selective Ceramic Membrane for Molten Salt Recycle*; 2014.

(6) Joshi, A. V; Steppan, J. J.; Taylor, D. M.; Elangovan, S. Solid Electrolyte Materials, Devices, and Applications. *J. Electroceramics* **2004**, *13* (1–3), 619–625 DOI: 10.1007/s10832-004-5168-x.

(7) SelectIon Technologies. “Technologies”. SelectIon Technologies official company website. www.select-ion.com/technologies.php (accessed October 1st, 2016).

(8) Sattar, S.; Ghosal, B.; Underwood, M. L.; Mertwoy, H.; Saltzberg, M. A.; Frydrych, W. S.; Rohrer, G. S.; Farrington, G. C. Synthesis of Di- and Trivalent Beta’’-aluminas by Ion Exchange. *J. Solid State Chem.* **1986**, *65*, 231–240.

(9) Meyer, G.; Ax, P. An Analysis of the Ammonium Chloride Route to Anhydrous Rare-Earth Metal Chlorides. *Mater. Res. Bull.* **1982**, *17* (11), 1447–1455 DOI: 10.1016/0025-5408(82)90231-8.

(10) Dell’Amico, D. B.; Calderazzo, F.; della Porta, C.; Merigo, A.; Biagini, P.; Lugli, G.; Wagner, T. Improved Preparation of Anhydrous Lanthanide Chlorides under Mild Conditions. *Inorganica Chim. Acta* **1995**, *240* (1–2), 1–3 DOI: 10.1016/0020-1693(95)04568-6.

(11) Freeman, J. H.; Smith, M. L. The Preparation of Anhydrous Inorganic Chlorides by Dehydration with Thionyl Chloride. *J. Inorg. Nucl. Chem.* **1958**, *7*, 224–227.

(12) Lee, H. 16 – Oxide Electroreduction and Other Processes for Pyrochemical Processing of Spent Nuclear Fuels: Developments in Korea. In *Reprocessing and Recycling of Spent Nuclear Fuel*; Elsevier Ltd, 2015; pp 415–436.

(13) Sakamura, Y.; Inoue, T.; Iwai, T.; Moriyama, H. Chlorination of UO_2, PuO_2 and Rare Earth Oxides Using $ZrCl_4$ in LiCl-KCl Eutectic Melt. *J. Nucl. Mater.* **2005**, *340* (1), 39–51 DOI: 10.1016/j.jnucmat.2004.11.002.

(14) Ying-Cai, W.; Mei, L.; Wei, H.; Yao-Chen, L.; Bin, L.; Yong-De, Y.; Mi-Lin, Z. The Chlorination of La_2O_3 by $MgCl_2$ in the LiCl-NaCl Melts. *Nucl. Sci. Tech.* **2015**, *26* (S10310) DOI: 10.13538/j.1001-8042/nst.26.S10310.

(15) Yang, Y.; Zhang, M.; Han, W.; Jiang, H. Selective Extraction of Gadolinium from Sm_2O_3 and Gd_2O_3 Mixtures in a Single Step Assisted by $MgCl_2$ in LiCl–KCl Melts. **2014**, 843–850 DOI: 10.1007/s10008-013-2333-7.

(16) Jain, A.; Hautier, G.; Ong, S. P.; Moore, C. J.; Fischer, C. C.; Persson, K. A.; Ceder, G. Formation Enthalpies by Mixing GGA and GGA + U Calculations. *Phys. Rev. B - Condens. Matter Mater. Phys.* **2011**, *84* (4), 1–10 DOI: 10.1103/PhysRevB.84.045115.

(17) Data from FTsalt – FACT salt databases. http://www.crct.polymtl.ca/fact/documentation/FTsalt/FTsalt_Figs.htm (accessed November 1st, 2016).

(18) Castrillejo, Y.; Bermejo, M. R.; Díaz Arocas, P.; Martínez, A. M.; Barrado, E. Electrochemical Behavior of Praseodymium (III) in Molten Chlorides. *J. Electroanal. Chem.* **2005**, *575* (1), 61–74 DOI: 10.1016/j.jelechem.2004.08.020.

(19) Yao, Y.-F. Y.; Kummer, J. T. Ion Exchange Properties of and Rates of Ionic Diffusion in Beta-Alumina. *J. Inorg. Nucl. Chem.* **1967**, *29* (9), 2453–2475 DOI: 10.1016/0022-1902(67)80301-4.

Chapter 7: Conclusions and recommendations

7.1 Important conclusions

Solid electrolytes have been shown to be useful in separating the *f*–elements from each other in two ways through separations of Eu and Sm. The first method utilizes ion exchange reactions between molten salts and the solid electrolyte BDPA. The second method utilizes selective ionic conduction of Eu^{2+} into a solid electrolyte BDPA membrane. The initial studies presented herein have provided a promising proof–of–concept demonstration and laid the groundwork for future studies in this exciting area of separation chemistry. It is expected that similar separations could be achieved for the other trivalent lanthanides as well as the minor actinides.

7.2 Recommendations for future work

Although these studies have answered the question of whether or not solid electrolytes can be used to accomplish separations involving the *f*–elements, there are numerous areas in which future research and development efforts could and should explore.

The work presented in Chapter 3 demonstrates the usefulness of LIBS to qualitatively and quantitatively analyze samples that are difficult to digest, such as BDPA, and have multiple *f*–elements present, which produce complex and often overlapping spectra. Future studies on LIBS to analyze difficult to digest samples containing the *f*–elements should be undertaken. However, before quantitative studies can be carried out it is crucial that the LIBS emission spectra for *f*-elements be expanded to

include all of the lanthanides and actinides. Currently, there is a lack of data in the literature on the LIBS emission spectra actinides, particularly the transuranics.

The work presented in Chapter 4 investigated the oxidation state behavior of Eu and Sm in BDPA. It would be very interesting to study the oxidation state behavior of other *f*–elements, both separately and in mixed samples, in the BDPA structure. Given the unique stability of divalent Eu, the reduction of other *f*–elements in the BDPA structure is of interest and quite possible. Studies synthesizing and characterizing a wide range of compositions under varied conditions should be undertaken. This could lead to an improved understanding of *f*–element chemistry as well as advanced materials for use in optics and separations. A robust effort to characterize structural dependence of the oxidation state behavior of Eu and other *f*-elements in BDPA should also be carried out. The role that site occupancy plays in the reduction and stabilization of Eu in BDPA is still unclear. In particular, studies using X-ray/neutron diffraction, Tunneling Electron Microscopy and Electron Energy Loss Spectroscopy techniques would particularly useful in elucidating this behavior.

The studies reported in Chapter 5 discussed the development of a novel *f*–element separation chemistry using ion exchange reactions between the BDPA solid electrolyte and molten chloride salts. The ion exchange reactions were shown to be dependent upon the processing history of the BDPA samples, exchange salts, reaction times, and atmospheric conditions. It is recommended that future studies investigate the use of this separation chemistry to accomplish separations other than those discussed herein. Future studies should also investigate the use of other solid electrolyte materials to accomplish

separations, such as beta– and beta″–ferrite as well as $Sc_2(WO_4)_3$–type materials that have also been shown to conduct lanthanides [1-6]. Included should be an in–depth investigation of the structural properties of the solid electrolyte materials and how they correlate with the separation dynamics. It is recommended that modeling efforts be performed in parallel with experimental studies. Specifically, it is of interest to gain an in-depth understanding of the conduction mechanism

Finally, Chapter 6 showed the exciting possibility of using a Na–BDPA as a membrane to selectively conduct certain species. Specifically, the separation of Eu and Sm by selective conduction of Eu^{2+} was accomplished with a high separation factor of 940.

7.3 References

(1) Kalogirou, O. Synthesis and Thermal Stability of Polycrystalline New Divalent Beta´´- and Beta-Ferrites Prepared by Ion Exchange. *Journal of Solid State Chemistry*. 1993, pp 318–331.

(2) Burmakin, E. I.; Shekhtman, G. S. Solid Electrolytes with Cesium-Cationic Conduction in the Fe_2O_3-TiO_2-Cs_2O System. *Russ. J. Electrochem.* **2009**, *45* (12), 1363–1367 DOI: 10.1134/S1023193509120088.

(3) Kobayashi, Y.; Egawa, T.; Okazaki, Y.; Tamura, S.; Imanaka, N.; Adachi, G. Trivalent Ion Conduction of the $Sc_2(WO_4)_3$–$Gd_2(WO_4)_3$ System. **1998**, *111* (May), 59–65.

(4) Adachi, G. Y.; Imanaka, N.; Tamura, S. Ionic Conducting Lanthanide Oxides. *Chem. Rev.* **2002**, *102* (6), 2405–2429 DOI: 10.1021/cr0103064.

(5) Imanaka, N.; Kohler, J.; Tamura, S.; Adachi, G. Trivalent Rare Earth Ion Conduction in the Rare Earth Tungstates with the $Sc_2(WO_4)_3$-Type Structure. *Eur. J. Inorg. Chem.* **2002**, 105–109 DOI: 10.1021/cm980157e.

(6) Higgins, B.; Graeve, O. A.; Edwards, D. D. New Methods for Preparing Submicrometer Powders of the Tungstate-Ion Conductor $Sc_2(WO_4)_3$ and Its Al and In Analogs. *J. Am. Ceram. Soc.* **2013**, *96* (8), 2402–2410 DOI: 10.1111/jace.12416.

Appendix

Table 3.1: Characteristics of laser and spectrometers

Laser Characteristics	
Wavelength	1064 nm
Energy per pulse	161 ± 2.25 mJ
Spectrometer Characteristics	
Wavelength ranges (nm)	FWHM (nm)
182.27 to 314.30	0.06
314.31 to 909.37	0.18

Table 3.2: Wavelengths of the emission lines used for univariate analysis

Element	Wavelength (nm)	Reference(s)
Eu	390.693	[8]
Eu	412.941	[8,9]
Eu	663.362	This work
Sm	425.624	This work
Sm	431.870	This work
Sm	474.556	This work
Al	308.205	[12]
Al	309.281	[12]

Figure 3.1: Full energy range spectra of (a) pure Al_2O_3 pellet, (b) Al_2O_3 pellet containing Eu_2O_3 at 5.320 wt %, (c) Al_2O_3 pellet containing Sm_2O_3 at 5.170 wt %, and (d) Al_2O_3 pellet containing both Eu_2O_3 at 5.300 wt % and Sm_2O_3 at 5.170 wt %.

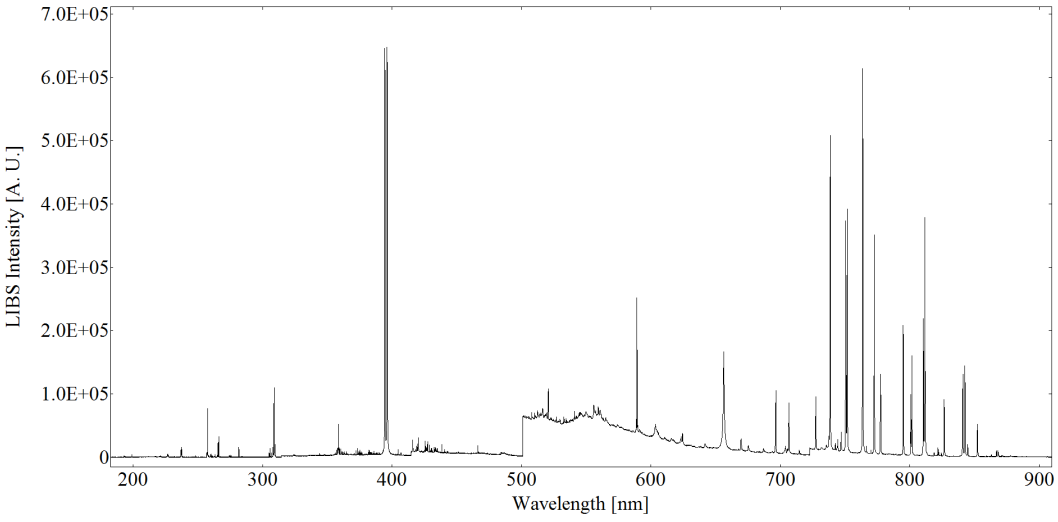

(a)

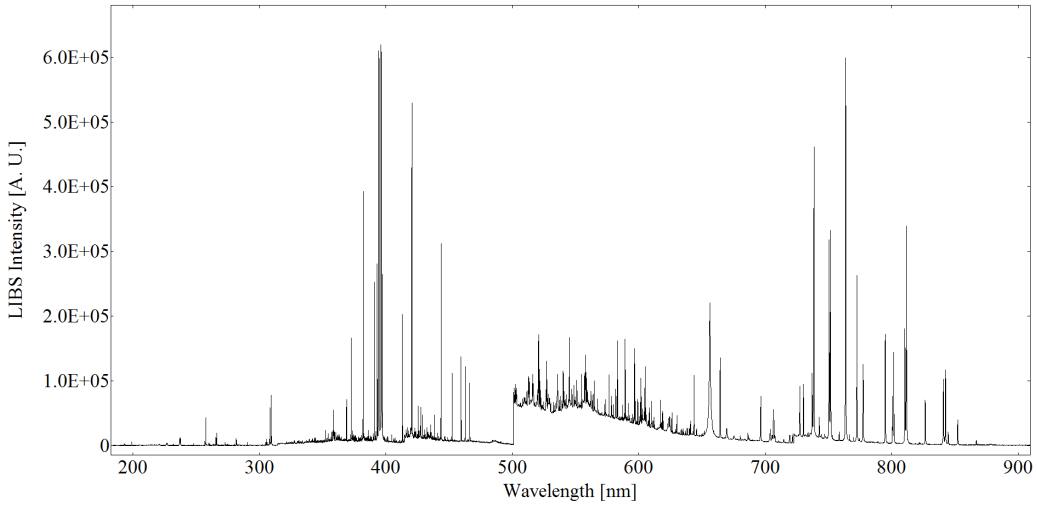

(b)

Figure 3.1 continued.

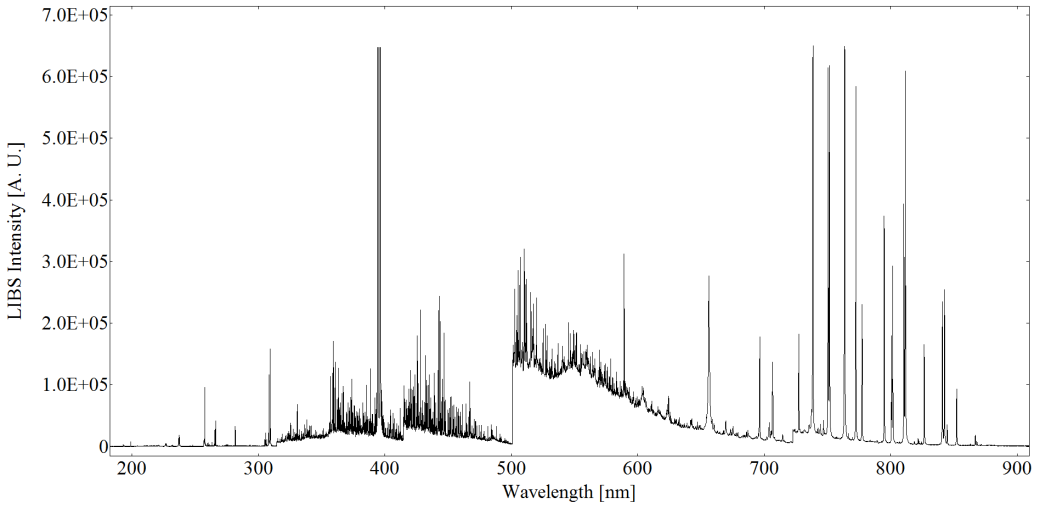

(c)

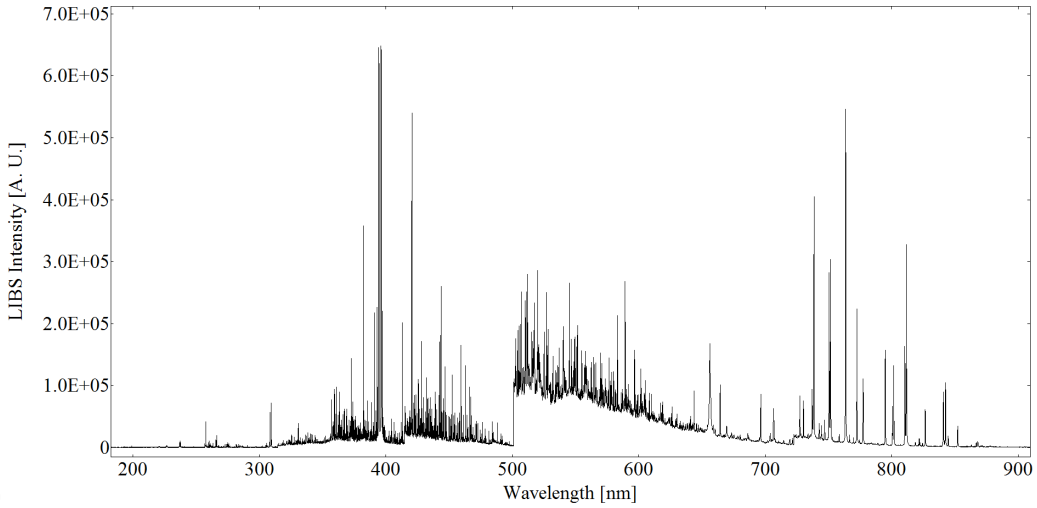

(d)

Figure 3.1 continued.

Figure 3.2: SLR calibration curves with the highest R^2 values for: (a) Eu in Eu_2O_3–Al_2O_3 using the Eu 663.362 nm emission line normalized to a nearby background region; (b) Sm in Sm_2O_3–Al_2O_3 using the Sm 474.556 nm emission line normalized using the Al 308.205 nm emission line; (c) Eu in Eu_2O_3–Sm_2O_3–Al_2O_3 using the Eu 390.693 nm emission line normalized to the Al 308.205 nm emission line; and (d) Sm in Eu_2O_3–Sm_2O_3–Al_2O_3 using the Sm 425.624 nm emission line normalized to the Al 309.281 nm emission line. The error bars represent the standard deviation for the measurements averaged to give the point on the graph.

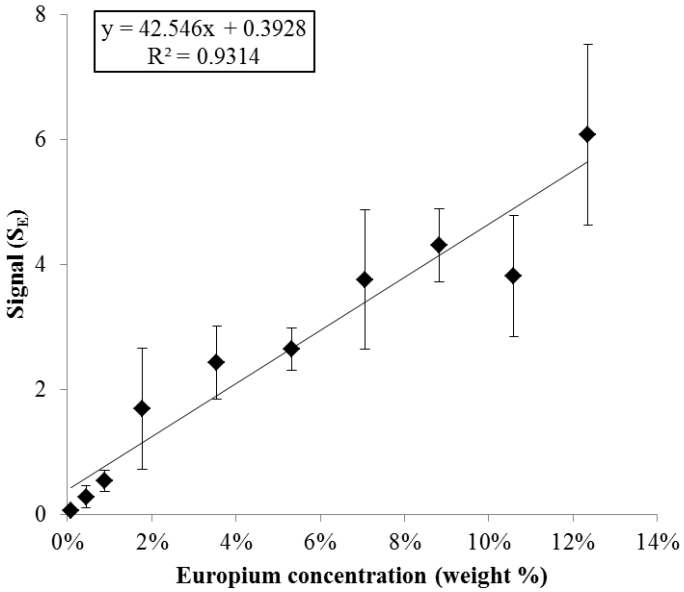

(a)

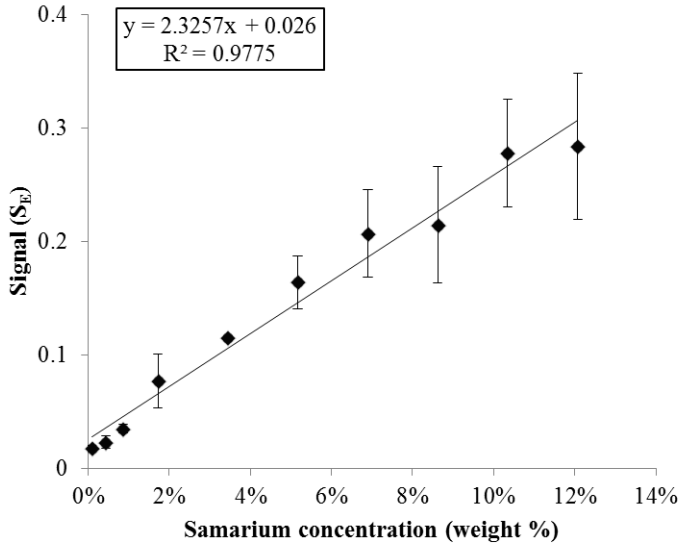

(b)

Figure 3.2 continued.

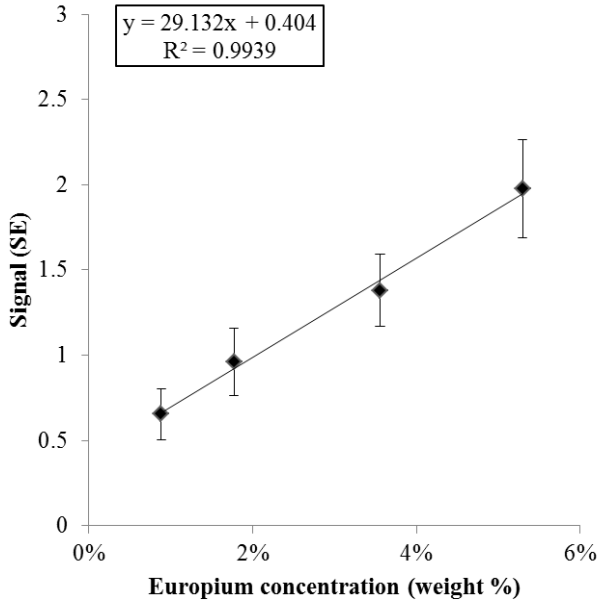

(c)

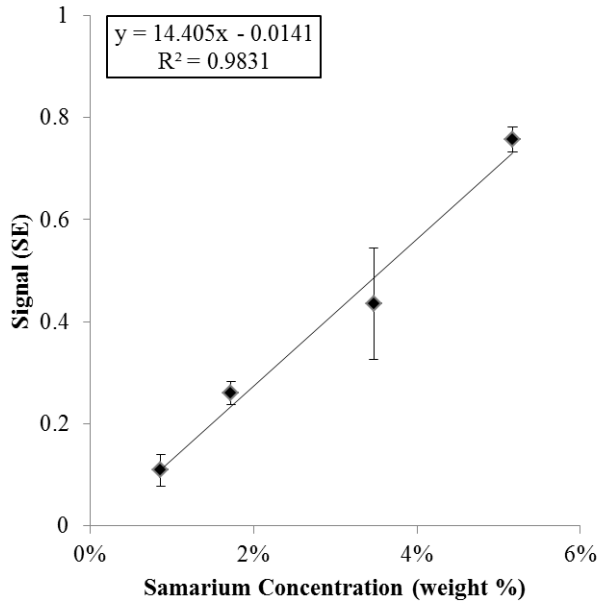

(d)

Figure 3.2 continued.

Table 3.3: Figures of merit for the Eu and Sm calibration curves built using univariate SLR analysis.

Univariate SLR Analysis for Single Element Samples				
Emission Line	Normalization	R^2	RMSE (wt %)	LOD (wt %)
$Eu_{390.693}$	Background	0.7670	0.023	0.006
$Eu_{390.693}$	$Al_{308.205}$	0.9192	0.013	0.002
$Eu_{390.693}$	$Al_{309.281}$	0.9218	0.012	0.012
$Eu_{412.941}$	Background	0.7649	0.023	0.005
$Eu_{412.941}$	$Al_{308.205}$	0.9255	0.012	0.001
$Eu_{412.941}$	$Al_{309.281}$	0.9283	0.012	0.010
$Eu_{663.362}$	Background	0.9314	0.012	0.008
$Eu_{663.362}$	$Al_{308.205}$	0.8860	0.015	0.004
$Eu_{663.362}$	$Al_{309.281}$	0.8966	0.014	0.037
$Sm_{425.624}$	Background	0.8565	0.017	0.018
$Sm_{425.624}$	$Al_{308.205}$	0.9736	0.064	0.006
$Sm_{425.624}$	$Al_{309.281}$	0.9711	0.007	0.053
$Sm_{431.870}$	Background	0.8338	0.018	0.023
$Sm_{431.870}$	$Al_{308.205}$	0.9710	0.007	0.007
$Sm_{431.870}$	$Al_{309.281}$	0.9682	0.008	0.050
$Sm_{474.556}$	Background	0.9185	0.012	0.054
$Sm_{474.556}$	$Al_{308.205}$	0.9775	0.006	0.025
$Sm_{474.556}$	$Al_{309.281}$	0.9745	0.007	0.183

Table 3.4: Figures of merit for the mixed Eu and Sm calibration curves built using univariate SLR analysis.

Univariate SLR Analysis for Multi–Element Samples				
Emission Line	Normalization	R^2	RMSE (wt %)	LOD (wt %)
$Eu_{390.693}$	Background	0.8830	0.006	0.010
$Eu_{390.693}$	$Al_{308.205}$	0.9797	0.002	0.004
$Eu_{390.693}$	$Al_{309.281}$	0.9939	0.001	0.032
$Eu_{412.941}$	Background	0.8481	0.007	0.028
$Eu_{412.941}$	$Al_{308.205}$	0.9476	0.004	0.006
$Eu_{412.941}$	$Al_{309.281}$	0.9694	0.003	0.038
$Eu_{664.362}$	Background	0.9321	0.005	0.035
$Eu_{664.362}$	$Al_{308.205}$	0.9528	0.004	0.015
$Eu_{664.362}$	$Al_{309.281}$	0.9508	0.004	0.108
$Sm_{425.624}$	Background	0.9218	0.005	0.013
$Sm_{425.624}$	$Al_{308.205}$	0.9801	0.002	0.002
$Sm_{425.624}$	$Al_{309.281}$	0.9831	0.002	0.013
$Sm_{431.870}$	Background	0.9015	0.006	0.010
$Sm_{431.870}$	$Al_{308.205}$	0.9745	0.003	0.001
$Sm_{431.870}$	$Al_{309.281}$	0.9400	0.004	0.010
$Sm_{474.556}$	Background	0.9651	0.003	0.011
$Sm_{474.556}$	$Al_{308.205}$	0.9709	0.003	0.005
$Sm_{474.556}$	$Al_{309.281}$	0.9680	0.003	0.040

Figure 3.3: Multivariate calibration curves built using PLS regression analysis for determining the concentration of: (a) Eu from the Eu_2O_3–Al_2O_3 single element standards; (b) Sm from the Sm_2O_3–Al_2O_3 single element standards; (c) Sm from the Al_2O_3 and Eu_2O_3–Sm_2O_3–Al_2O_3 multi–element standards; (d) Eu from the Al_2O_3 and Eu_2O_3–Sm_2O_3–Al_2O_3 multi–element standards; (e) Sm from all of the standards; and (f) Eu from all of the standards.

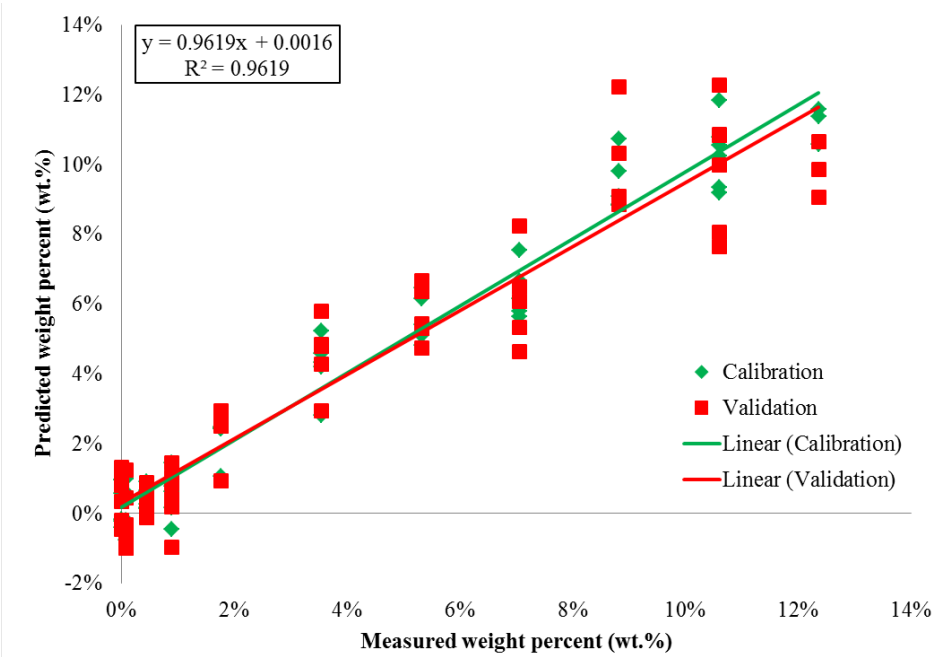

(a)

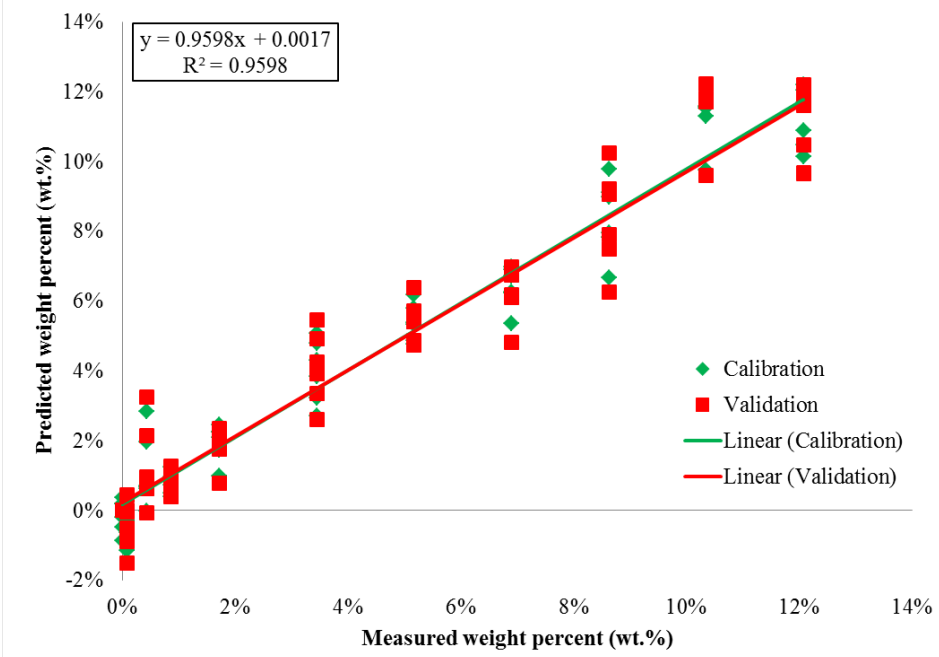

(b)

Figure 3.3 continued.

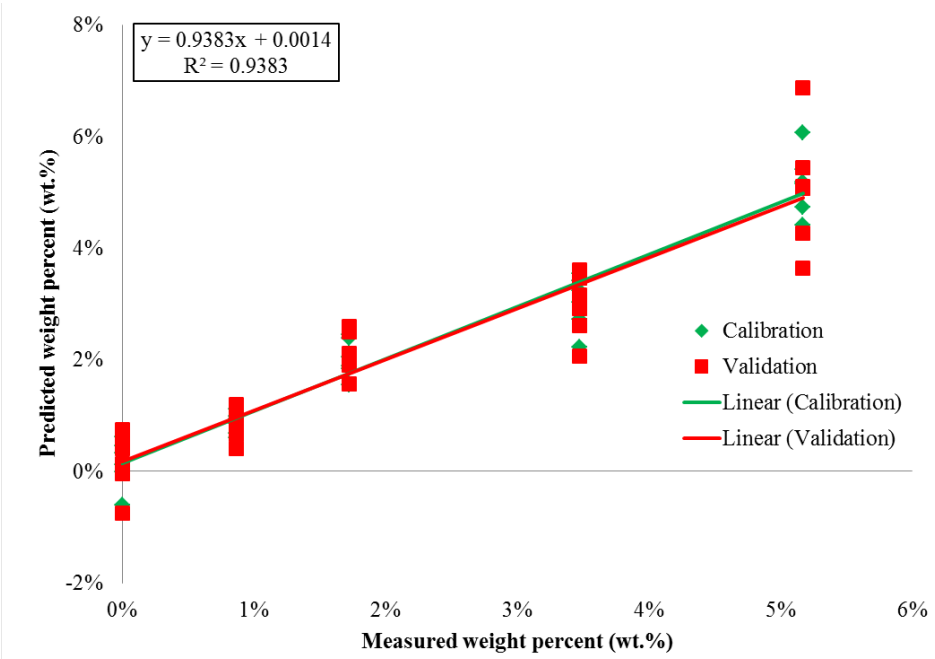

(c)

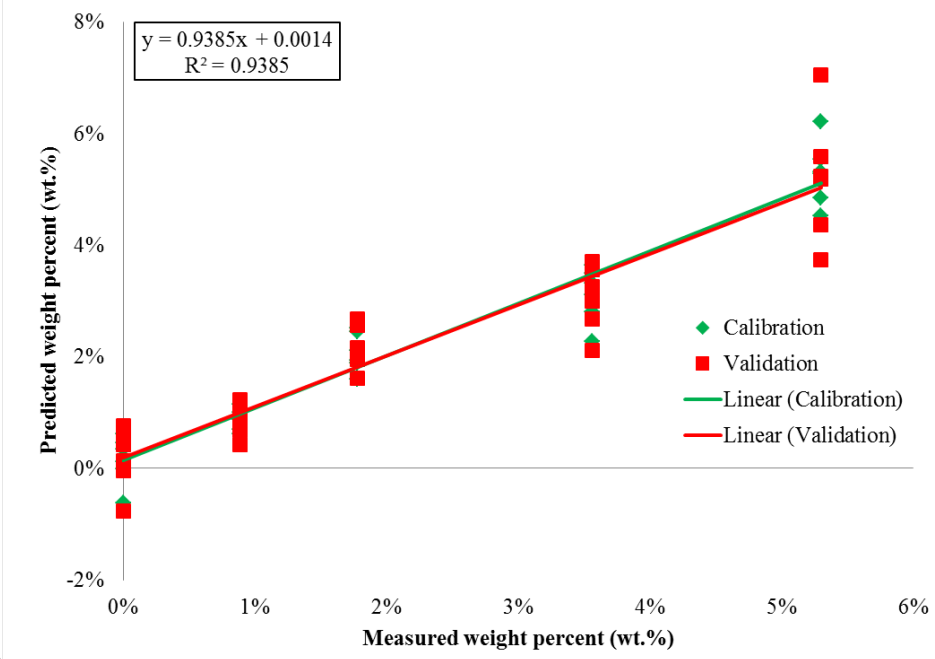

(d)

Figure 3.3 continued.

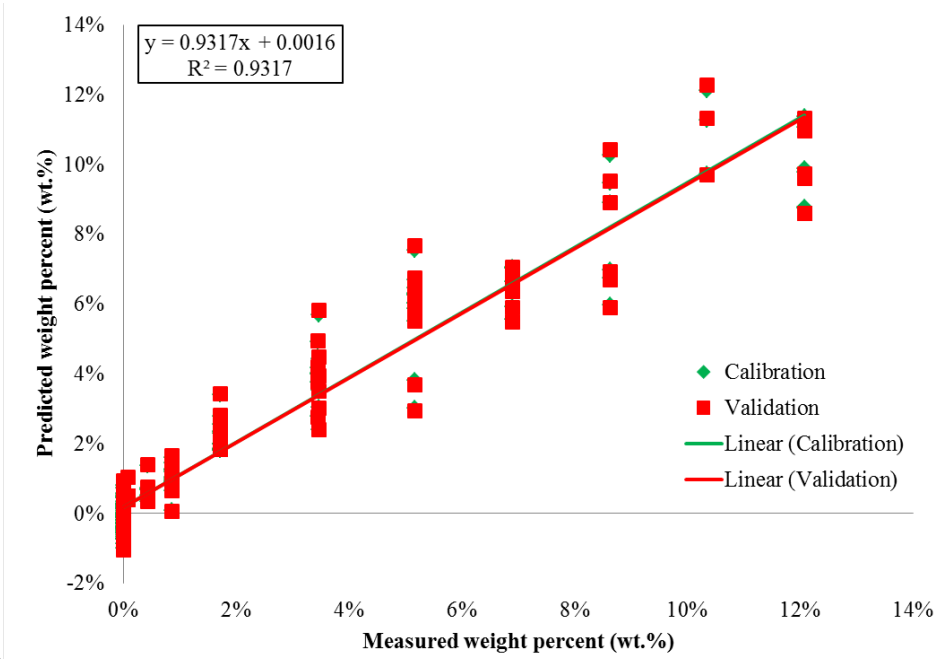

(e)

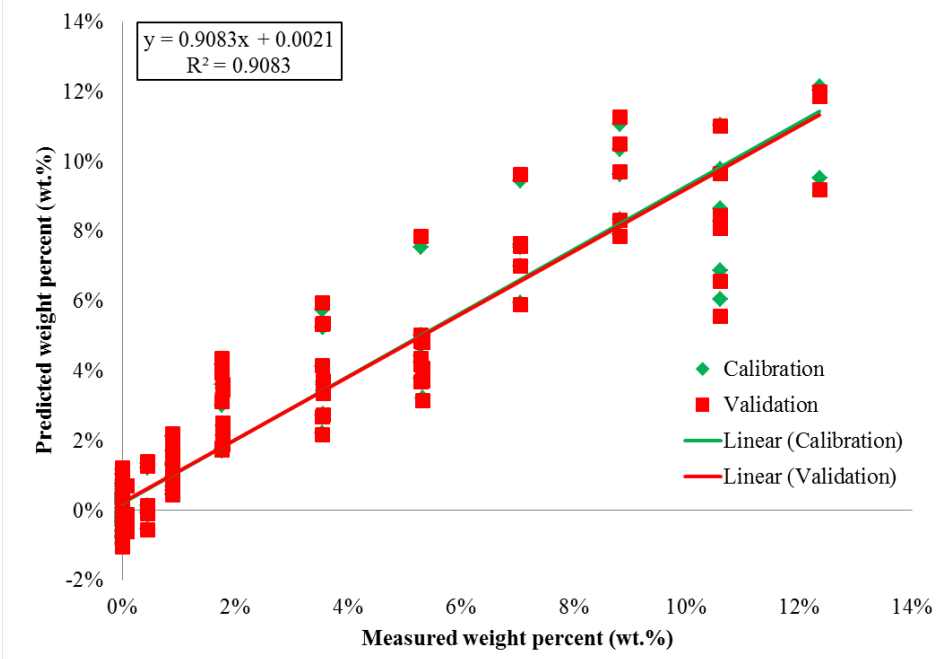

(f)

Figure 3.3 continued.

Figure 3.4: Percentage of the total residual variance as a function of the number of principal components for the calibration curves built using PLS regression analysis of the LIBS spectra data from (a) the Eu_2O_3–Al_2O_3 single element standards, (b) the Sm_2O_3–Al_2O_3 single element standards, (c) the Al_2O_3 and Eu_2O_3–Sm_2O_3–Al_2O_3 multi–element standards, and (d) all of the standards.

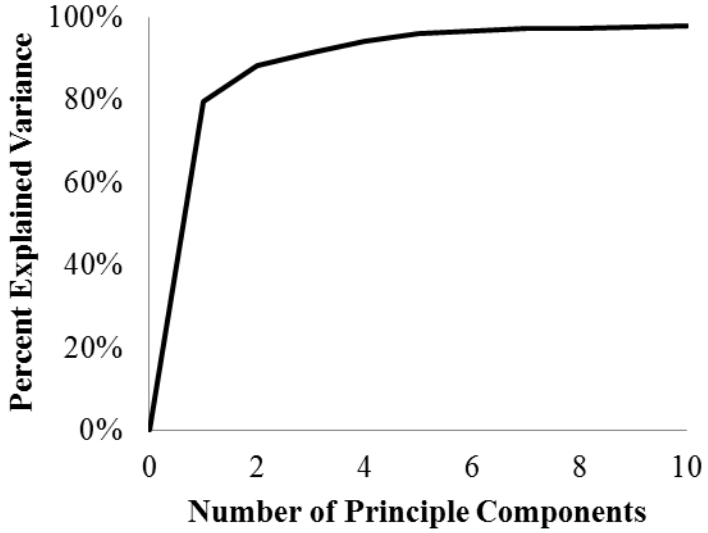

(a)

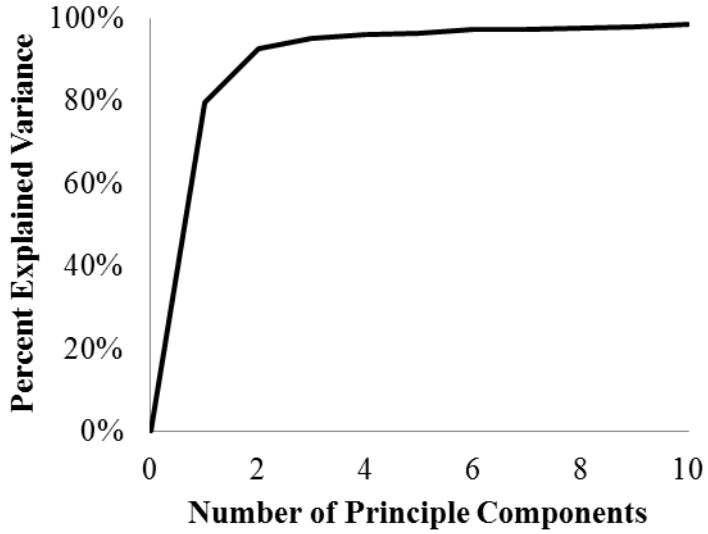

(b)

Figure 3.4 continued.

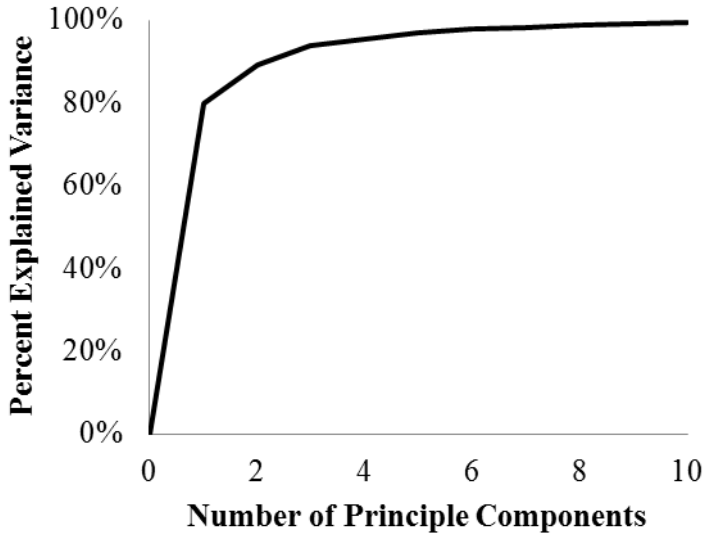

(c)

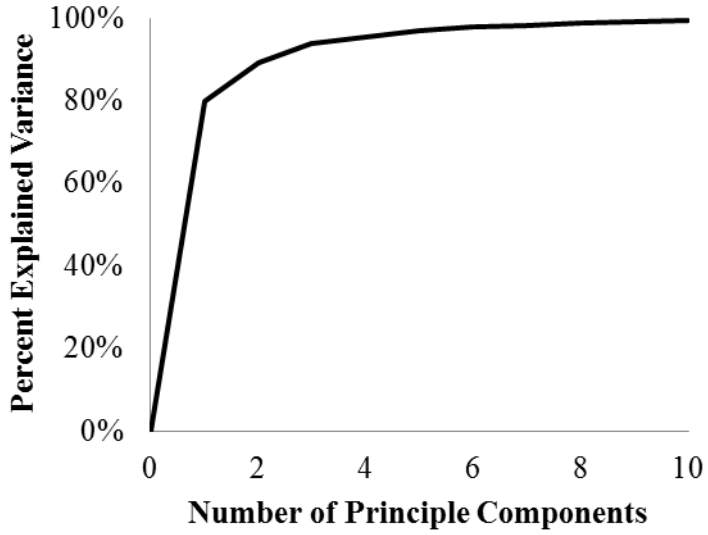

(d)

Figure 3.4 continued.

Table 3.5: Figures of merit for the calibration curves built using PLS regression analysis.

Multivariate PLS Analysis for Eu				
Standards	PC Factors	R^2	RMSE (wt %)	LOD (wt %)
Single element	5	0.9619	0.008	0.019
Multi–element	3	0.9385	0.005	0.014
All	4	0.9083	0.010	0.013
Multivariate PLS Analysis for Sm				
Standards	PC Factors	R^2	RMSE (wt %)	LOD (wt %)
Single element	4	0.9598	0.008	0.015
Multi–element	3	0.9383	0.005	0.014
All	4	0.9317	0.009	0.005

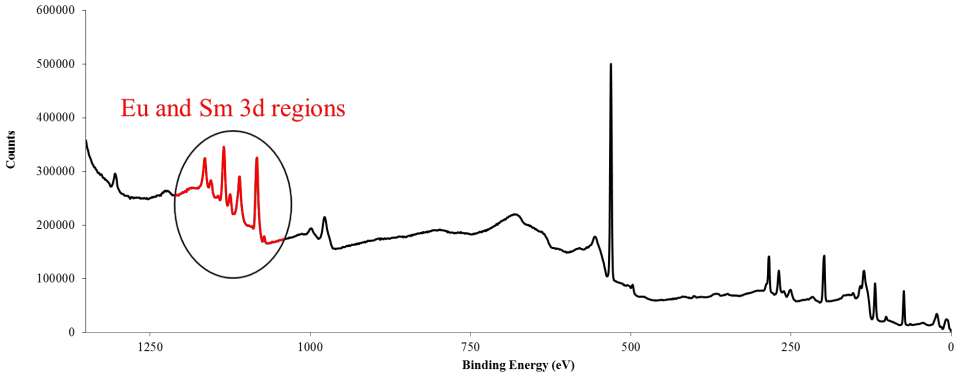

Figure 4.1: Spectra obtained from full survey scans of Eu/Sm–BDPA produced from ion exchange of Na–BDPA with $EuCl_3$–$SmCl_3$ [50:50] at 650 °C for 24 hours under an argon atmosphere. The Eu and Sm 3d regions are highlighted.

Figure 4.2: Spectra of the Eu 3d spectral line regions from the XPS measurements of Eu/Sm–BDPA (Eu to Sm ratio of 1:1) synthesized under an atmosphere of (a) air, (b) argon, (c) vacuum, and (d) argon with an excess of NH_4Cl.

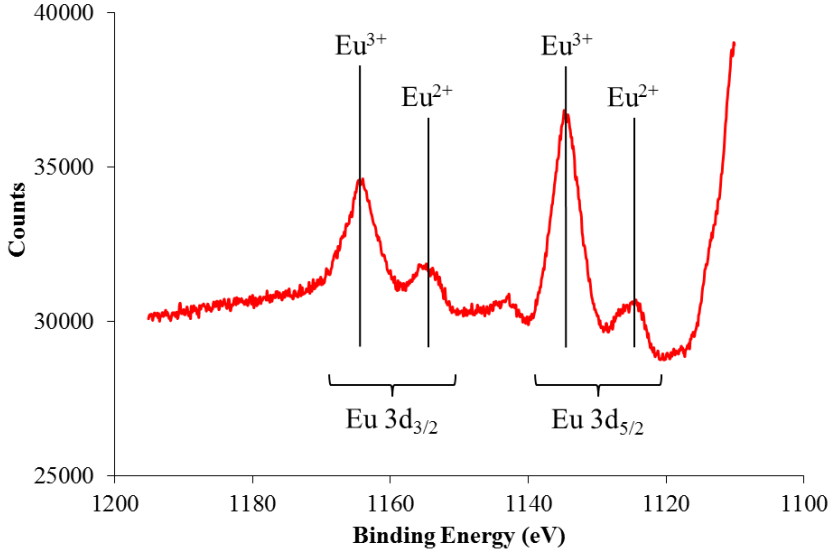

(a)

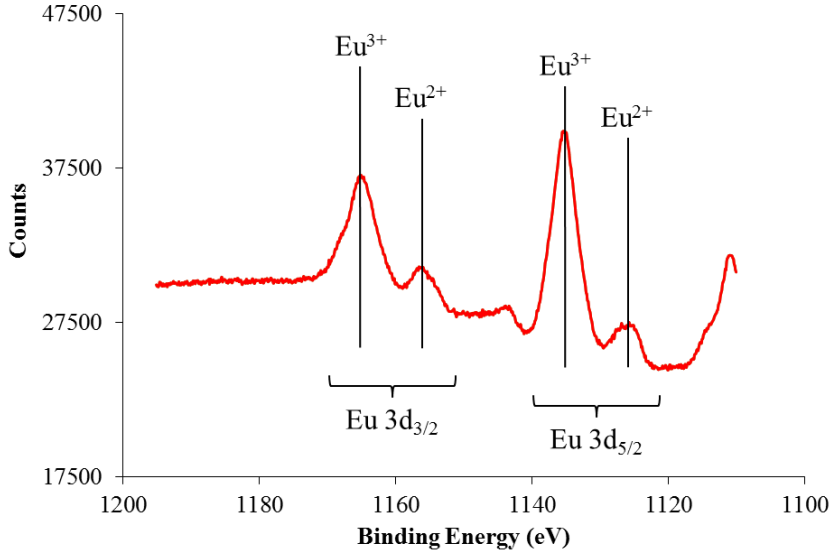

(b)

Figure 4. 2 continued.

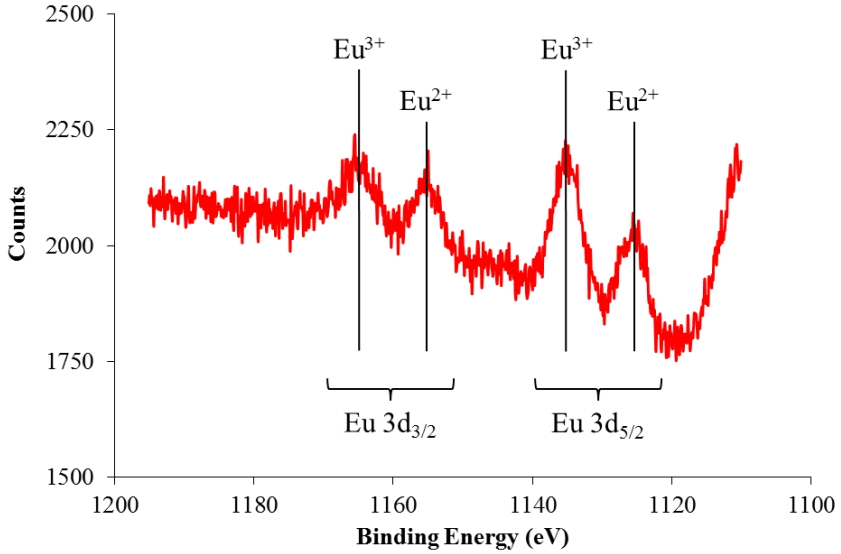

(c)

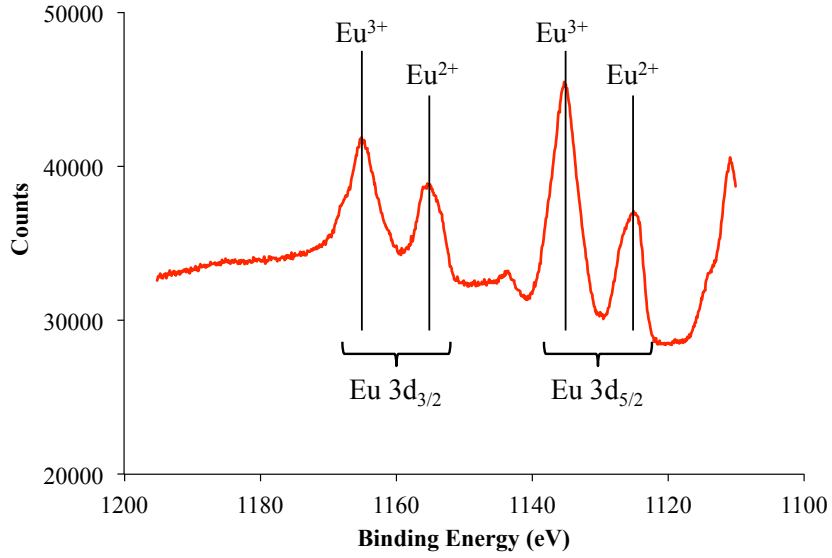

(d)

Figure 4.2 continued.

Figure 4.3: Spectra of the Sm 3d and spectral line regions from the XPS measurements of Eu/Sm–BDPA (Eu to Sm ratio of 1:1) synthesized under an atmosphere of (a) static air, (b) flowing argon gas, (c) static vacuum, and (d) argon with an excess of NH_4Cl.

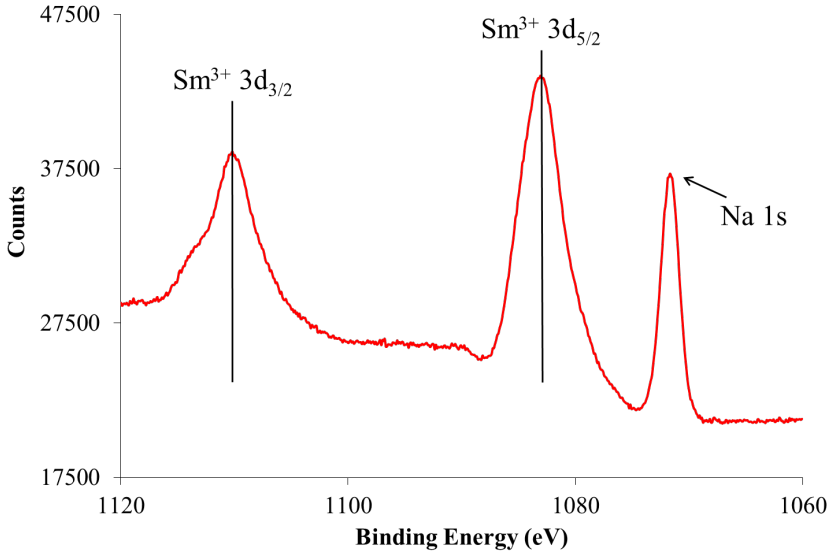

(a)

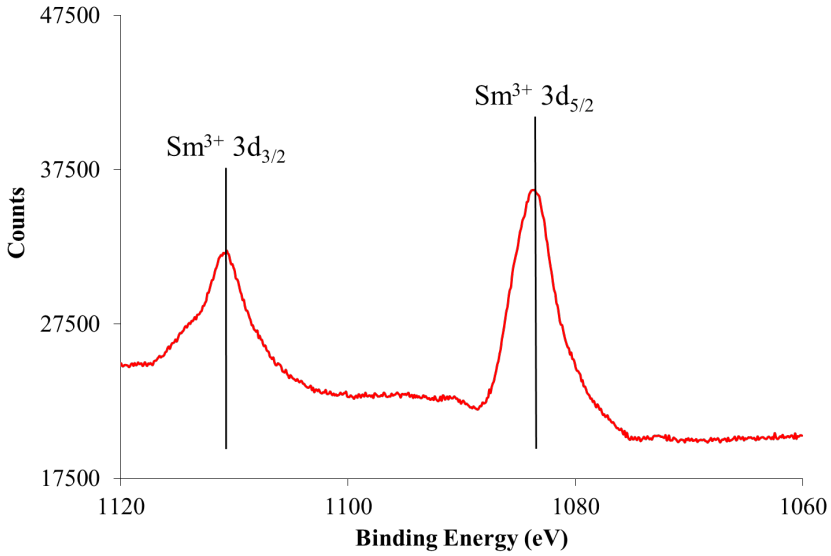

(b)

Figure 4.3 continued.

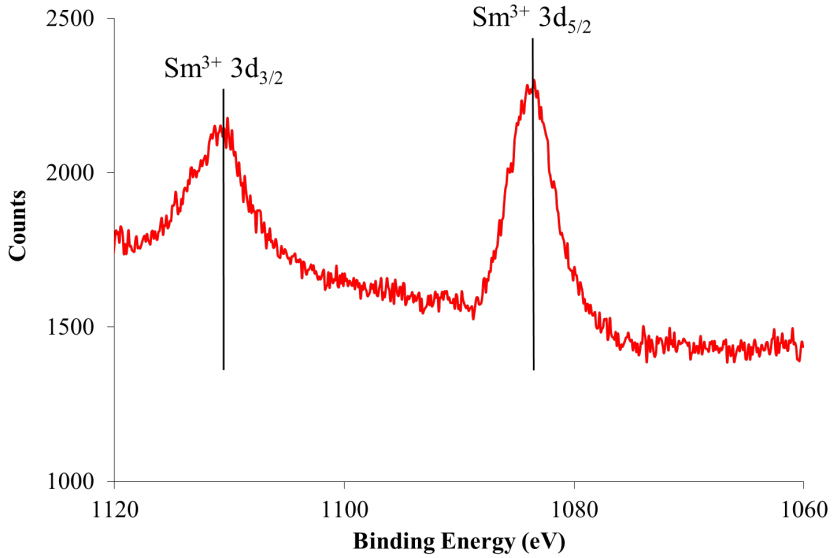

(c)

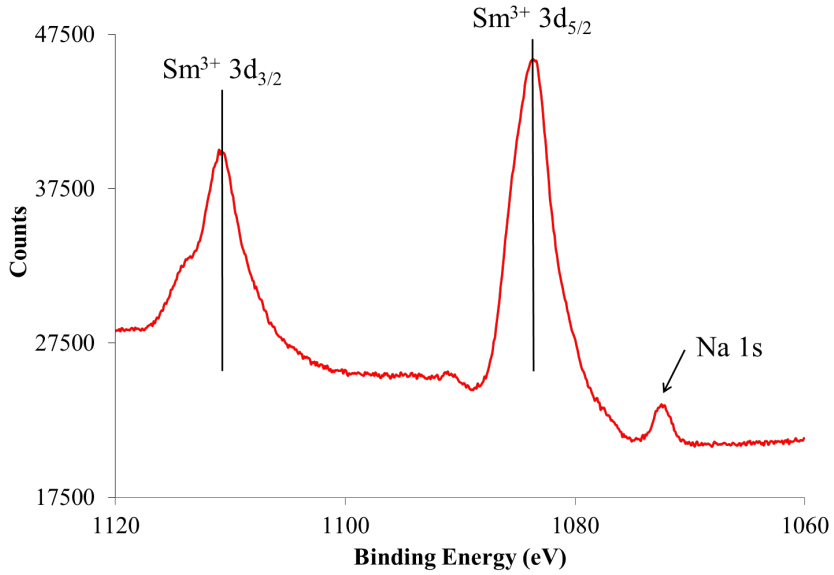

(d)

Figure 4.3 continued.

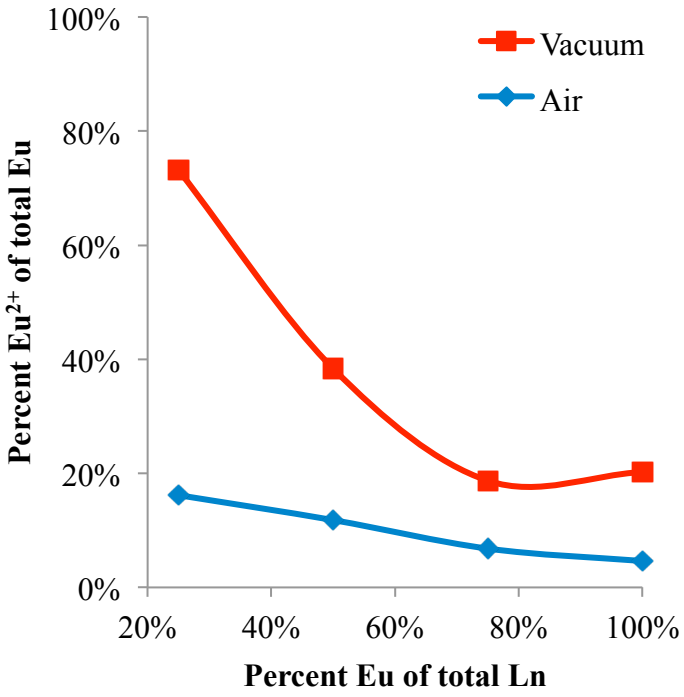

Figure 4.4: Percent Eu^{2+} of the total Eu content as a function of the percent of Eu of the total Ln content in Eu/Sm–BDPA derivatives synthesized in air (blue line) and vacuum (red line).

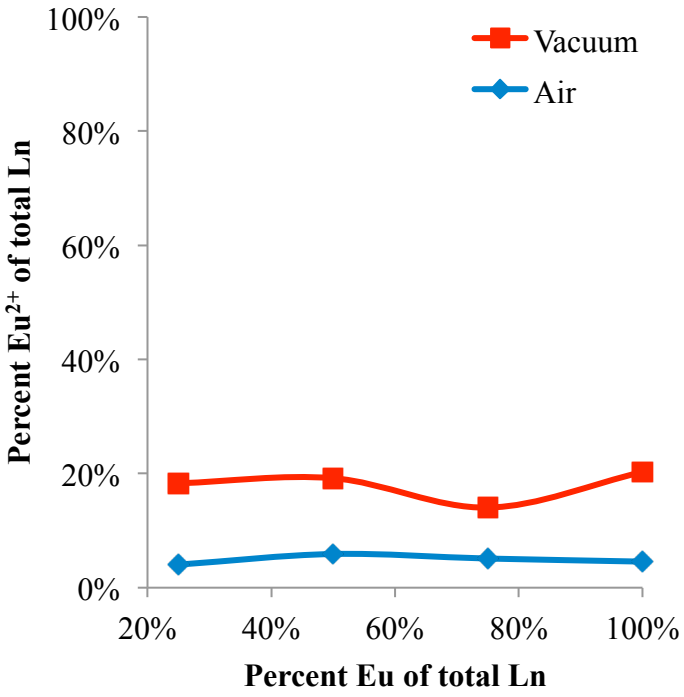

Figure 4.5: Percent Eu^{2+} of the total Ln content as a function of the percent Eu of the total Ln content in Eu/Sm–BDPA derivatives synthesized in air (blue line) and vacuum (red line).

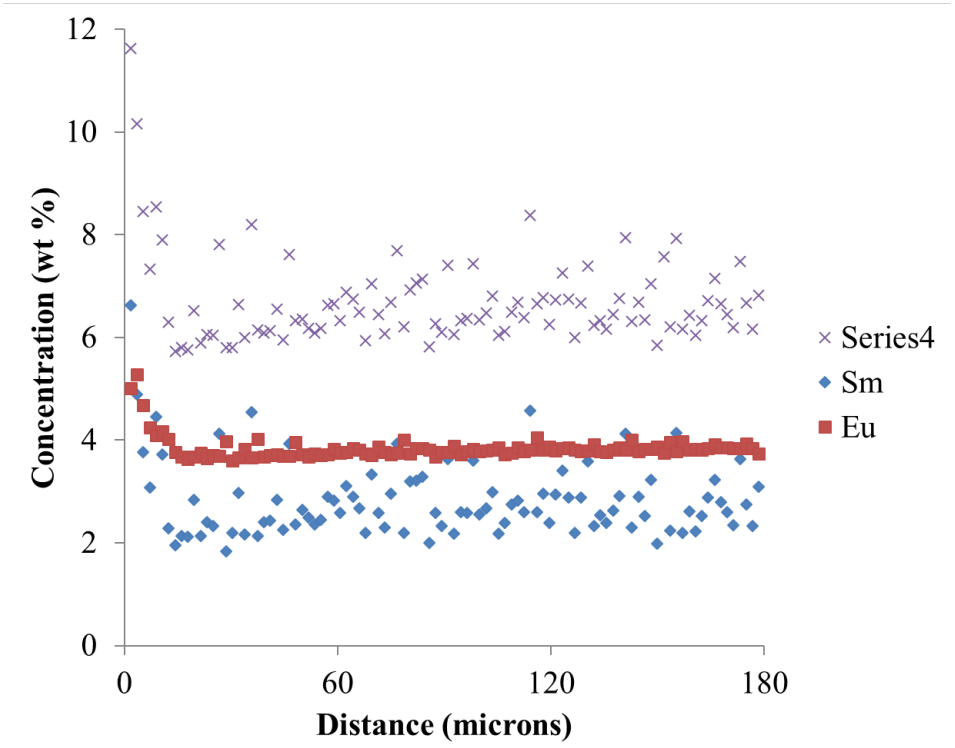

Figure 5.1: Concentration of Eu and Sm as a function of distance into a Eu/Sm–BDPA sample produced from an ion exchange reaction between Na–BDPA, $EuCl_3$–$SmCl_3$ hydrate, and an excess of NH_4Cl at 700 ˚C for 24 hours under an argon atmosphere.

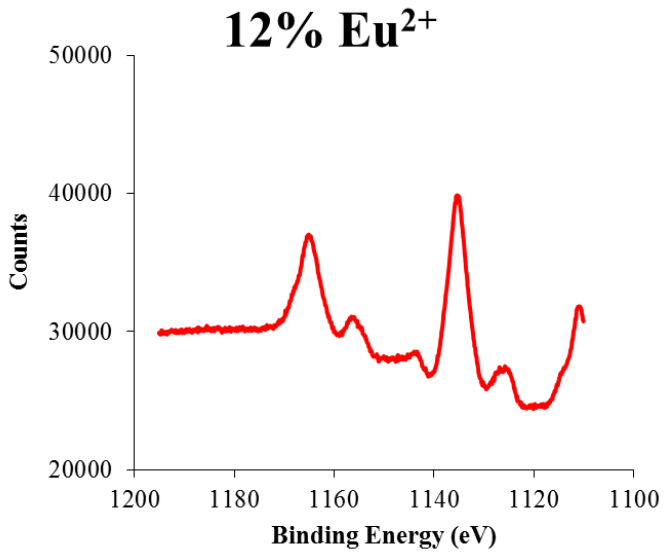

(a)

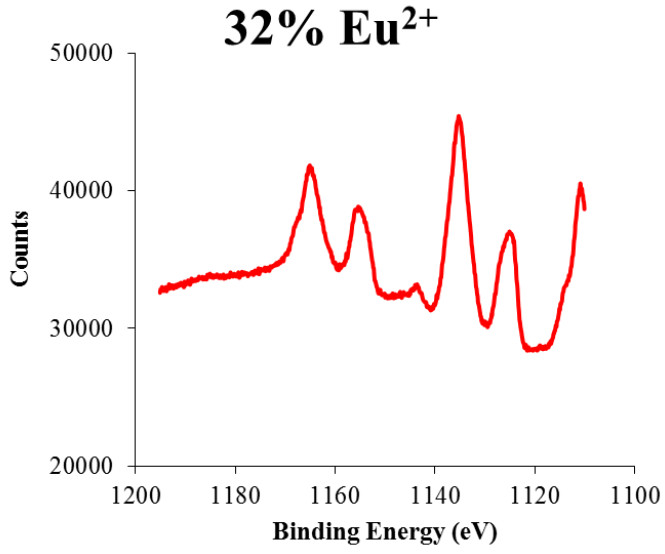

(b)

Figure 5.2: XPS spectra of the Eu 3d regions in Eu/Sm–BDPA samples prepared by ion exchange of Na–BDPA with $EuCl_3$–$SmCl_3$ [50:50] hydrate mixtures and excess NH_4Cl under argon atmospheres for 24 hours. The samples were designated as having (a) low Eu^{2+} and (b) high Eu^{2+} content.

Table 5.1: Results from ion exchange reactions at 815 °C between molten NaCl and Eu/Sm–BDPA starting materials with low Eu^{2+} content.

Atmosphere	**Time (h)**	**% Eu Extracted**	**% Sm Extracted**	**SF_{Sm}**	**SF_{Eu}**	**D_{ex}**
Air	2	20%	57%	0.5	1.9	5.3
Air	24	12%	31%	0.8	1.3	3.5
Argon	2	8%	27%	0.8	1.3	4.2
Argon	24	12%	38%	0.7	1.5	4.6
Vacuum	2	10%	37%	0.7	1.4	5.4
Vacuum	24	13%	36%	0.7	1.4	3.8

Table 5.2: Results from ion exchange reactions at 550 °C between molten CsCl–NaCl and Eu/Sm–BDPA starting materials with low Eu^{2+} content.

Atmosphere	**Time (h)**	**% Eu Extracted**	**% Sm Extracted**	**SF_{Sm}**	**SF_{Eu}**	**D_{ex}**
Air	2	15%	55%	0.5	1.8	7.0
Air	24	4%	52%	0.5	2.0	25.5
Argon	24	11%	33%	0.7	1.3	4.0
Vacuum	24	11%	14%	1.0	1.0	1.3

Table 5.3: Results from ion exchange reactions at 550 °C between molten $CaCl_2$–NaCl and Eu/Sm–BDPA starting materials with low Eu^{2+} content.

Atmosphere	**Time (h)**	**% Eu Extracted**	**% Sm Extracted**	**SF_{Sm}**	**SF_{Eu}**	**D_{ex}**
Air	2	18%	45%	0.7	1.5	3.8
Air	24	10%	44%	0.6	1.6	6.8
Argon	24	2%	3%	1.0	1.0	1.3
Vacuum	24	15%	16%	1.0	1.0	1.0

Table 5.4: Results from ion exchange reactions at 550 °C between molten CsCl–NaCl and Eu/Sm–BDPA starting materials with high Eu^{2+} content.

Atmosphere	**Time (h)**	**% Eu Extracted**	**% Sm Extracted**	**SF_{Sm}**	**SF_{Eu}**	**D_{ex}**
Air	2	38%	~0%*	1.7	0.6	1.3E+07
Argon	24	~0%*	6%	0.7	1.5	510.0
Vacuum	2	35%	32%	1.1	1.0	1.2
Vacuum	24	16%	29%	0.8	1.2	2.1

* values at or below the LOD of 0.005 wt % Sm or 0.013 wt % Eu.

Table 5.5: Results from ion exchange reactions at 550 °C between molten $CaCl_2$–NaCl and Eu/Sm–BDPA starting materials with high Eu^{2+} content.

Atmosphere	**Time (h)**	**% Eu Extracted**	**% Sm Extracted**	**SF_{Sm}**	**SF_{Eu}**	**D_{ex}**
Air	2	~0%*	~0%*	~	~	~
Argon	24	~0%*	~0%*	~	~	~
Vacuum	2	35%	30%	0.9	1.1	1.3
Vacuum	24	16%	18%	1.0	1.0	0.9

* values at or below the LOD of 0.005 wt % Sm or 0.013 wt % Eu.

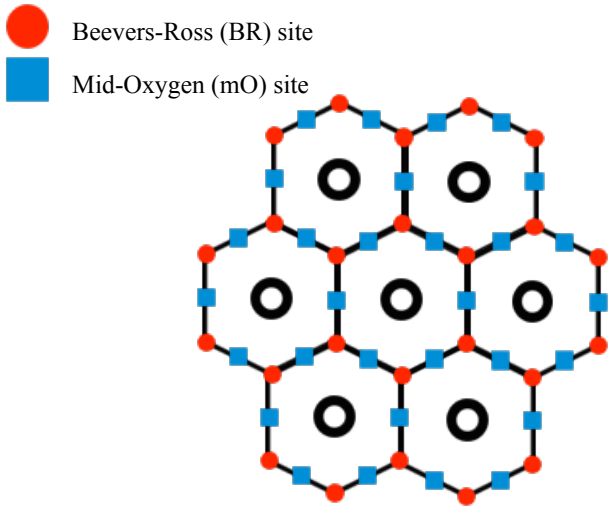

Figure 5.3: Graphical representation the conduction plane in the BDPA structure as an aerial view. The black circles in the middle of each hexagon denote the pillar oxygen species.

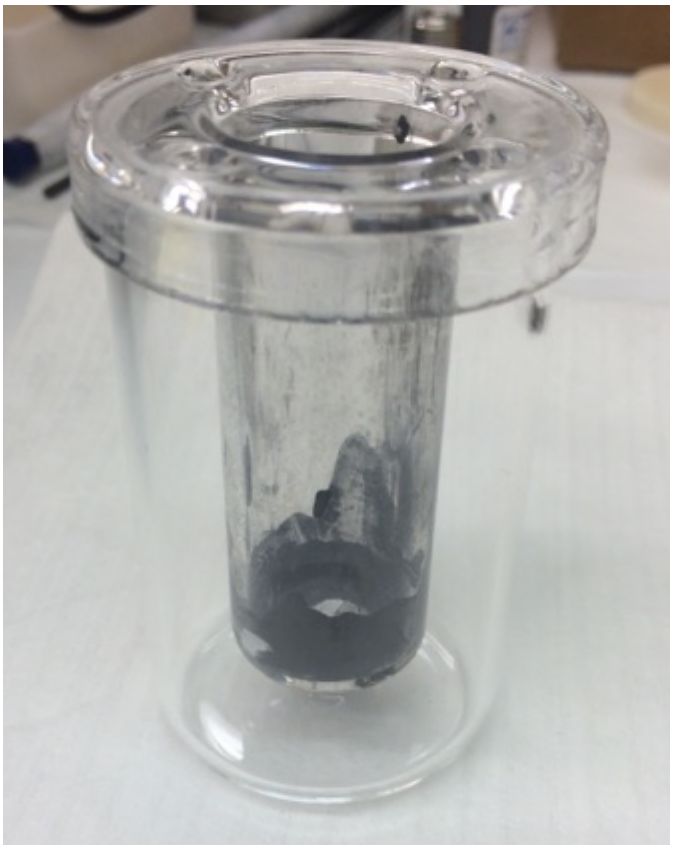

Figure 6.1: Picture of the quartz used for the electrolytic separation of Eu from Sm. The Na–BDPA disc is pasted into the quartz using a high–temperature carbon paste from PELCO.

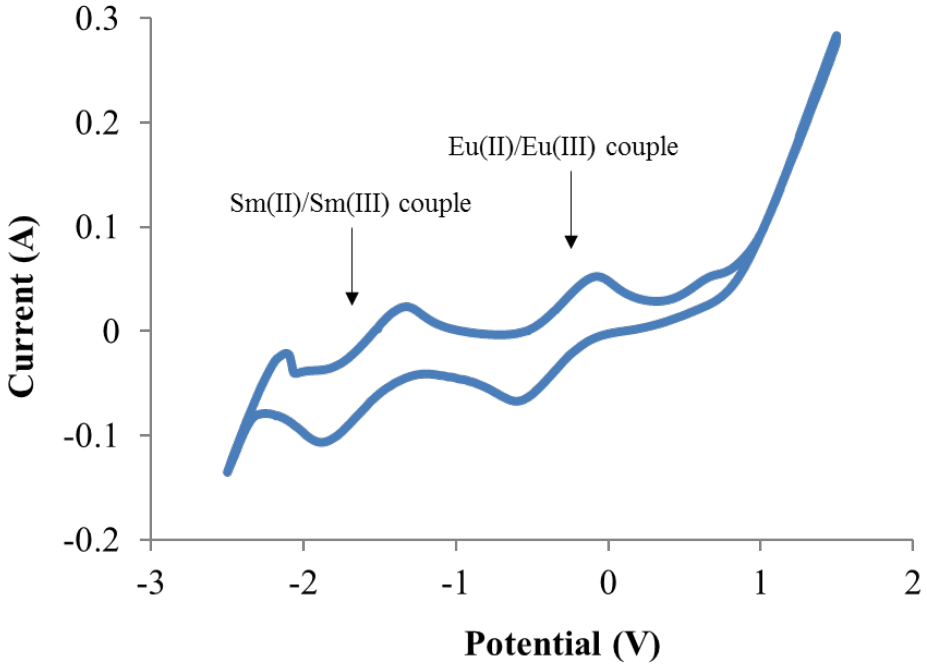

Figure 6.3: Cyclic voltammogram of CsCl–$MgCl_2$–Eu_2O_3–Sm_2O_3 at taken 1 V s^{-1} with glassy carbon rods as the electrodes. The measurements were taken at 550 °C under a flow of argon gas.

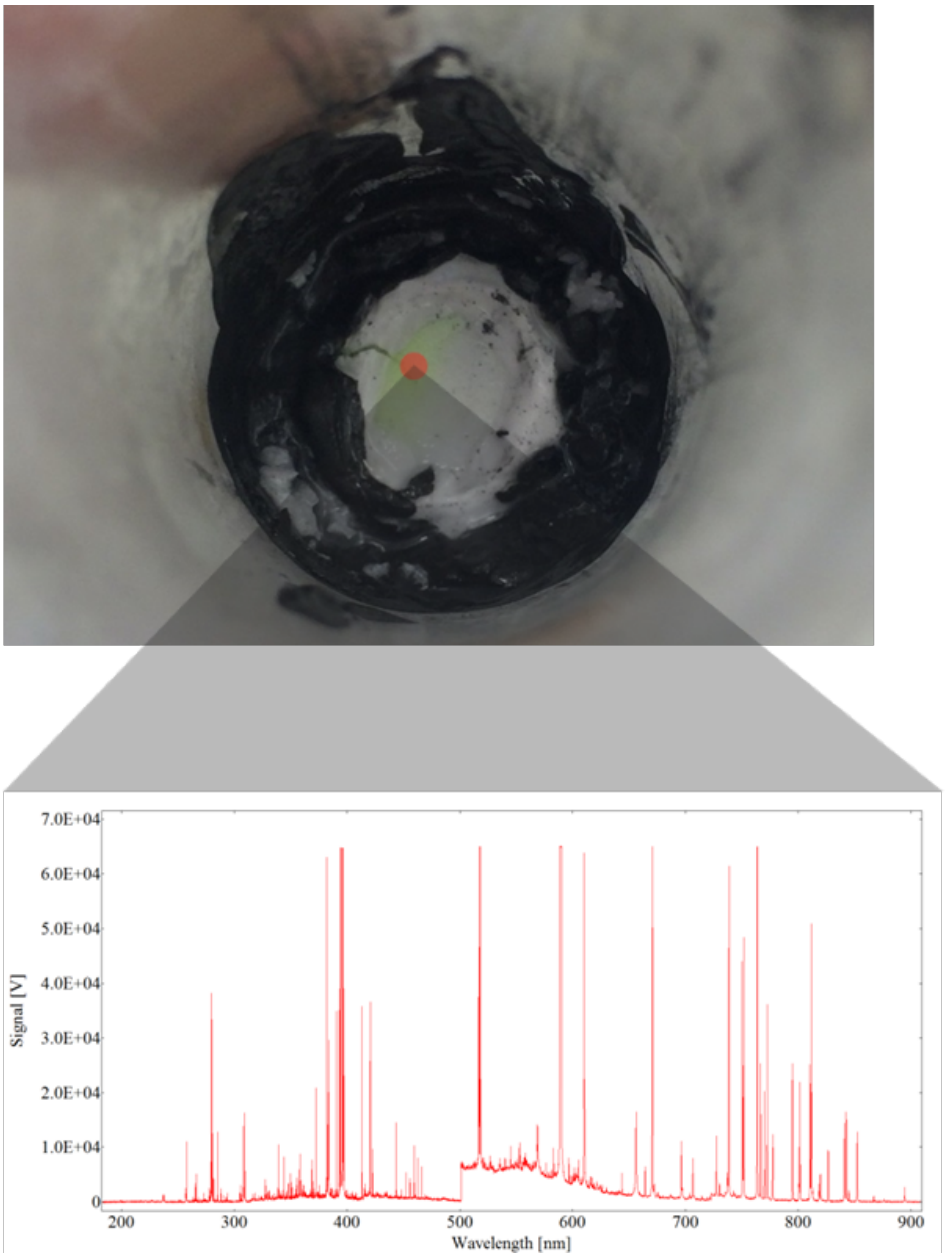

Figure 6.4: Picture of the receiving solution side of the electrochemical cell showing the green coloration of the BDPA indicative of the presence of Eu^{2+}. The LIBS analysis spot is highlighted with a red see–through dot to show where the LIBS spectra were acquired. An example spectrum is included in the picture.

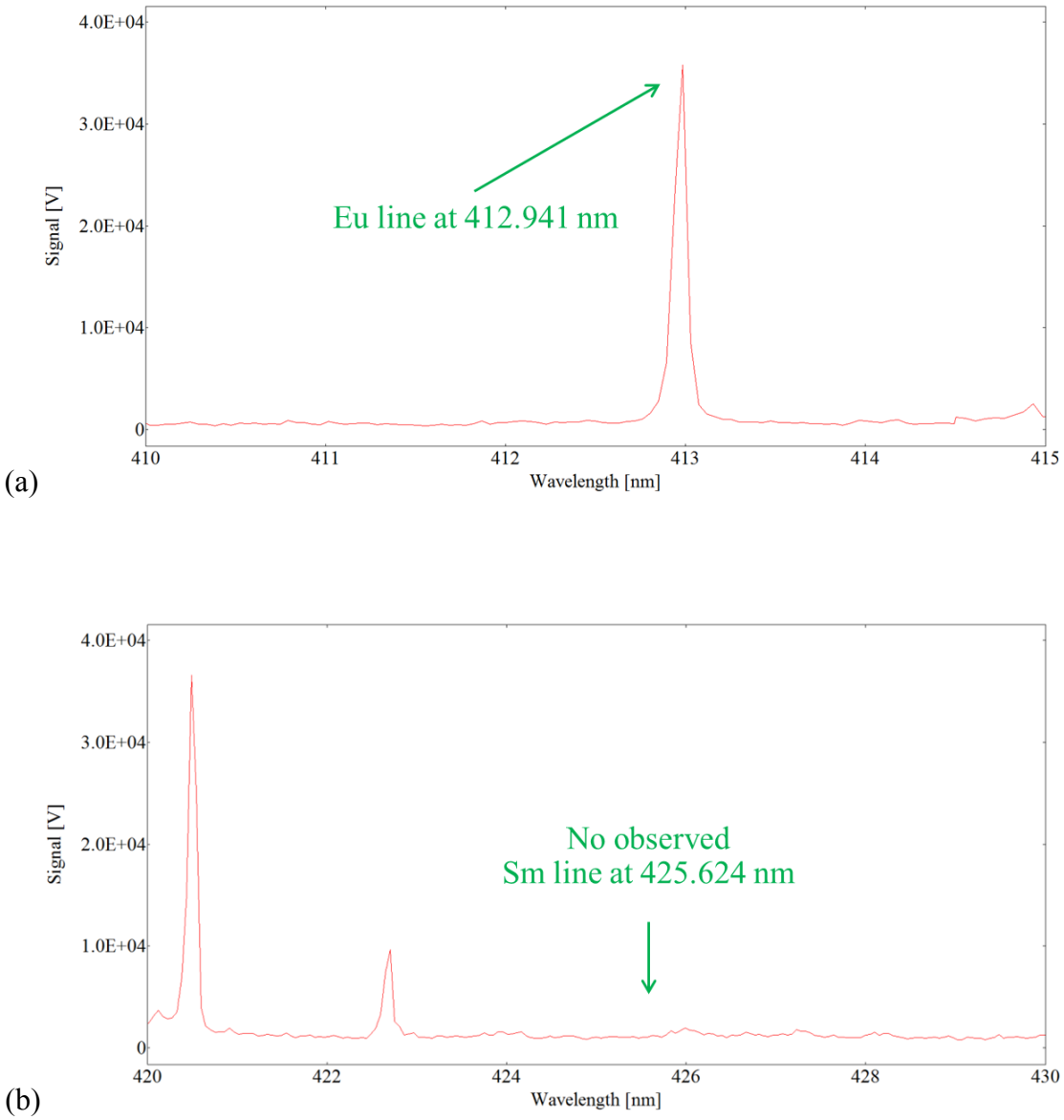

Figure 6.5: Zoomed in regions from (a) 410 nm to 415 nm and (b) 420 nm to 430 nm of LIBS spectra acquired from measurement of the receiving solution side of the Na–BDPA membrane showing the presence of Eu and absence of Sm.

Vita

Kristian Guy Myhre was born in Seattle, Washington in 1991 to Franck and Kimberly Myhre. During his last two years of high school, he attended Shoreline Community College full–time through Washington State's Running Start program. He graduated from high school in 2009 and completed his associate's degree one year later. Afterwards, he transferred to Seattle Pacific University, where he earned his B.S. Chemistry degree in 2013. During his time at Seattle Pacific University, he worked as an undergraduate research student under Dr. Scott Wilbur in the University of Washington Medical Center's Radiation Oncology Radiochemistry Research Laboratory. It was through that student work–study position that Kristian first was exposed to radiochemistry. He also partook in the Department of Homeland Security's Nuclear Forensics Summer School in 2012 at the University of Missouri in Columbia. Through that experience, he learned about the opportunity to continue his studies through the University of Tennessee and ORNL's joint Ph.D. program housed within the Bredesen Center. He then moved to Knoxville, Tennessee to partake in the Bredesen Center's Energy Science and Engineering Ph.D. program. Shortly after starting the program, he met his beautiful wife Bethany and married her in March, 2015.